NASA CR-72989

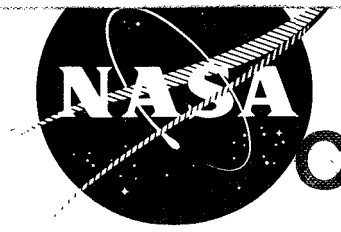

DEFLECTABLE BEAM LINEAR STRIP CESIUM CONTACT ION THRUSTER SYSTEM

By

C. R. Dulgeroff, D. E. Zuccaro, S. Kami,
D. E. Schnelker, and J. W. Ward

Contract NAS 3-13724

April 1971

Prepared for

NATIONAL AERONAUTICS AND SPACE ADMINISTRATION

HUGHES RESEARCH LABORATORIES
A DIVISION OF HUGHES AIRCRAFT COMPANY
3011 Malibu Canyon Road
Malibu, California 90265

1. Report No.	2. Government Accession No.	3. Recipient's Catalog No.
CR-72989		

4. Title and Subtitle	5. Report Date
DEFLECTABLE BEAM LINEAR STRIP CESIUM CONTACT ION THRUSTER SYSTEM	April 1971
	6. Performing Organization Code
7. Author(s)	8. Performing Organization Report No.
C.R. Dulgeroff, D.E. Zuccaro, S. Kami, D.E. Schnelker and J.W. Ward	
	10. Work Unit No.
9. Performing Organization Name and Address	11. Contract or Grant No.
Hughes Research Laboratories 3011 Malibu Canyon Road Malibu, Calif. 90265	NAS 3-13724
	13. Type of Report and Period Covered Contract Report
12. Sponsoring Agency Name and Address	14. Sponsoring Agency Code
National Aeronautics and Space Administration Lewis Research Center Cleveland, Ohio	

15. Supplementary Notes

16. Abstract

A dual beam thruster system suitable for two-axis attitude control has been designed, constructed, and tested. The system is comprised of two orthogonal strips, each capable of producing 0.30 mlb thrust and beam deflections of more than ±20°. The nominal specific impulse is 5000 sec ± 500 sec. The thrust level from each strip can be varied from 0 to 100%. The system power required for clean ionizers is approximately 200 W. Neutralizer filaments were developed and life tested over 2000 hours producing more than 40 mA of electron emission per watt of input power.

17. Key Words (Suggested by Author(s))	18. Distribution Statement
Ion Thruster System, Dual Beam Thruster, Thrust Vectorable Beam, Cesium Feed System, Neutralizer Filamental, Analytical Vibration Study	Unclassified - Unlimited

19. Security Classif. (of this report)	20. Security Classif. (of this page)	21. No. of Pages	22. Price*
Unclassified	Unclassified	138	$3.00

* For sale by the National Technical Information Service, Springfield, Virginia 22151

TABLE OF CONTENTS

LIST OF ILLUSTRATIONS

LIST OF TABLES

ABSTRACT

A dual beam thruster system suitable for two-axis attitude control has been designed, constructed, and tested. The system is comprised of two orthogonal strips, each capable of producing 0.30 mlb thrust and beam deflections of more than ±20°. The nominal specific impulse is 5000 sec ± 500 sec. The thrust level from each strip can be varied from 0 to 100%. The system power required for clean ionizers is approximately 200 W. Neutralizer filaments were developed and life tested over 2000 hours producing more than 40 mA of electron emission per watt of input power.

SECTION I

SUMMARY

The objective of this program was to design, build, and test a dual deflectable beam ion thruster system. This system employs two orthogonal linear strips with deflectable beams and is suitable for two-axis attitude control and single direction station keeping of a synchronous satellite. Each aperture provides a variable thrust from 0 to 0.3 mlb at a nominal specific impulse of 5000 sec ± 500 sec.

The electrode design evolved with the aid of a computer program and deep electrolytic tank. The computer program established a design for electrodes which give deflection angles of greater than ±20° with a minimum amount of ion interception. The deep tank was used to study the end effects of the strip geometry.

The design of the thruster incorporated the LE-1 strip engine, an advanced ion engine developed previously at Hughes Research Laboratories. The feed system design was similar to a zero-g capillary type system used successfully on a Hughes-built μ-thruster. This feed system used an integrated thermal valve and vaporizer to control the cesium flow.

The neutralizers used on the thruster also were developed as part of this program. A set of parameters for producing uniform carburized thoriated tungsten filaments was obtained. Two such neutralizers were life tested for more than 2,000 hours, terminating at the end of the contract period. Life expectancy is 15,000 hours. A vibration analysis was made with the aid of a Hughes Aircraft Company computer program. The results of this study suggested several changes; these were made to the original design, so the system would be constructed to withstand vibrations of an actual launch.

The critical temperatures and ionization efficiencies of the ionizers were obtained with the aid of two neutral detectors. The ionization efficiency for a clean ionizer was about 1% for a 7 mA/cm^2 ion density.

The beam deflections were measured with two beam scanning collectors. Deflections as high as 24° were recorded.

The performance characteristics of the system were obtained during an intensive testing period. The final test called for a 24 hour test at Hughes Research Laboratories. After the 24 hour test and some neutralization tests, the thruster was delivered to NASA Lewis Research Center. Hughes personnel successfully operated the thruster for an eight hour period at LeRC, as required by the contract.

The thruster system as it now exists, requires approximately a 200 W power input with clean ionizers. The total efficiency for the system is about 40%. Several improvements are suggested for the present design.

SECTION II

INTRODUCTION

Hughes Research Laboratories has been developing surface contact ion engines since 1959. During this time, ion thrusters using porous tungsten buttons, rings, multistrip and single strip engines have been built and operated. The work on these thrusters was devoted to optimizing thruster performance, ion optics, beam neutralization, and other related areas. One of the important tasks performed during this period was the operation of a strip thruster for 2000 hours to demonstrate the lifetime of this type of thruster.[1] The most recent thrusters that had been built prior to the present contract were a 20 μlb button thruster[2] and a 4.6 cm strip thruster. The latter (described in Ref. 3), is readily adapted for beam deflection and is the basic thruster unit for the program covered in this report.

Surface contact ion thrusters offer potential advantages for various space applications. In particular, a complete dual deflectable ion thruster system has, as one possible use, the two-axis attitude control and single direction station keeping of a medium weight (1500 lb to 3000 lb), stable platform type satellite in a synchronous earth orbit. In order to effectively use a dual beam thruster for this application, two linear strip thrusters with deflectable beams have their principal thrust axes parallel, and orthogonal thrust vector deflection planes.

The objective of this program was to design, construct, and test a thruster system, based on past work on the linear strip thruster designated as the LE-1 thruster by Hughes Research Laboratories. The system was designed to demonstrate the following nominal performance goals.

a. Design thrust: 0.30 mlb ± 0.03 mlb at each aperture along the principal axis for a total of 0.60 ± 0.06 mlb.
b. Specific impuse: 5000 sec ± 500 sec along principal axis. Maximum deviation, 1000 sec at 30° deflection angle.
c. Net voltage: 1.67 kV nominal.
d. Ionizer current density: 7.0 ± 0.5 mA/cm^2.
e. Input power: less than 200 W total.
f. Beam deflection goal: from 0° to ±30° (Minimum acceptable ±20°).
g. Beam deflection stability: stable to within ±10% at any angle.
h. Thrust control: at 0, 25%, 50%, 75%, and 100% of design level.
i. Lifetime goal in excess of 15,000 hours.

The neutralizers for the system were also developed. The design goal of the neutralizers was to produce 20 mA of space-charge limited thermionic electron current per watt of input power with a life expectancy of 15,000 hours.

The design phase of the thruster was composed of three parts: optics, hardware, and vibration analysis. After the evolution and 24 hour test of the system at HRL, the thruster was delivered to NASA Lewis Research Center. Hughes Research Laboratories provided the necessary personnel for subjecting the thruster to an 8 hour acceptance test. The results of this program show that the dual beam system has great potential for attitude control and station keeping of a synchronous satellite.

SECTION III

DESIGN OF THE DUAL DEFLECTABLE BEAM THRUSTER SYSTEM

The object of this program was to design, build, and test a dual beam contact ion thruster system. The basis for this design was the past work on a linear strip thruster, designated the LE-1 thruster by Hughes Research Laboratories.

The thruster design can be described best with aid of a cross section of the system shown in Fig. 1 and side view photograph in Fig. 2. This is a reproduction of part of the assembly drawing that was sent to the NASA Project Manager. The ionizer designated as Strip 2 is shown in the left side of the drawing. It is orthogonal to Strip 1, which is hidden behind a shielded insulator, and the edge of the focus electrode in the right side of the drawing. The orientation of strips can be seen better in Fig. 3 which shows the top view of the thruster. Item (1) in Fig. 1 is the feed system for one strip. Immediately above the ionizer in Fig. 1, are the accel electrodes and exit electrode. A photograph of the complete system is shown in Fig. 4. The components are described in the following section.

A. IONIZER

The ionizer material was supplied by NASA Lewis Research Center. It was originally made by Hughes Research Laboratories under Contract NAS 3-7105 and was called slab 333-S. It was sintered from spherical tungsten powder. The slab had an average pore spacing of 4.42 μm and an average pore size of 2.58 μm. A photograph of the surface of the ionizer after etching and polishing is shown in Fig. 5.

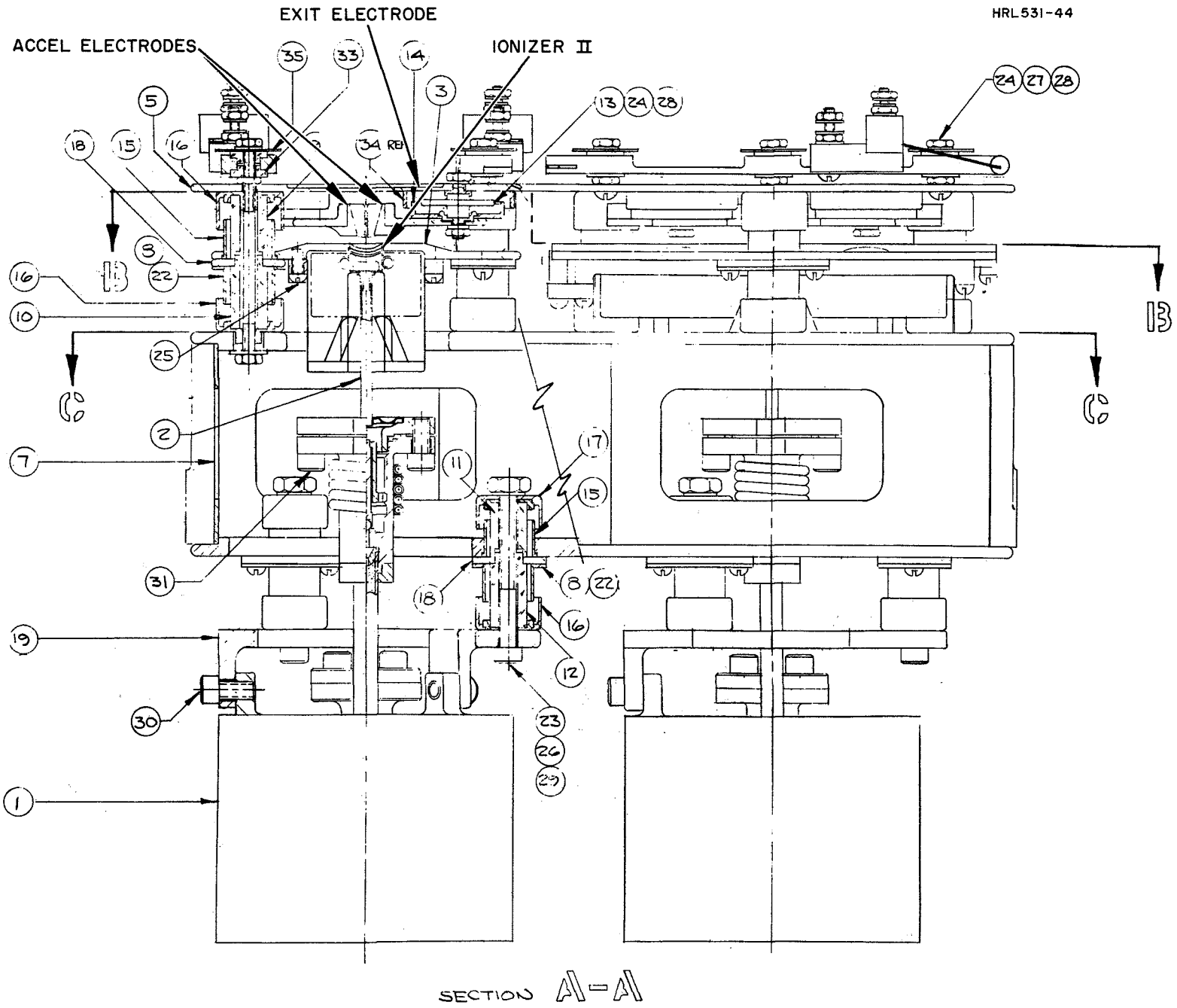

Fig. 1. Cross Section of Dual Deflectable Beam Thruster System.

M 7618

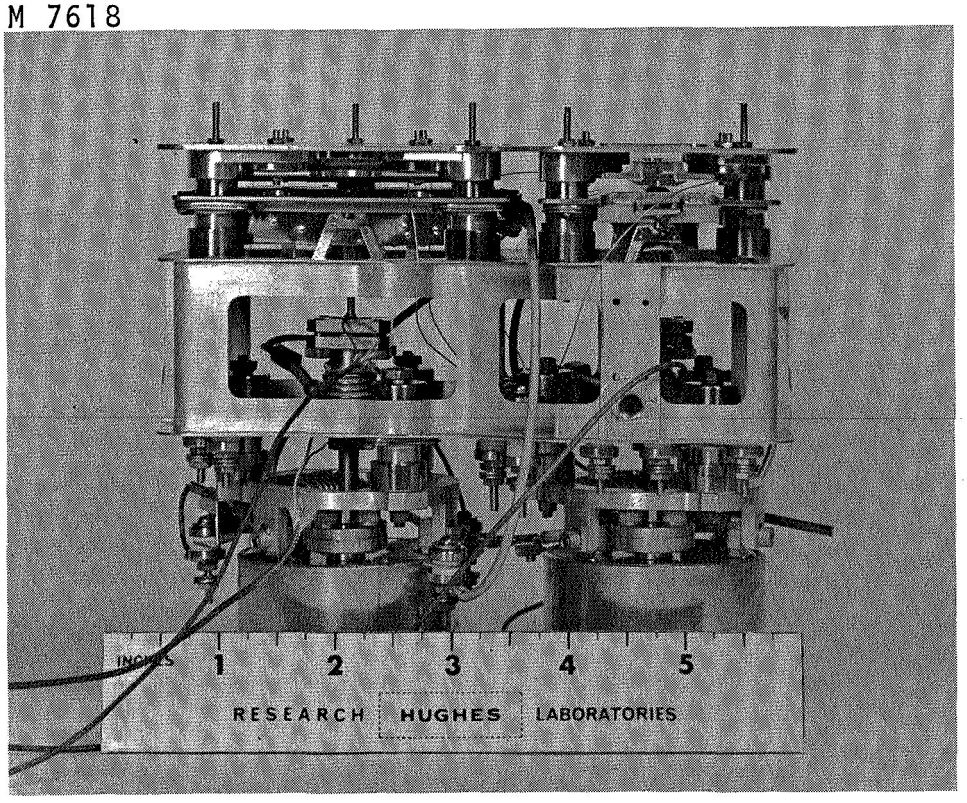

Fig. 2. Photograph of Side View of Thruster.

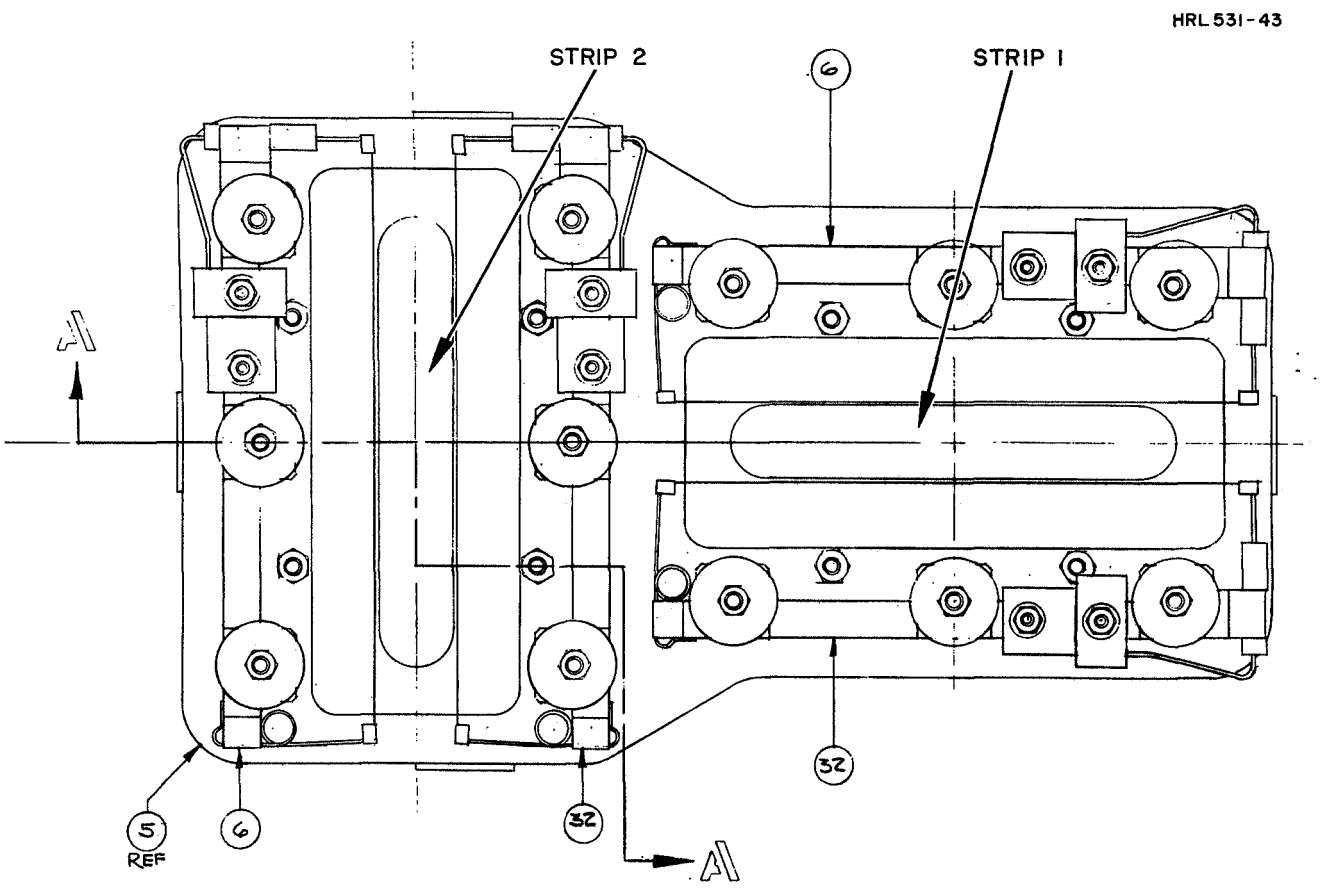

Fig. 3. Top View of Thruster.

M 7739

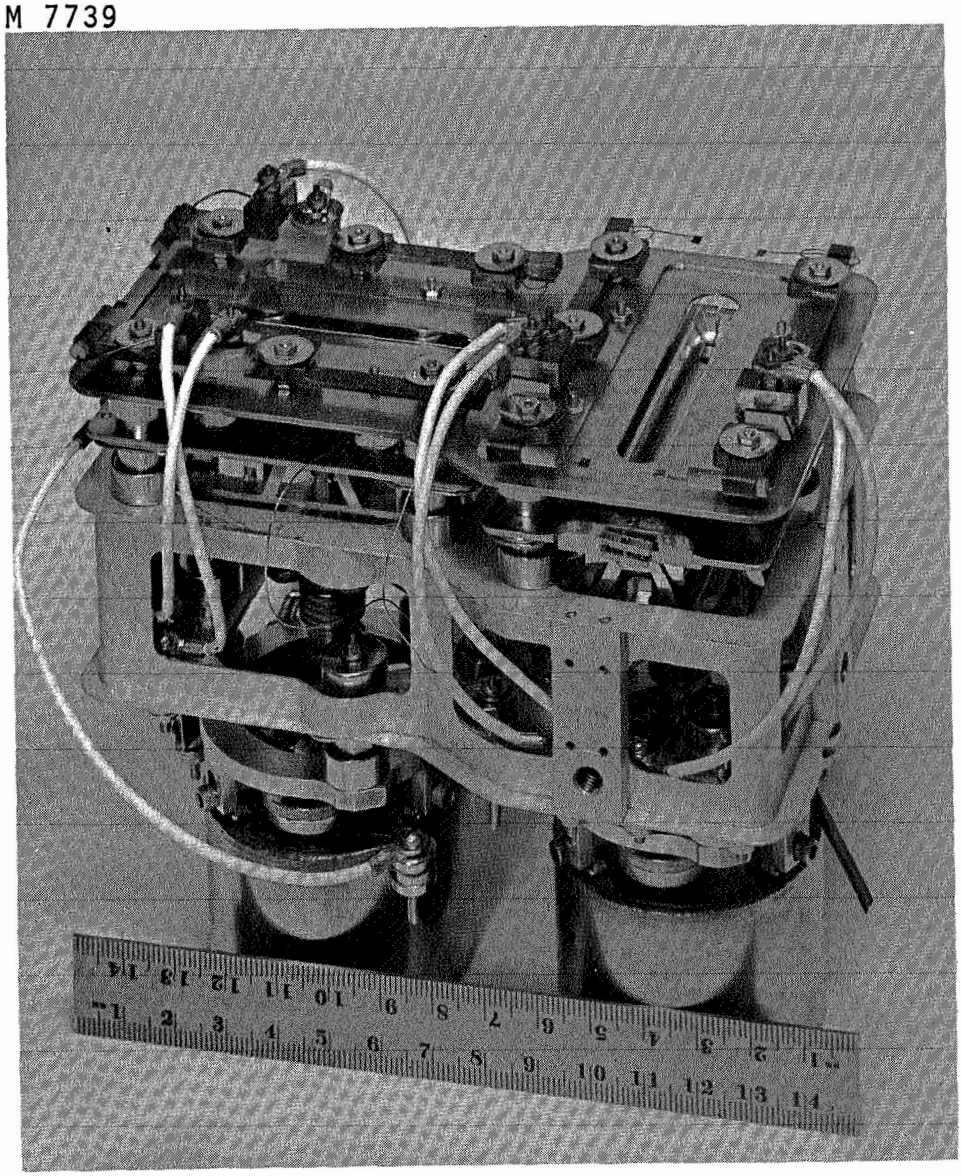

Fig. 4. Photograph of Dual Deflectable Beam Thruster System.

M 7882

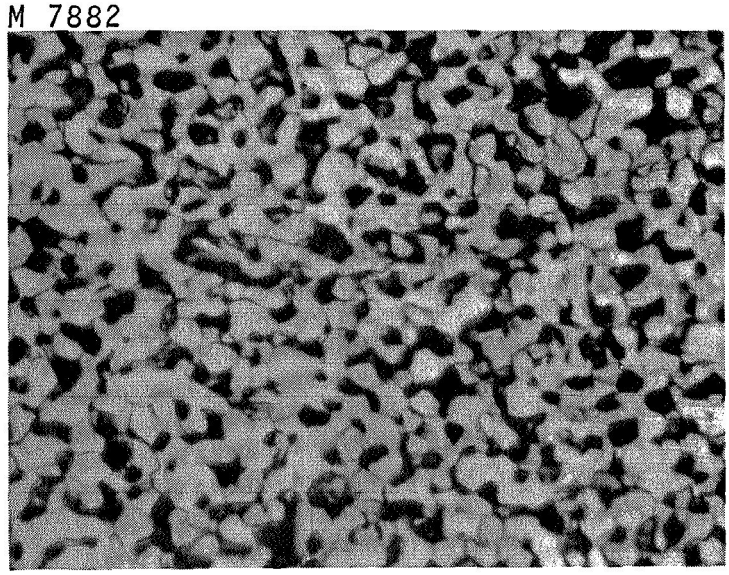

Fig. 5. Ionizer Surface after Etching and Polishing (1000x).

The ionizer was the same low mass ionizer as that used on the LE-1 thruster.[3] A photograph of a cross-section of this type of ionizer is shown in Fig. 6. The contour of the ionizer was obtained from the Model 70 optics. Figure 6 also shows the position of two tungsten tubes that serve as sheaths for the heaters. Electron beam welding was used to attach the sheaths and back of the ionizer manifold to the porous tungsten. The heating element was coiled helix wire, made from 97% tungsten and 3% rhenium. The emittance of the heater coil was increased by depositing a ceramic coating on the wire. The heaters were placed into a cylindrical ceramic spacer prior to insertion into the metal sheaths (shown in Fig. 7). Figure 8 shows the basic elements of the ionizer and heater. The welded ionizer, sheaths, and support straps are shown in Fig. 9. Before attaching the flange which joined the feed system, the heat shields were placed around the ionizer. Results of tests made on heaters of this type are reported in Ref. 3.

B. FEED SYSTEM

Item (31) in Fig. 1 shows the ionizer assembly which is attached to the flange on the feed system with four screws. There is a shear-seal copper gasket between the flanges.

Each linear strip has its own propellant tank, vaporizer, and thermally activated valve as a positive shutoff. The design was based on a feed system used successfully at HRL.

Each propellant feed system was required to reliably supply a minimum of 70 grams of cesium in a 0 to 1 g environment, and to operate in a 0 g environment in any attitude. The design of the system permits operation in any attitude over the range of 0 to 1 g; it is a capillary-type feed system in which the liquid cesium is moved by controlled

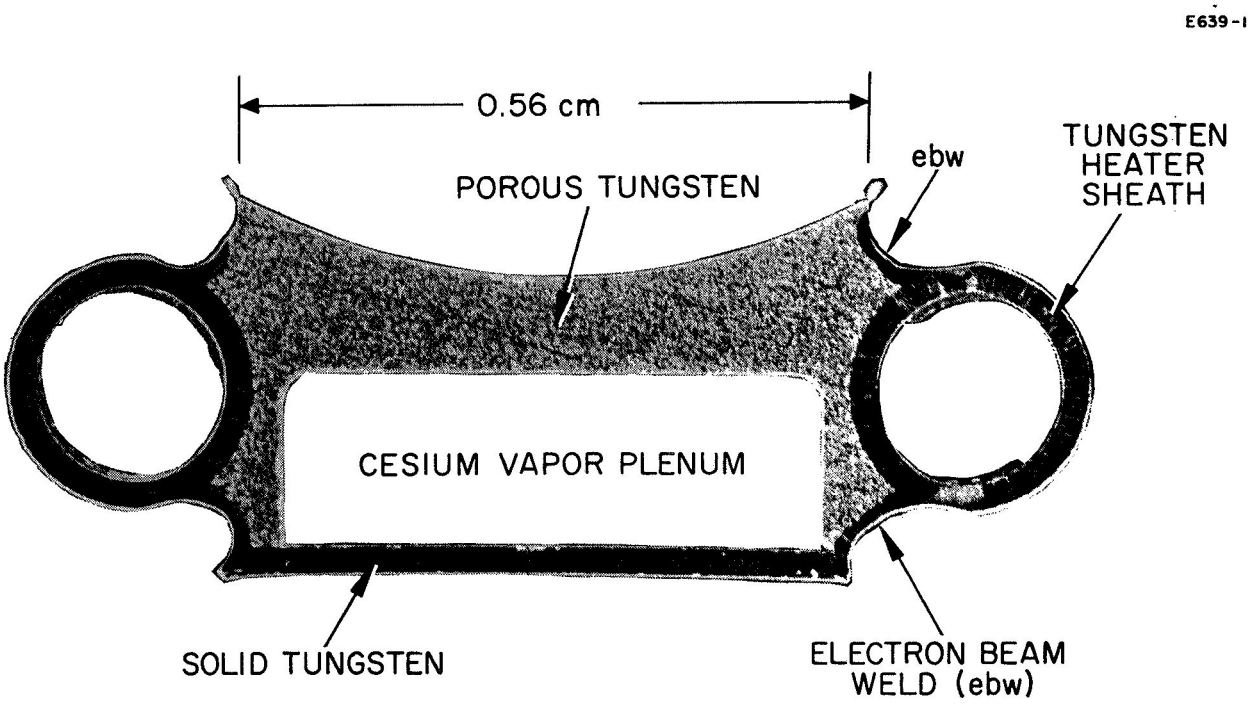

Fig. 6. Photograph of Low Mass Ionizer Cross Section.

M 4530

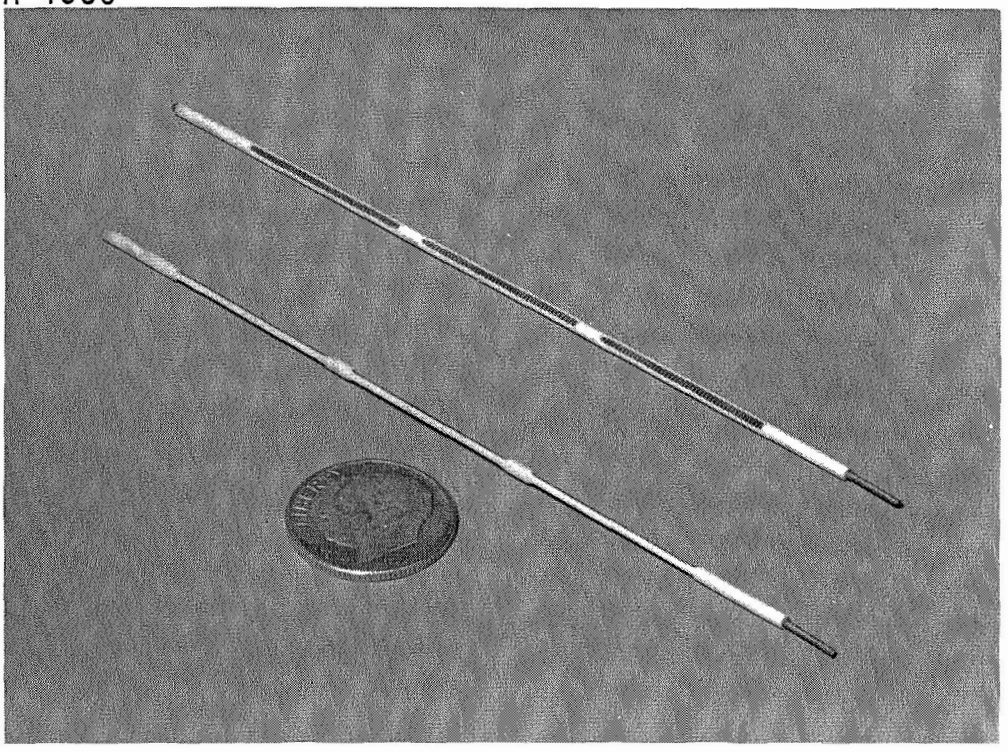

Fig. 7. Photograph of Two Low Mass Ionizer Heaters.

M 4429

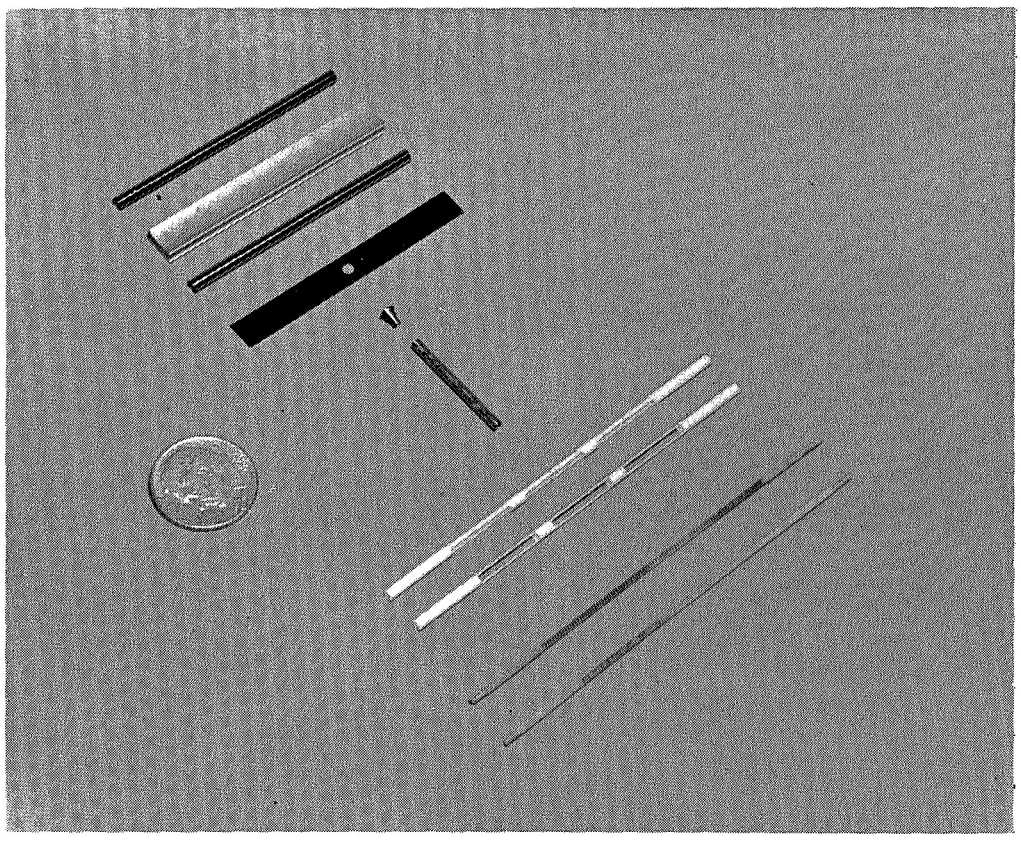

Fig. 8. Parts Comprising the Basic Elements of a Low Mass Ionizer.

M 3515

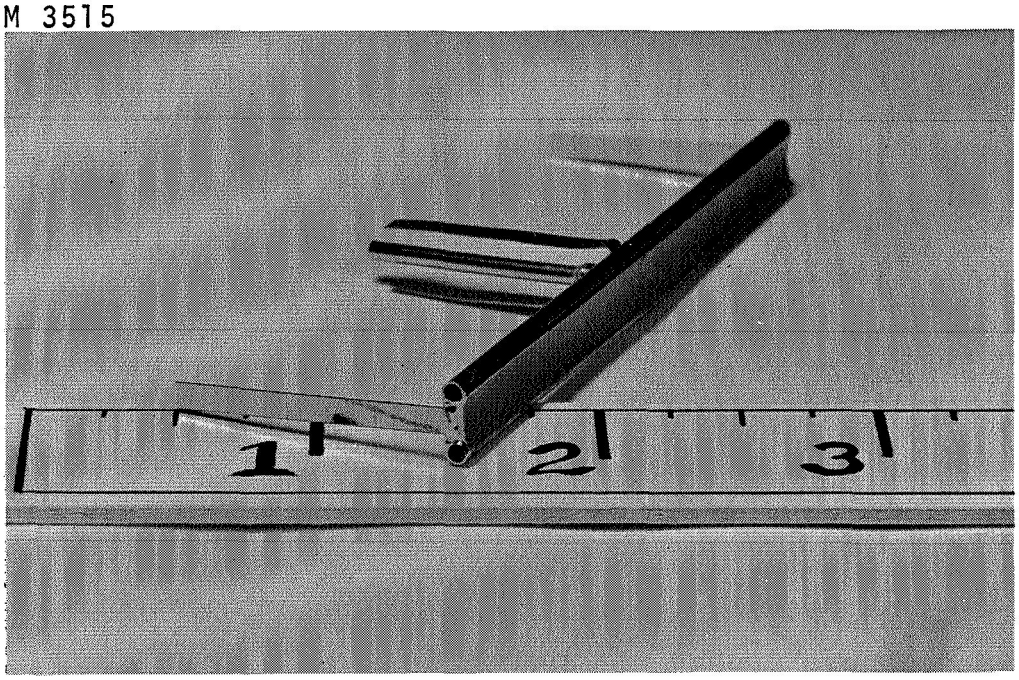

Fig. 9. Low Mass Ionizer Showing Heater Tubes, Manifold Plates, Support Straps, and Feed Tube, All Electron-Beam Welded to the Porous Emitter (Scale in Inches).

surface tension forces to a predetermined position, where local heat is applied for vaporization of the liquid cesium. The present state of the art for this type of system, including long term tests,[3-5] demonstrates long life and high propellant expulsion efficiency.

The four major elements of the system, are cesium storage, liquid-metal transfer, vaporization, and thermal valve.

1. Cesium Storage

Because of Hughes Research Laboratories' experience with propellant storage systems in which the cesium is stored as a liquid in a Feltmetal sponge for either vapor-transfer or capillary-type feed systems, the porous-metal storage approach was used. It is inherently reliable as a result of its simplicity. Figure 10 illustrates a reservoir made from the porous sponge material.

2. Liquid Metal Transfer

Surface tension pumping of the liquid cesium to the desired liquid vapor interface is achieved by gradation of the Feltmetal pore size. For a wetting liquid, the surface tension forces are in the decreasing pore size direction. Hughes Research Laboratories has developed a means of accurately controlling a continuous variation in pore size in Feltmetal sponges. The storage reservoir material is machined to an octagonal cross section and then subjected to a hydraulic pressing operation to achieve the required dimensions. This procedure results in a continuous decrease of the Feltmetal pore size from the outer periphery of the cylindrical storage sponge to the inner surface. Typical as-received densities for nickel Feltmetal were 12 to 13%. After selective

M 5329

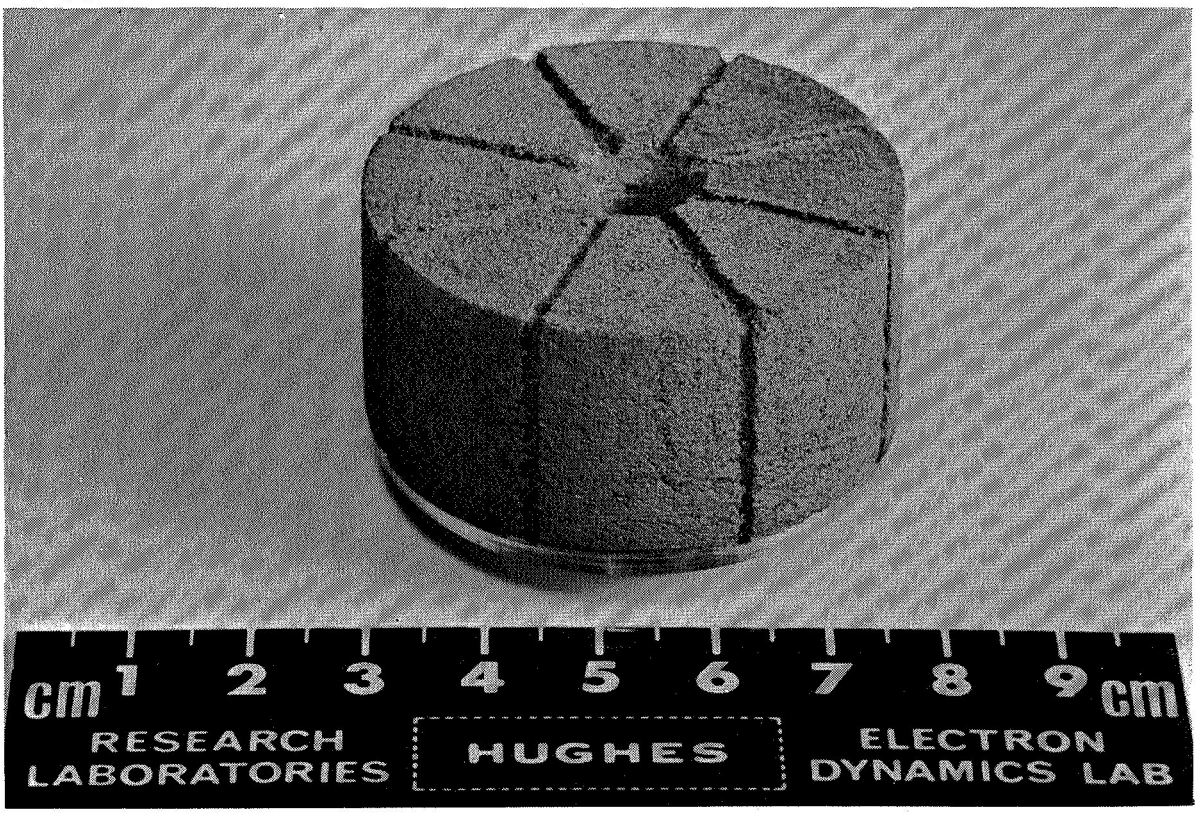

Fig. 10. Photograph of Nickel Feltmetal for Liquid Cesium Storage.

recompression to obtain the desired variation of pore size by the method outlined above, the completed reservoir fillers have a weight density of about 16% that of solid nickel. In practice, some of the pores in the Feltmetal are not interconnecting; therefore, in terms of liquid storage capabilities, the equivalent Feltmetal density is 20%. Figure 11 shows the variation in pore size from the central wick zone to the outer periphery of the storage material. This approach to the surface tension pumping of liquid cesium has demonstrated over-all high propellant expulsion efficiency. Experimental tests have shown that the propellant expulsion efficiency is >99%.

Wetting of the nickel by liquid cesium is vital to the successful operation of liquid-metal capillary type feed systems. Particular attention was given to cleaning procedures and preprocessing steps to provide porous nickel and other surfaces which are essentially free of surface contaminants. Our established and documented methods result in rapid wetting. In addition, cesium is a very good getter of oxygen, and any trace of oxygen remaining on the nickel surfaces is readily reduced by the cesium at temperatures on the order of 180 to 200°C.

3. Vaporizer

The cesium vaporizer is a small porous (80% dense) metal nickel wick that is inserted through the center of the storage medium. Feltmetal wick densities of 80% have good performance results in capillary-type feed systems used at Hughes Research Laboratories.

Figure 12 shows the results of an analysis in which capillary pressure was calculated; the results indicate that stable operation, using surface tension forces as the

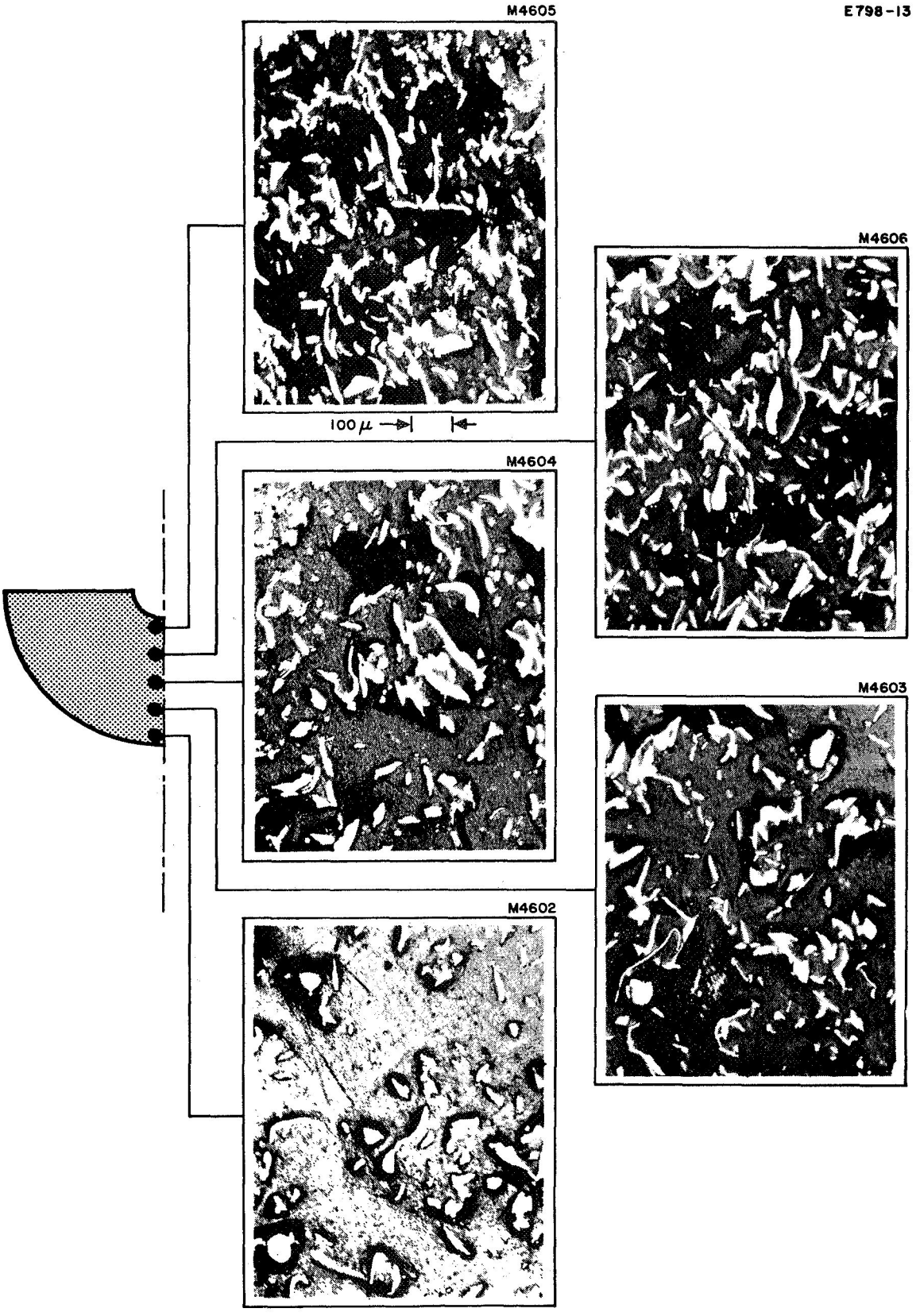

Fig. 11. Photomicrographs of a Graded-Pore Feltmetal Reservoir.

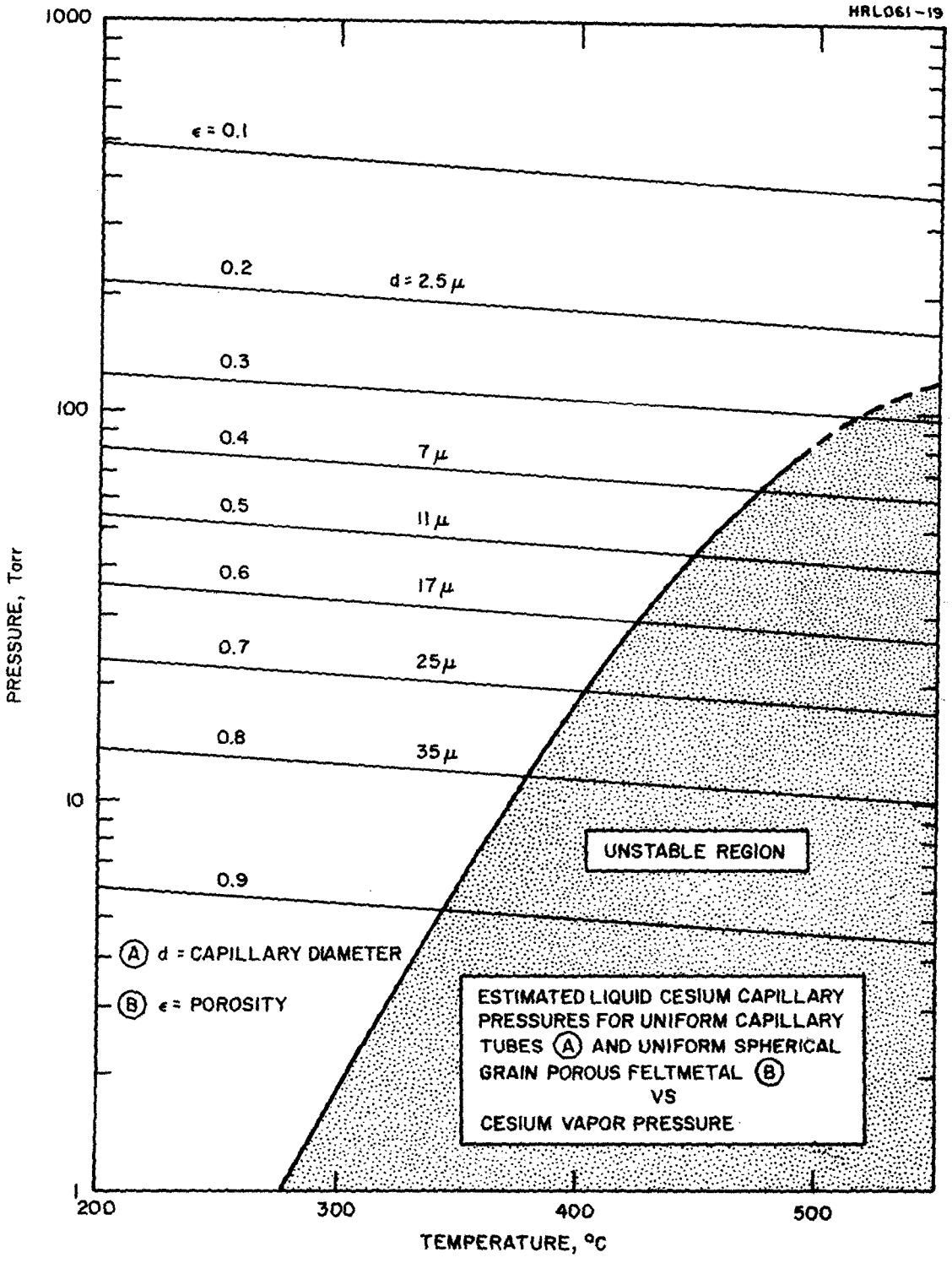

Fig. 12. Approximate Liquid Cesium Capillary Pressures for Uniform Tubes and For Uniform Spherical Grain Porous Nickel.

driving mechanism, is obtainable over a wide range of temperature, pressure, and pore size conditions.[6] This analysis is conservative in the sense that the contact angle between the liquid cesium and the nickel was assumed to be 30°. Contact angles approaching 0° are realizable with the liquid cesium-nickel system when oxygen impurities are removed. As shown in Fig. 12, the liquid cesium in an 80% dense Feltmetal wick develops a capillary pressure in excess of 180 Torr at the liquid-vapor interface for a temperature of 380°C. (This corresponds to a cesium vapor pressure of 10 Torr.) Therefore, the liquid-vapor interface could not move upstream in the wick until operating temperatures in excess of 550°C were reached.

Control of the liquid vapor interface position is essential for successful repeatable operation of a capillary-type feed system. A typical capillary tube with a wetting liquid such as cesium is shown schematically in Fig. 13. Flow of the liquid is in the direction of the capillary force until a discontinuity is encountered. For a wetting fluid, the discontinuity is typically a sudden enlargement, as shown on the right side of Fig. 13. Any increase in upstream pressure which overcomes the surface tension force will lead to breakaway of the column of liquid from the liquid-vapor interface. If the liquid cesium is forced to the right until the interface enters the small tube, the desired interface surface could not readily restore itself. Instead, the liquid would continue to flow to the right as a result of capillary forces, if the radius of the free liquid surface within the reservoir were larger than the tube radius on the right.

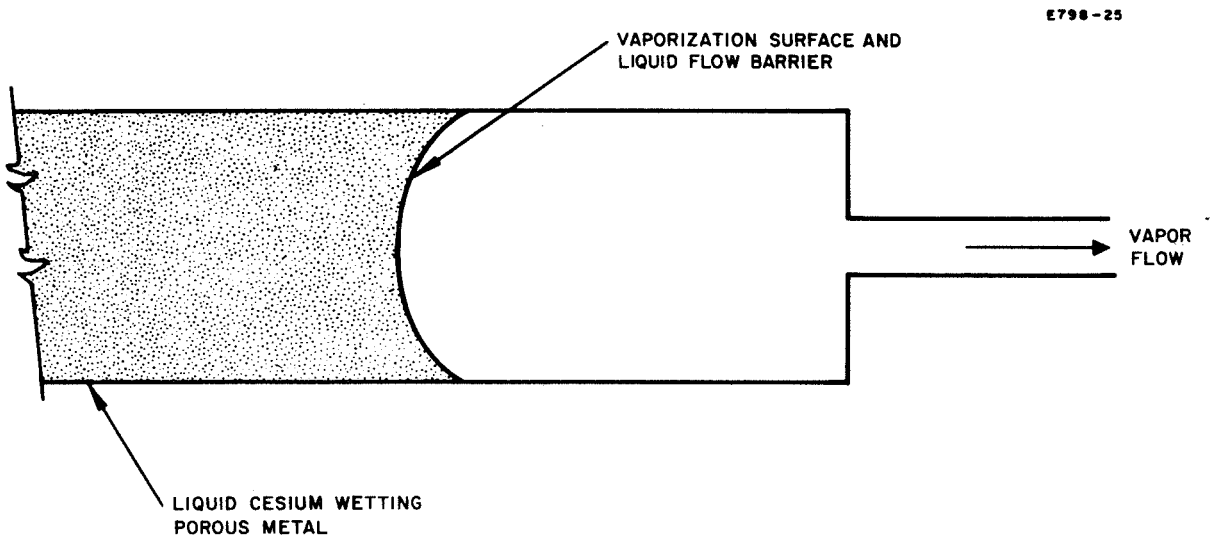

Fig. 13. Schematic Diagram of Wetting Fluid in a Capillary Tube and Downstream Region Typical for Ion Engines.

In this type of feed system design, Hughes Research Laboratories has taken two steps to avoid or overcome this cesium liquid breakaway situation. First, the porous Feltmetal used as a sponge has a maximum average pore radius of approximately 35 μm. In the ion thruster design no capillary or tubing exists on the downstream side of the vaporizer with a dimension approaching this small value. Therefore, if liquid cesium breakaway occurs, forcing liquid downstream from the end of the wick, the surface will restore itself as a result of the reversed surface tension forces. In addition, a "liquid metal trap" was incorporated immediately downstream from the vaporizer wick end. This trap consists of an in-line metallic insert (item (E), Fig. 14), shaped to provide conical surfaces where any liquid cesium which breaks away from the wick will condense and be retained in a minimum free surface energy condition (point I in Fig. 14). The insert has a hole with a conical shape (point II, Fig. 14)

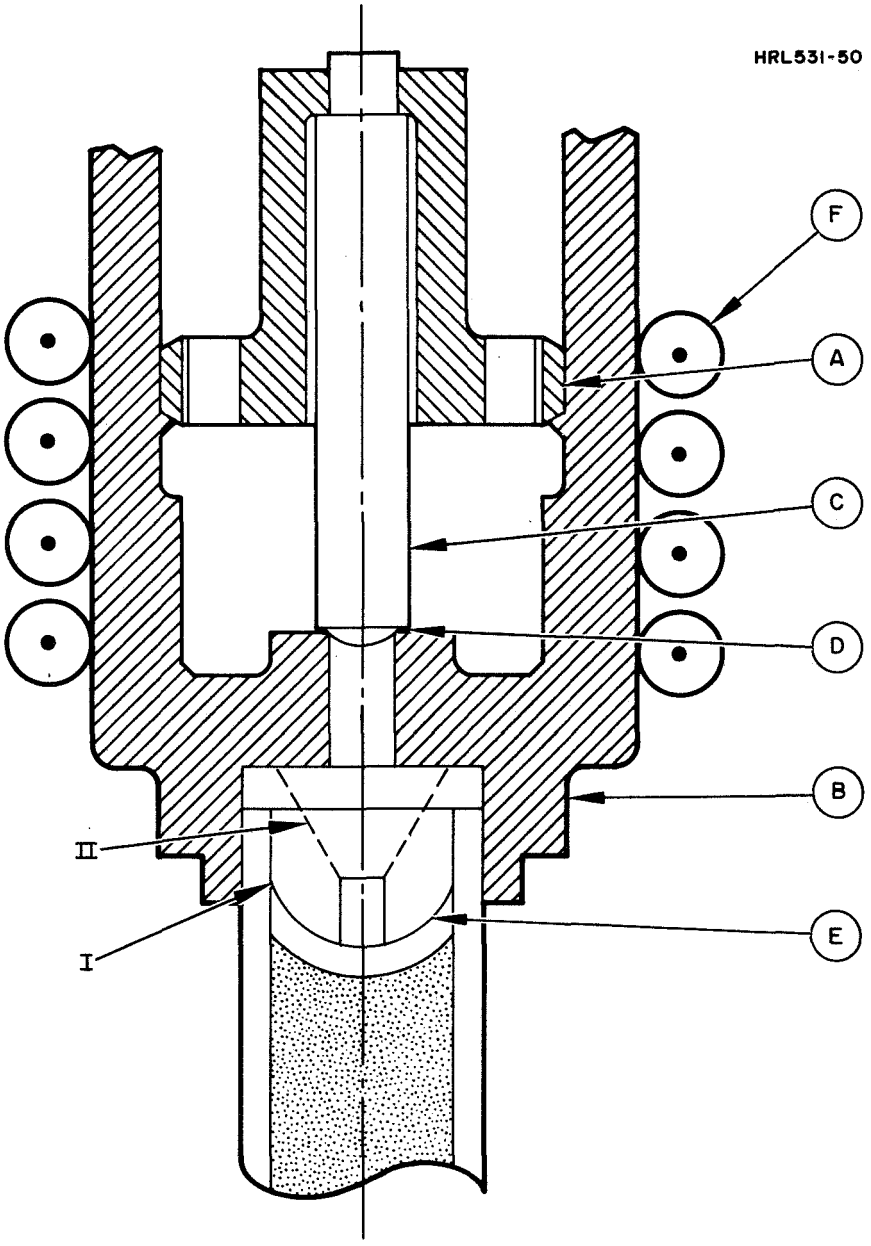

Fig. 14. Cross-Sectional Drawing of the Bi-metal Valve and Vaporizer Section.

on the downstream side so any liquid cesium coming through the hole will collect and form a minimum free energy surface in this region also. Thus, if cesium droplets break away from the end of the wick, the liquid metal trap provides a twofold passive safety feature. In such an event, the cesium vapor to the ionizer still will originate in a region very close to the wick.

4. Thermal Valve

The feed system design also incorporates a thermal valve in the downstream exit region of the cesium feed system. Inclusion of this valve results in a number of significant system advantages which increase the over-all reliability of the ion propulsion system. Specific advantages of this bimetal valvular element are the following: (1) operational test of an actual flight propulsion system can be carried out on-board the actual spacecraft during thermal-vacuum qualification tests, without the necessity for removing and/or reloading the ion propulsion system; (2) the valve provides a hard vacuum seal, and therefore prevents oxidation of cesium during long term storage; and (3) the valve response time is sufficiently fast to shut off the cesium vapor flow in the event of an unexpected total power failure in the propulsion system.

The bimetallic valvular element used in a typical feed system is shown in Fig. 14. The valve operates according to the following principles: Activation of the vaporizer heater F raises the temperature of the housing B, which causes the plunger to lift because of the difference of the coefficients of expansion of the Kovar plunger and stainless parts A and B. The plunger C is preloaded by the screw adjustment A which supplies seating pressure to the ball

D on the valve seat. As the preload element C is displaced due to an increase in temperature, the Kovar plunger moves the ball to open the valve.

The valve may be set to open at any desired temperature, by adjustment of the threaded disk A. Repeatable valve opening and closing temperatures have been demonstrated experimentally over the range of 125 to 400°C.

The liquid metal trap that was discussed earlier is located between the valve and the vaporizer face. When the thruster restarts, any entrapped liquid will be near the heater H and will vaporize before the cesium at the wick surface. Any small amounts of liquid cesium downstream from the vaporizer thus can be trapped and removed (by vaporization) before they reach the ionizer feed tube. Figure 15 shows a schematic of the feed system as used on each strip.

C. SUPPORT STRUCTURES

The main support structure of the thruster is an aluminum frame (item (7) in Fig. 1). The feed system is supported from this frame in three places. A typical support subassembly of the feed system is comprised of two mating insulators and shields. These are held in compression with a bolt, nut, and washer ((23) , (26) , and (29) in Fig. 1) The ceramic is alumina and provides an electrical isolation for the beam voltage of 2 kV. The focus electrode of the ionizer assembly and exit electrode are supported by common subassemblies. One subassembly is visible to the left of the ionizer; there are three such assemblies for each strip. The exit electrode is made electrically common to the support structure by the bolt and nut that holds the insulators and shields

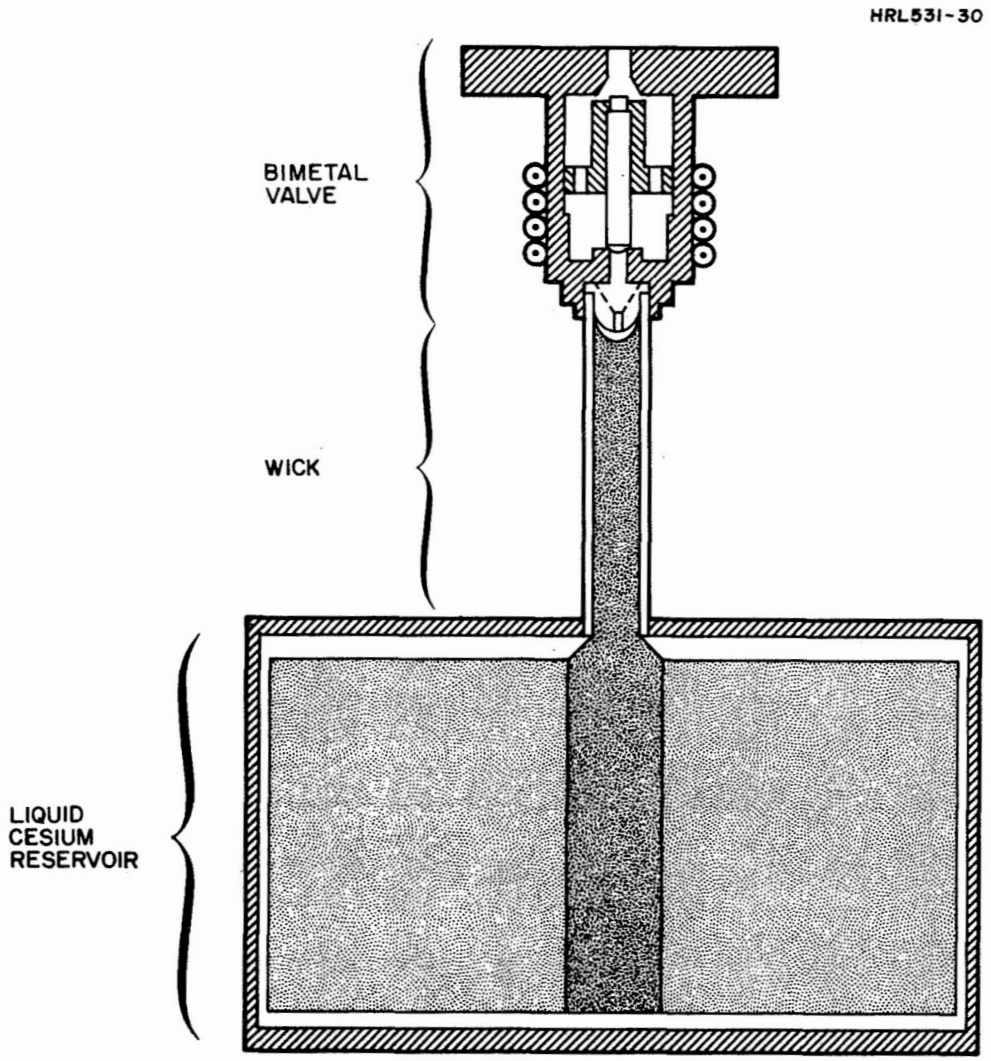

Fig. 15. Schematic of Reservoir, Vaporizer, and Valve Integration.

together. The focus electrode is midway between the main support structure and exit electrode and is electrically isolated from them by alumina ceramics. As in the case of the feed system insulators, these insulators also stand off the beam voltage of 2 kV. Each strip has two accel electrodes which are shaped alike but are electrically isolated from one another. This permits bias voltages to be applied to them for beam deflection. The accel electrodes are mounted from the exit electrodes with insulators, labeled (13), (24), and (28) in Fig. 1. Each accel is supported in two places. The accel electrodes are copper and stainless steel. The electrode surfaces near the ionizer are copper pieces that are brazed on the stainless steel that provides a rugged support. The actual design of the focusing and deflecting part of the accel electrode is presented in more detail in Section III-D.

The neutralizers are 0.002 in. diameter thoriated-tungsten wire. Each strip has two neutralizers which are mounted to, but electrically isolated from, the exit electrode. This can be seen on each side of the strips in Fig. 4. The dimensions and processing used on the neutralizers are presented in Section IV.

Electrical terminals are attached to the main structure. These serve as the points for leads from components of thrusters such as leads to accel electrode, neutralizer, and vaporizer. A rear view photograph in Fig. 16 shows these terminals on the support structure around the cesium reservoirs.

M 7617

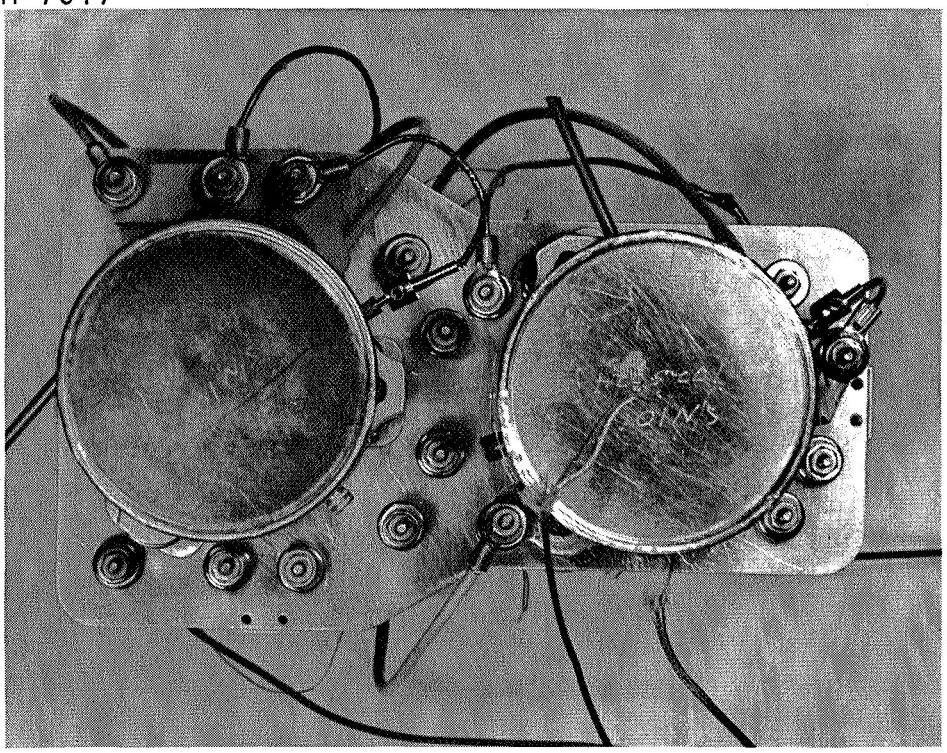

Fig. 16. Photograph of Rear View of Dual Beam Thruster System.

D. OPTICS DESIGN

The objectives of this task were to design the deflection optics for the strip engine to produce a ±30° deflection angle with minimum deflection voltage while maintaining good ion optics (i.e, very low direct interception). It is important to minimize the deflection voltage, which also minimizes the ionizer current density variations and direct interception. For all these investigations, the basic extraction geometry (emitter focus to upstream accel) was the Model 70 optics which has been studied previously both in the trajectory tracer and experimental thrusters. The deflection optics design was accomplished by digital computer

simulations in which a number of iterations were required to arrive at the final optimized design. The areas investigated with the digital computer were (1) deflectable geometry, (2) partial space charge operations, (3) ionizer neutral flow distributions, and (4) the shape and position of the downstream boundary. Ion trajectories, including space charge, were computed and plotted each of the geometries, and the average deflection angle was computed for each of these cases. In addition to the digital computer investigations, the deep electrolytic tank was used to design end effect electrodes for the final geometry.

1. Geometry Investigation

All the geometries studied were configurations in which a segmented accel serves as the deflecting structure. Although this method has the advantage of simplicity, it produces a nonuniform gradient at the emitter, thus producing a variation in current density capability across the ionizer. The actual dependence of the current density variations on the transverse voltage is minimized by a high deflection sensitivity. An alternative method of beam deflection not used here, is downstream deflection of the accel electrode, with either a segmented decel electrode, or with an electrode intermediate between the accel and decel electrode. These methods have the advantage because the ionizer is shielded from the deflecting fields, and the deflection takes place in a region of lower axial velocity where the deflection sensitivity is greater. However, the effect of a transverse field on the neutralizer electrons is a problem that must be resolved experimentally before the method can be considered practical. Another problem of the post accel deflection

is that space charge expansion produces a broader beam near the decel, requiring wider deflection plates (lower sensitivity), to prevent direct interception.

The basic deflection geometry investigated using the digital computer is shown in Fig. 17. The distance a is fixed since Model 70 optics were maintained for all cases. The two variables we have at our disposal are the taper ratio m = c/a, and the normalized deflection length L = b/a. Simple theory for the deflection angle of tapered plate geometry has been determined[7] showing that

$$\tan \theta = \frac{1}{2} \; L \left(\frac{2 \; \Delta V}{V_o} \right) \; \frac{\ln m}{m - 1} \quad . \tag{1}$$

Derivation of this formula assumes, (1) no space charge, (2) constant axial velocity (e.g., no decel), and (3) parallel incidence. Since none of these assumptions are satisfied, we would not expect this formula to be quantitatively correct, though qualitatively we would expect the deflection sensitivity to increase with increasing L and decreasing m. Digital computer trajectories were run for three different geometries. The first two geometries had a normalized length of L = 1.2 with taper ratios of m = 3.06 (Case I) and m = 1.6 (Case II) while the final geometry (Case III) had a normalized length of 1.7 with the same taper angle as Case II. The computer generated trajectories showed that all three geometries produced well-focused beams with no direct interception. Each of these geometries were run with a number of deflecting voltages to determine the dependence of the average deflection angle on the normalized deflection voltage $(2 \; \Delta V)/V_a$. The average deflection angle for each run was computed as follows:

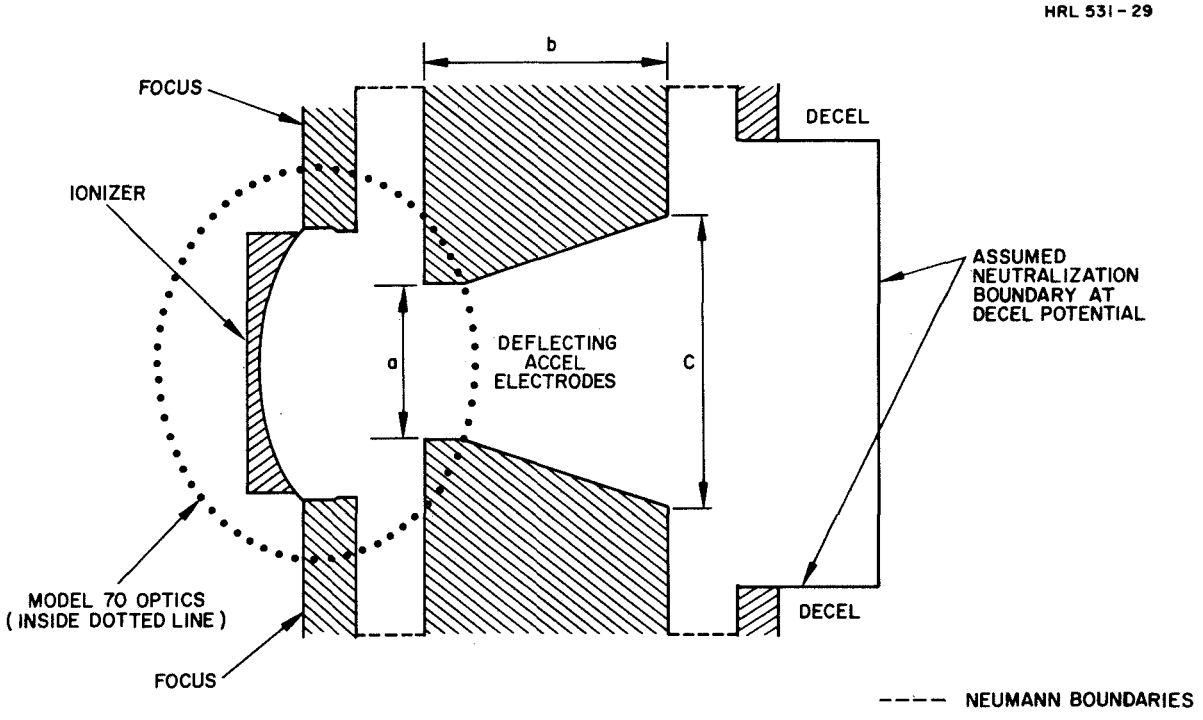

Fig. 17. Basic Deflection Geometry.

$$\theta_{avg} = \frac{\sum_{i=1}^{27} I_i \theta_i}{\sum_{i=1}^{27} I}$$

This method weights each of the 27 computed trajectories according to the current of each ray times its deflection angle in order to give a quantitative measure of the actual transverse thrust. Empirically, these calculations showed the average deflection angle, computed in the manner described above, was for most cases, about 10% lower than the deflection computed for the central ray. For all the cases it was found the deflection angle was a linear function of the deflection voltage. A summary of the digital computer geometry investigation is listed below. In this listing the deflection sensitivities are normalized with respect to the value obtained for the Case III geometry.

Summary of Digital Computer Geometry Investigations

Geometry	Normalized Length, L = b/a	Taper Ratio, m = c/a	Normalized Deflection Sensitivity
Case I	1.2	3.06	0.54
Case II	1.2	1.6	0.65
Case III	1.7	1.93	1

It is seen that the deflection sensitivity for Case II is approximately 20% higher than Case I, because the narrower taper produces a stronger transverse field for

a given normalized deflection voltage. However, the increase is not proportional to ln m/(m - 1) as eq. (1) predicts, because as the taper ratio increases, the decel field penetrates farther upstream into the deflecting region producing a lower axial velocity. This tends to increase the deflection sensitivity while the weaker transverse field from the increasing taper ratio decreases the deflection sensitivity. As a result, the deflection sensitivity is a weaker function of the taper ratio than predicted in eq. (1). Thus, eq. (1) would predict that deflection sensitivity would increase ∿60%, going from the wide to narrow taper, while the actual increase was only ∿20%. The listing also shows the effect of changing the deflection length while keeping the taper angle constant. It is seen the deflection sensitivity has increased ∿54% going from the Case II to the Case III geometry which approximates the increase in normalized deflection lengths ∿42%. The Case III geometry was chosen for the final design because it was believed any increase in deflection sensitivity resulting from a longer deflection region or a narrower taper would produce trajectories which would come too close to the decel electrode. Figure 18 shows the computed trajectories for the Case III geometry with full space charge.

2. Effect of Partial Space Charge

For all the cases considered so far, the trajectories were calculated for the full space charge condition. In these cases the currents were calculated assuming space charge limited current conditions at the emitter. This implicity assumes the operating point occurs on the space charge limited perveance line and the neutral flow distribution across the ionizer matches the space charge limited current capability of the optics. However, in actual practice the engine is operated flow limited, it was necessary

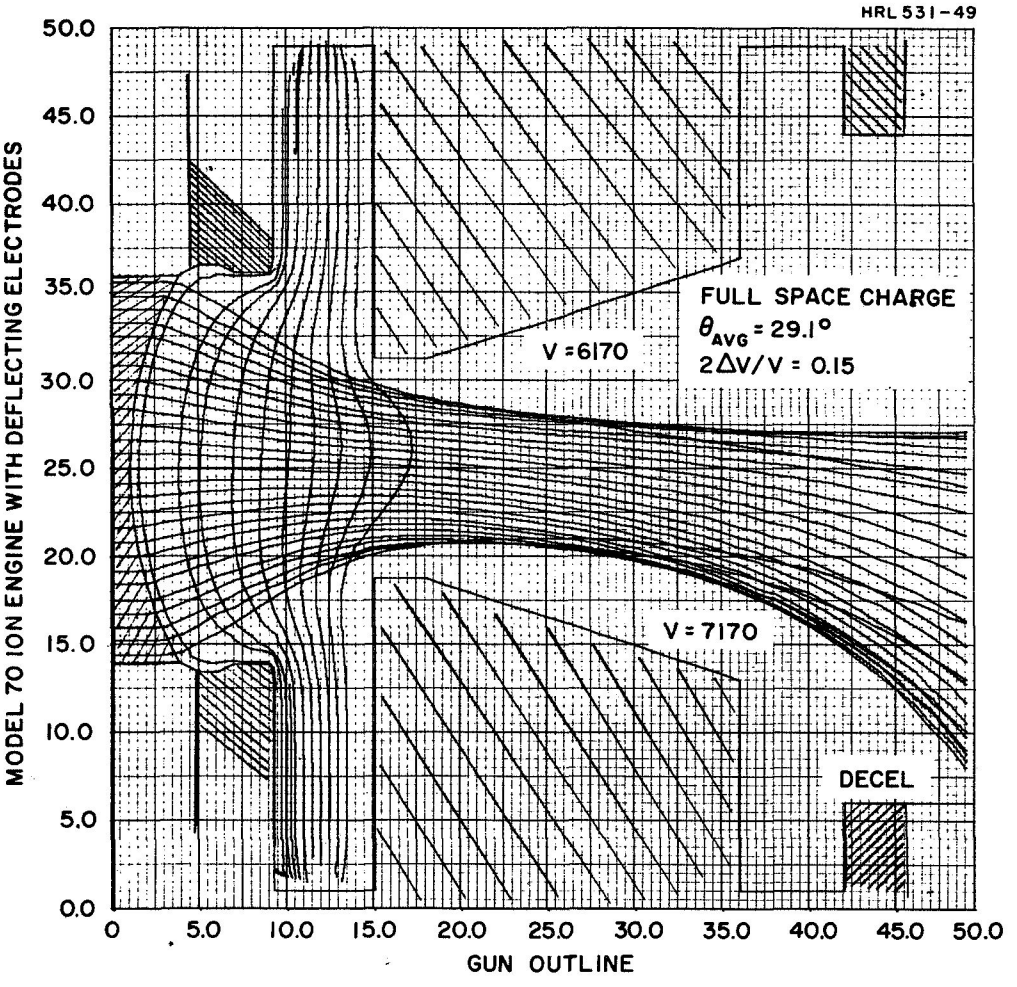

Fig. 18. Computer Generated Trajectories for Case III Geometry.

to determine that the computed deflection angle and trajectories for the partial space charge condition were not appreciably different from the full space charge conditions. To produce a large effect, the space charge limited currents were multiplied by 1/20 and the program was rerun with the Case III geometry. In this case the appearance of the trajectories is quite different (see Fig. 19) because the beam has nearly "collapsed" because of the absence of any appreciable space charge forces. The computed deflection angle for this case showed there was a 25% decrease in the deflection angle compared with the full space charge value. Extrapolating this extreme case to the 25% thrust value ($\sim$1/5 space charge) would predict a 1/4 x 25% $\simeq$ 6% decrease in deflection angle (i.e., decreasing from the 100% thrust level to the 25% thrust level). This reduction in deflection sensitivity for partial space charge operation is inevitable because of the nature of deflecting fields. Figure 20 shows a plot of the potential versus radius at a representative cross section in the deflection region. This figure shows that the slope of this curve increases in either direction away from the centerline. Because the transverse force is proportional to the slope of this curve the partial space charge cases, which have a larger percentage of the current in the central region, will not be deflected as much as the full space charge cases which utilize the region closer to the deflecting electrodes where the transverse gradient is higher.

3. Ionizer Neutral Flow Distribution

An ideal ionizer would have a neutral flow distribution which exactly matched the current capability of the optics. For the Model 70 optics, Fig. 21 shows the digital computer

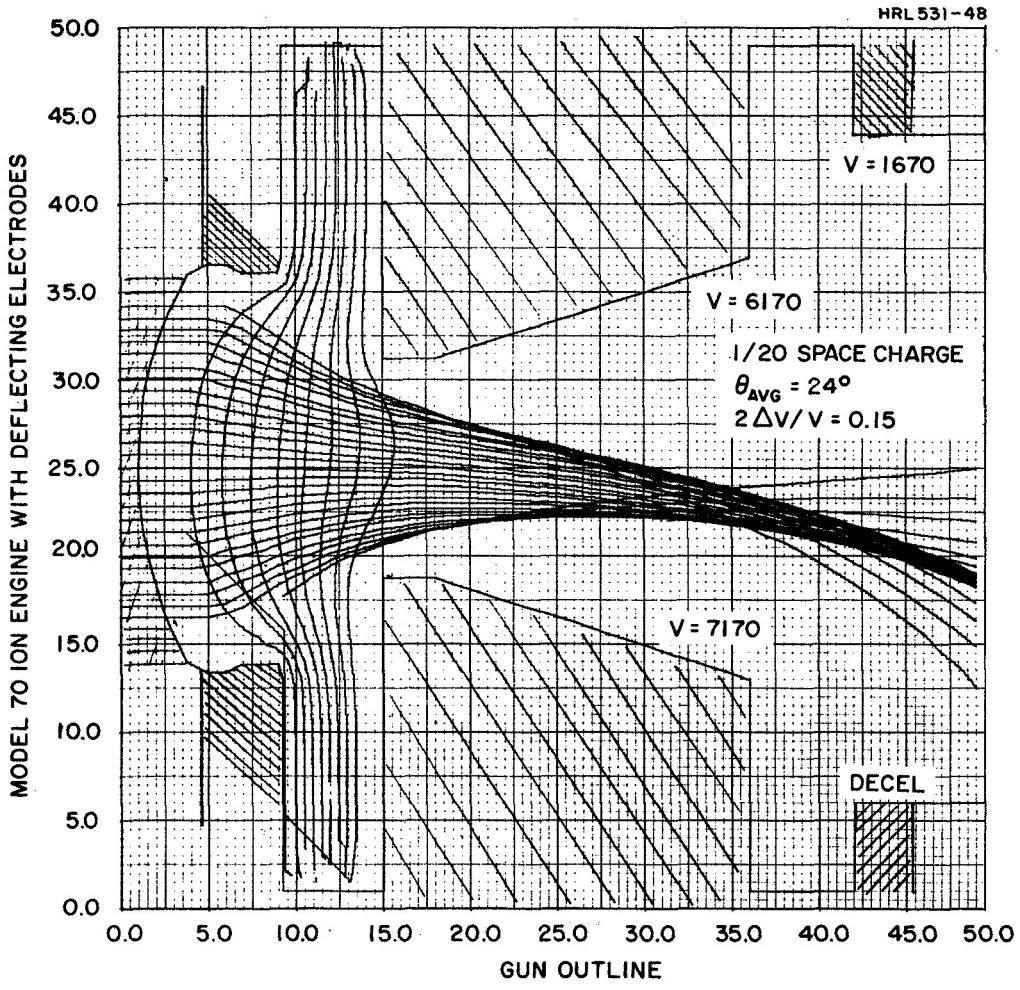

Fig. 19. Computer Generated Trajectories for Case III Geometry with Neglgible Space Charge.

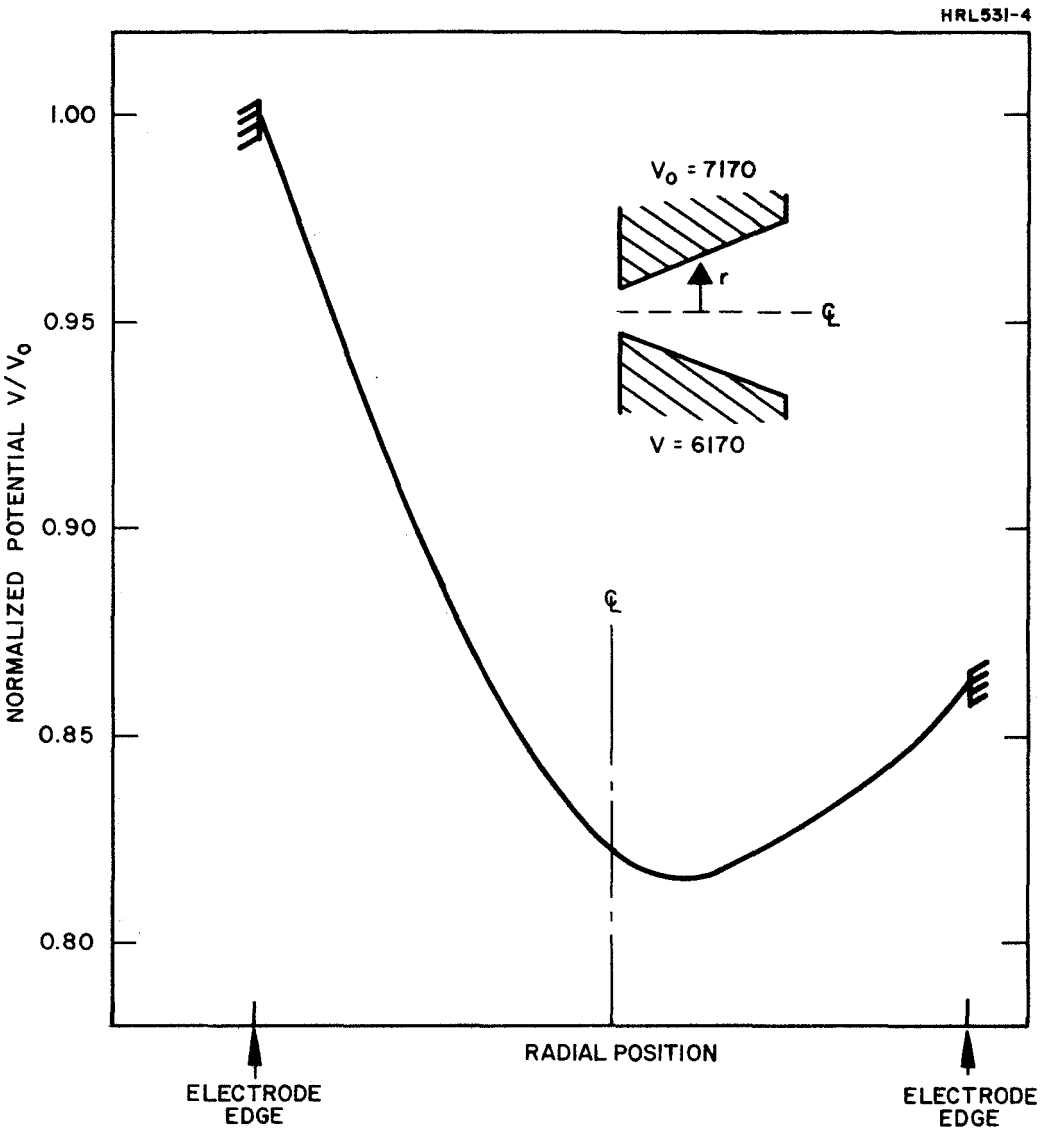

Fig. 20. Normalized Potential Versus Radius at Midpoint of Deflection Region.

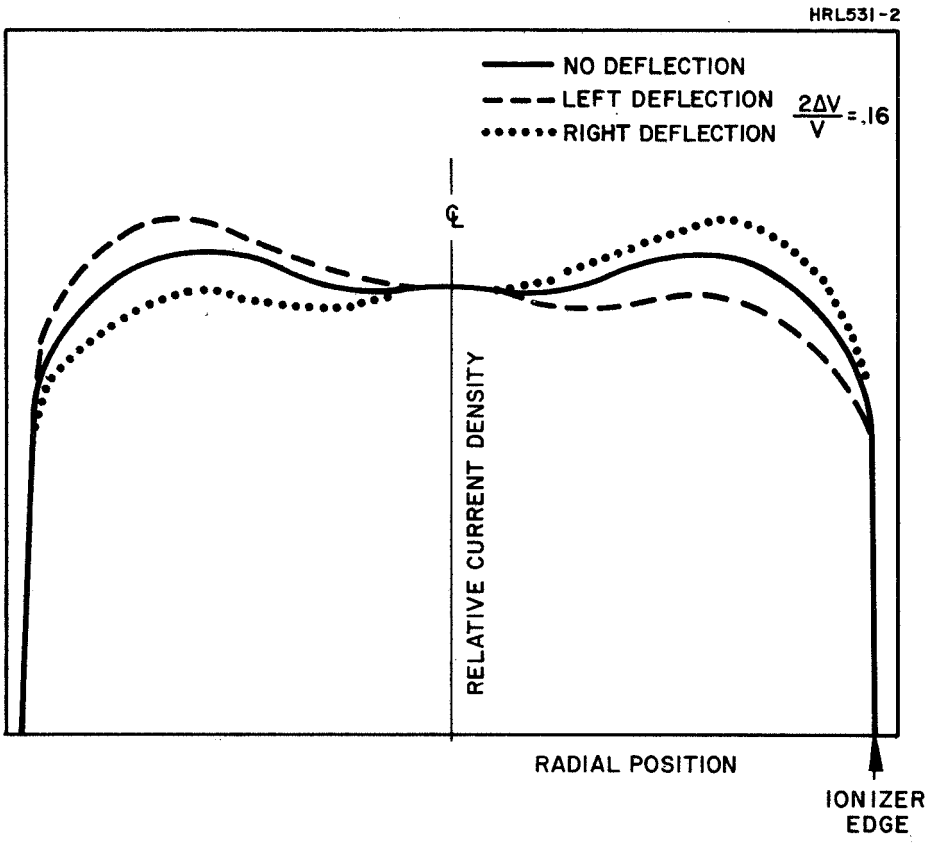

Fig. 21. Computed Ionizer Current Density Capability for Model 70 Optics with no Deflection, Left Deflection, and Right Deflection for a Normalized Deflection Voltage of 0.16.

calculation of the variation in the space charge limited current capability of the optics for no deflection, left deflection, and right deflection for a normalized deflection voltage of 2 $\Delta V/V = 0.16$ and a total (average) voltage of 6.67 kV. The undeflected case produces a substantially uniform distribution, while the deflected cases produce distributions which are tilted about the center of the undeflected case in a direction toward the high voltage side. The amount of this tilt is approximately equal to the normalized deflection voltage ($\sim$16%). An ideal neutral flow distribution would exactly match the current capability of the optics for all the cases and is obviously impossible. The optimum physically realizable distribution would be a neutral flow, symmetric about the centerline, which matched the lowest combination of the three curves and is the composite distribution consisting of the two low voltage sides, of the deflected distributions. This ideal composite distribution is also substantially uniform with a very slight peak in the center. If this ideal distribution could be closely approximated, the engine could be operated in the flow limited regime a very slight distance to the right of the perveance curve, and there would be little "rounding" as the transition from space charge limited to flow limited operation took place. In this case the total current handling capability of the optics could be achieved with the minimum possible voltage. In actual practice there is considerable rounding of the perveance curve because there is not a perfect match between the current handling capability (which is substantially uniform), and the neutral cesium arrival rate. The present ionizer has a flat upstream side so the center thickness is a minimum. The resulting neutral flow distribution is, therefore, peaked at the center, and thus requires a higher voltage to achieve flow limited operation at the center

than at the edges. The exact neutral flow distribution is determined by a nonlinear differential equation, describing molecular flow through an assemblage of capillaries. In each of these capillaries, Knudsen flow occurs[8] and is too complicated to justify an attempt at an analytical solution. An estimate of how "peaked" the neutral flow distribution actually is in an operating engine, was obtained by trial and error methods of assuming a neutral flow distribution, and integrating to find the total current under the trial curve for a given peak amplitude. By comparing this current with the theoretical space charge limited current (see Fig. 21) having the same peak amplitude in the center, an estimate was obtained of how far to the right of the perveance curve it would be necessary to operate to achieve flow limited operation for the trial neutral flow distribution. By iterating the trial neutral distributions, a distribution was found which would produce an operating point which agreed with the experimentally measured break point occurring to the right of the space charge limited perveance curve. Figure 22 shows the neutral distribution obtained by this trial and error method for the 100% (18 mA) thrust level. The distribution is quite peaked, having a peak-to-edge current density of approximately three to one. When this distribution was run with the digital computer program it was found there was a reduction of only about 1° for the computed value of the average deflection angle, compared to the full space charge case. Thus, from this study it was concluded that the neutral flow distribution produced only a second-order effect on the computed deflection angle.

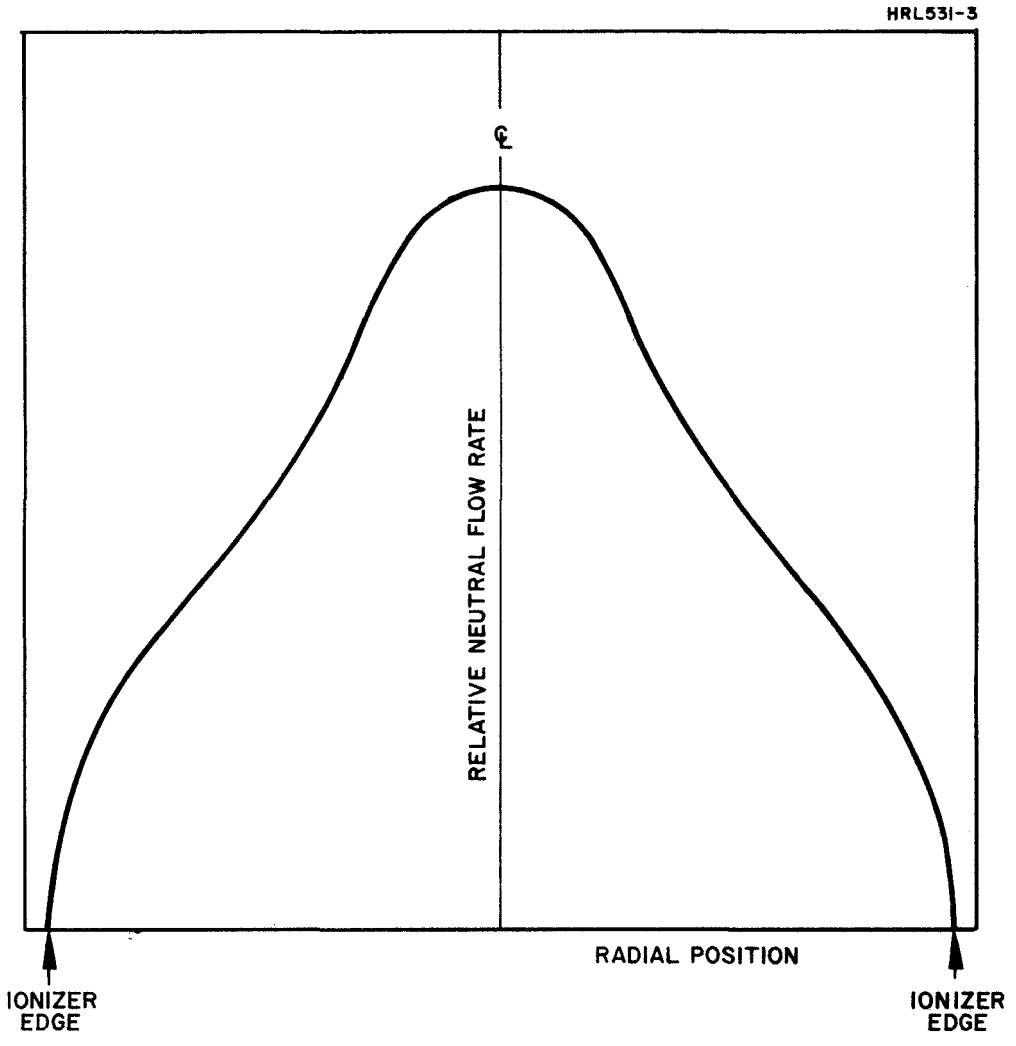

Fig. 22. Neutral Flow Distribution which Produces Experimentally Observed Operating Point on Perveance Curve for 100% Thrust Level.

4. Shape and Position of Downstream Boundary

The other remaining area investigated was the position of the downstream boundary at decel (ground potential). All the previous cases used a downstream boundary as shown in Fig. 17. In actual operation this boundary is the plasma "meniscus" which separates the pure ion flow from the downstream neutralized plasma, where ideally the ions travel in straight lines since this is a field free region. A completely rigorous treatment would require this boundary to be located self-consistently with the ion flow. This would require a considerable number of iterations to find a boundary where the normal gradient was zero, and on which the potential was a constant equal to the plasma potential, which is typically a few volts positive with respect to the grounded decel to trap the neutralizing electrons.

Because of time limitations this was not done but a number of downstream boundaries were tried to see how sensitive the computed deflection angle was to the shape and position of the boundary. All these cases used ionizer currents computed for the 100% thrust level with the peaked neutral distribution discussed in the previous section.

These studies indicated that the position of the downstream plasma meniscus was more important than its shape in determining the average deflection angle. By running a number of cases in which the simulated plasma meniscus was a straight boundary at decel potential, separated from the actual decel electrode by Neumann boundaries on the two axes of symmetry, it was found the computed deflection angle initially decreased then stabilized at a constant value as this boundary was moved downstream from the position shown in Fig. 17. The trajectories for the final iteration of this procedure are shown in Fig. 23 which predicts a nominal 20° average deflection for a normalized deflection voltage of 0.15.

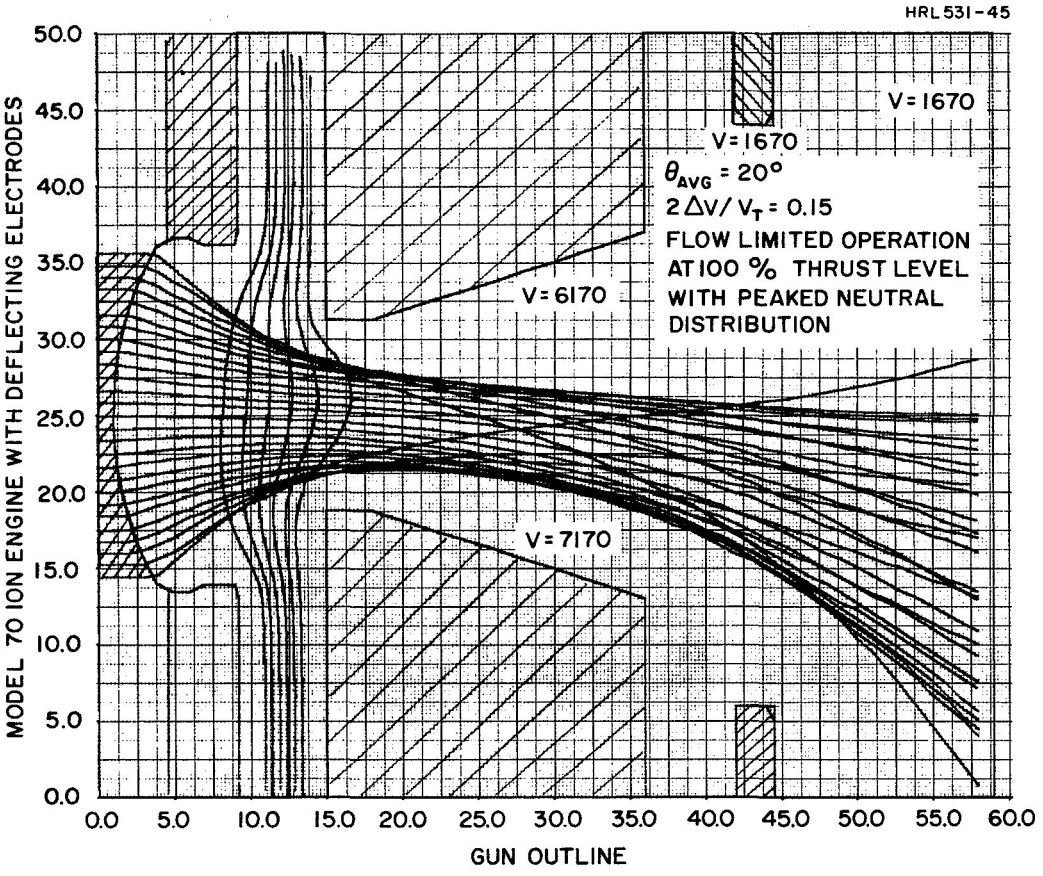

Fig. 23. Computer Generated Trajectories for Case III-a Geometry with Downstream Neutralization Plane at z = 59.

5. End Effects Design

The digital computer studies discussed previously, analyzed the flow of ions in a representative cross section of the beam which was assumed to be infinite in length. In actual practice, the strips terminate, making it necessary for the ion optical design to properly focus the ions at the end of the ionizer. Before this study was begun, it was not known whether the segmented accel required for beam deflection would be a problem area. Therefore, the electrolytic tank was used to investigate the end effects problem for the final design derived from the ditial computer studies. The basic idea used in this study was the same as that used by Kramer and Todd[9] for the undeflected strip optics. This method is to first design the two dimensional electrode shapes (for use along the length of the beam), including space charge, either in the electrolytic tank or with the digital computer. When the design is complete a potential plot is taken on the central plane of the gun. A model of the end of the gun is then placed in an electrolytic tank and the central plane potential is matched along the simulated end beam boundary by a modified Pierce technique used by Brewer[10] and described by Gallagher.[11] This approach cancels any transverse electric field at the beam end so it may pass through the engine without hitting any electrodes. Figure 24 shows the electrolytic tank setup used to design end effect electrodes for the strip ion beam with deflecting accel electrodes. Because of the lack of any symmetry plane when deflection voltage is ,applied, it was necessary to use the deep tank and model the complete end effect electrode geometry rather than using a wedge section as described in Ref. 9. This required the construction of a special probe which could measure potentials below the surface of

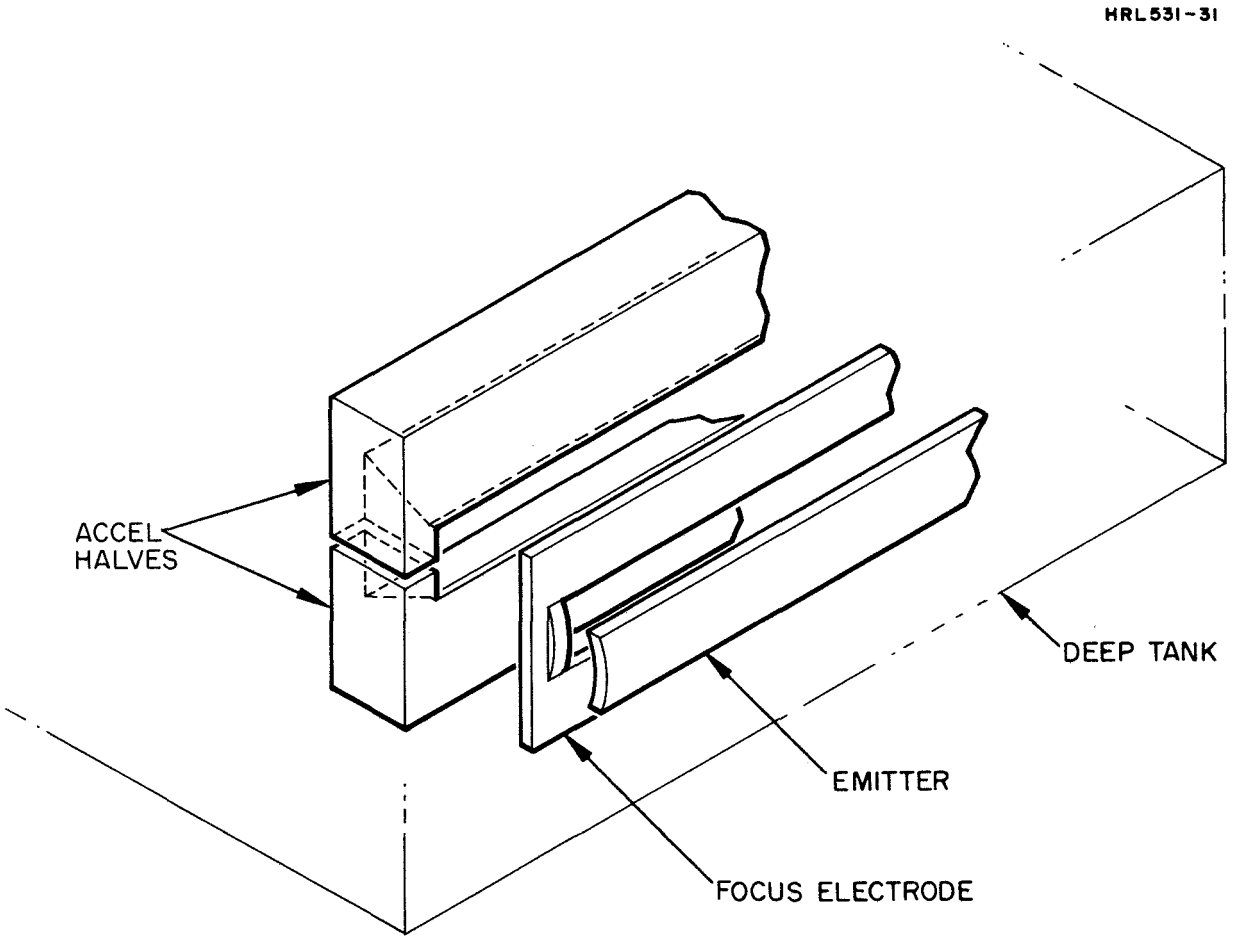

Fig. 24. Electrolytic Tank Setup Used for End Effects Study.

the water. The results of the potential measurements from this study (Fig. 25) show the potential calculated in the central plane by the digital computer along with the potentials measured in the electrolytic tank for different focus-emitter distances at the beam end. This figure shows how a focus too close to the emitter causes the potential at the beam edge to be too low, while the reverse is true when the focus is too far away. Reference 11 has shown that for cylindrical beams, when the potential along the beam boundary is too low, the beam is compressed or overfocused while it diverges for the opposite case. Figure 25 also shows that at intermediate distances a very good potential match is obtained showing that the segmented accel design can be employed with no harmful ion optical effects. The optimum distance of 0.0445 in between the focus and emitter was found from this study and was incorporated in the final design.

6. Comparison of Theory and Experiment

Table I summarizes the main conclusions predicted by the computer modeling and the experimental observations. As indicated in the table there is good agreement between theory and experiment. The difference between the measured and calculated values for the deflection sensitivity are within the experimental measurement errors.

E. VIBRATIONAL ANSLYSIS

The original vibrational environment specified in this program for the dual beam thruster system follows.

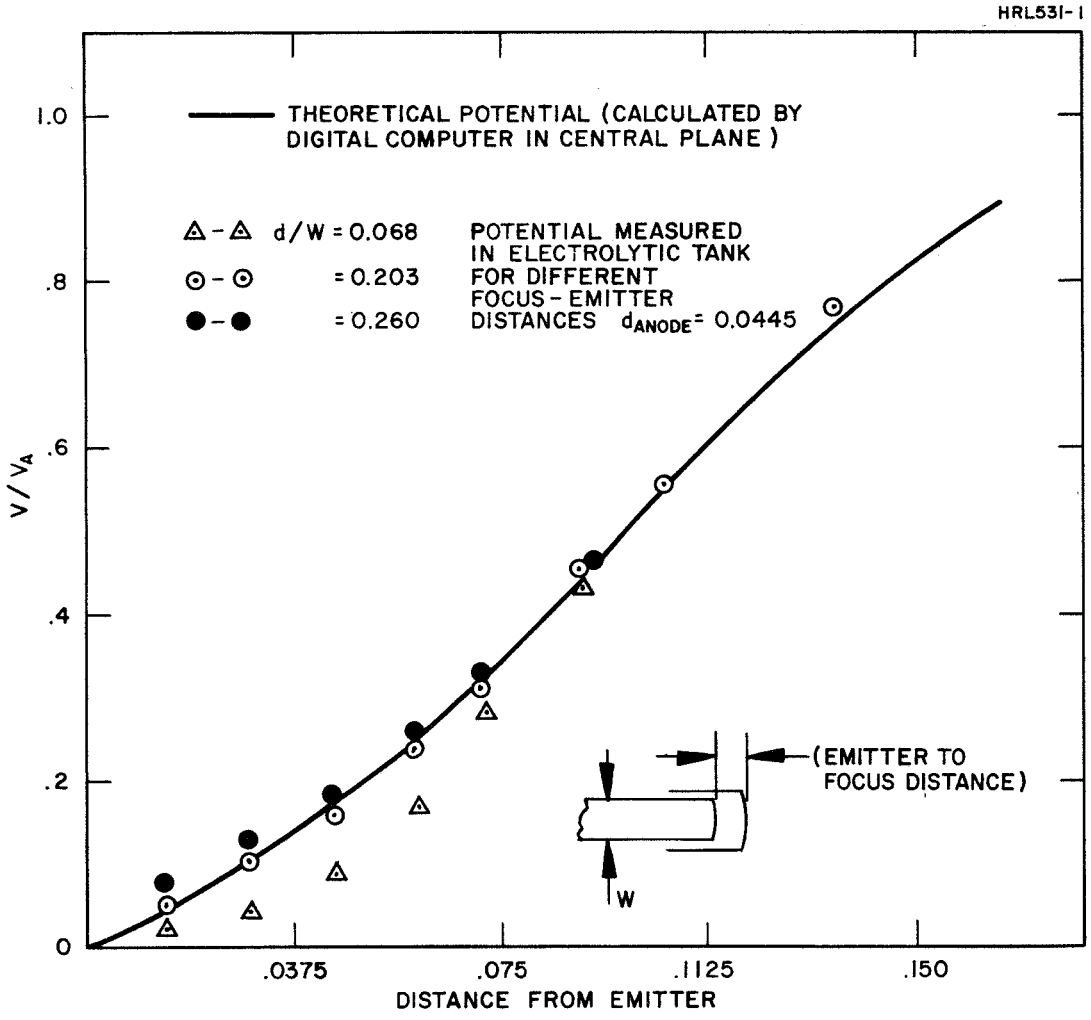

Fig. 25. Graph Showing Potential Distributions Measured in Electrolytic Tank at Beam End Along with that Calculated in Central Plane by Digital Computer.

TABLE I

Main Conclusions and Experimental Observations
Predicted by the Computer Modeling

Theory	Experiment
Very low direct interception.	Verified.
Computed deflection sensitivity of 2 $\Delta V/V_{tot}$ = 0.18 for 24° deflection.	Measured deflection sensitivity of 2 $\Delta V/V_{tot}$ = 0.2 for 24° deflection at 100% thrust level.
End effects design for deflected beam.	Design verified. No erosion seen near ends.
Linear variation in θ versus 2 $\Delta V/V_{tot}$.	Quantitatively verified.
Decrease in deflection sensitivity as beam current is reduced.	Qualitatively verified, experimental data shows faster decrease with current than theory predicts.

T190

- All components and subsystems shall be designed for nominal operation after being subjected to shocks of 35 g's and sinusoidal vibrations of 3.0 g's peak amplitude, 10 to 2000 Hz, along each of three mutually perpendicular axes at a sweep rate of 2.0 octaves/min.

Subsequent discussions with the NASA Project Manager modifed these specifications to read:

- All components and subsystems shall be designed for normal operation after being subjected to shocks of 35 g's, one-half sine wave for 8 msec, and sinusoidal vibrations of 3 g's ± 3 g's peak amplitude, 20 to 2000 Hz along each of three mutually perpendicular axes at a sweep rate of 2.0 octaves/min.

In practice, components and subsystems are qualified at one and one-half times the sinusoidal vibration; therefore, the design qualification for this sinusoidal vibration was 9.0 g's. This study was analytical in nature because shake test of the hardware was not required under this program.

The study began with a review of the vibration analysis of programs that were used on other strip thrusters and new programs which could be applied to the present system. Discussions with other Hughes Aircraft Company personnel, who were responsible for handling vibration programs for space hardware supported this initial investigation. The first computer program considered for use was called DYNM 2. This program is a completely general program which computes the steady-state response of a linear N degree-of-freedom system of masses, springs and dampers subjected to a sinusoidal excitation of one or more masses at any desired frequency. The input consists of the elements of the inertia, stiffness, and damping matrices, and vectors of the amplitudes of the forcing function. The output consists of displacement amplitudes and phase of each mass. Natural frequencies then

are estimated by plotting the results of the displacement computations to determine the frequency or frequencies when large displacements occur. Further studies showed a MARS (Matrix Analysis Routine for Structures) computer program was more suitable for the analysis. The MARS program is an improved version of the LESAR (Linear Elastic Structural Analysis Routine) program, used on other strip thruster vibration studies. The MARS program is written for a GE 635 computer used at Hughes Aircraft Company. The MARS program has the advantage of directly computing the required stiffness, inertia, and damping matrices from the dimensions and material constants of the system. The DYNM 2 programs required these matrices to be computed in advance and presented as input data.

1. MARS Computer Program

The vibrational analysis of the linear strip ion thruster system was performed by the MARS I and MARS II computer programs. The MARS I program, used in this analysis, computes the natural frequencies and modes of a structural model which consist of beams and shell elements. Structural masses are "lumped" at node points which represent the element extremities. A model may contain as many as 60 mass nodal stations and an unlimited number of connecting elements. This is equivalent to 360° of freedom; at each mass point there may be three translational and three rotational degrees of freedom. Figure 26 is a schematic of the MARS computer program. The input requirements to the GE 635 computer consist of the mass and rotational inertia at each node, coordinates, element cross-sectional properties, material constants, and node numbers which define the element

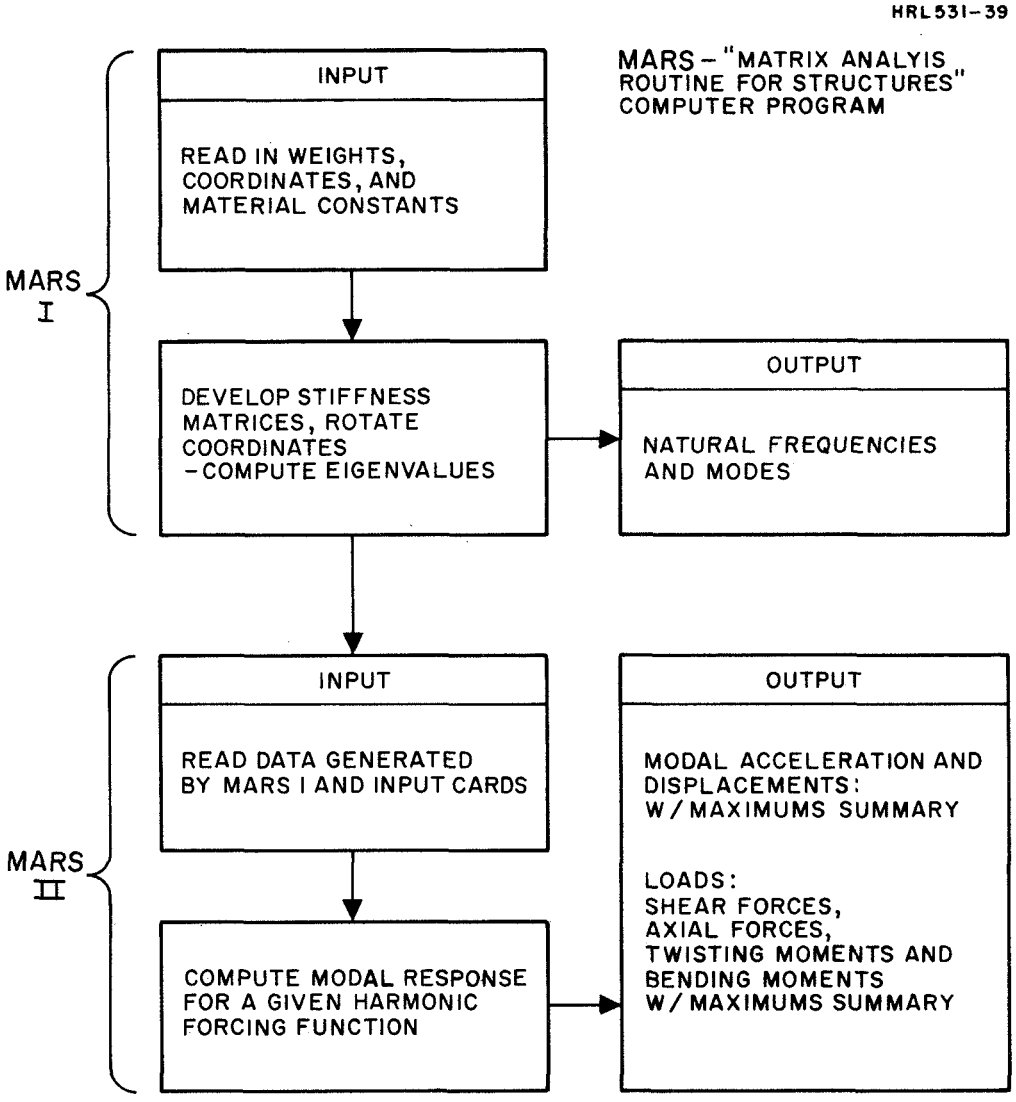

Fig. 26. MARS Computer Program.

end points. The flexible elements are entered into the program data by the programmer in any of the following three types.

Type 1: Elemental stiffness matrix is externally generated by the programmer and is coded by hand.

Type 2: Symmetrical elements — elemental stiffness matrix is generated by the computer program using the dimensions of circular elements.

Type 3: Nonsymmetrical elements — elemental stiffness matrix is generated by the computer using moments of inertia calculated by the programmer.

The MARS II program determines the dynamic response of the model, using the frequencies and mode shapes computed by MARS I. Frequencies and amplitudes of the excitation forces are the only additional input data.

The mass stations are chosen at points throughout the structure where dynamic response is required. Structural and component weight is lumped in proportion to the number of mass stations in a given area. The coordinates of each station are input using any arbitrary reference system, and the computer program formulates the elemental stiffness matrices and rotates them into system coordinates. It then compiles the system stiffness matrix and solves for eigenvalues and eigenvectors. The transmissibility of each mass station then is determined by applying a unit load (1.0 g) at the base. The response to any sinusoidal input specification is then found by multiplying the transmissibilities by the input level at each natural frequency for every mass station. Next, bending and twisting moments are found by multiplying the stiffness matrix by the displacements to compute the shear loads and moments from the moment-arm distances between mass stations.

2. Description of Mathematical Model

The thruster assembly is composed of two identical halves, or subassemblies. The symmetry of the design enabled the programmer to make a detailed model of one-half of the total assembly and a less complicated model of the other half. A total of 60 mass stations and 96 connecting elements were used in the model shown in Fig. 27. The left side of the assembly (in the positive x-direction) is modeled in detail and the right side modeled to ensure that the over-all system flexibility and mass properties are adequately simulated.

Mass Stations 1-20 represent a detailed model of the aluminum main support housing. Stations 4, 8, and 13 are the attachment points, and are used as the base for sinusoidal vibrational and shock input. The ionizer subassembly is a critical part of the thruster assembly and is represented in detail. The porous tungsten emitter and manifold assembly is shown by mass Stations 27, 29, and 36. The emitter assembly is supported by Mo/Re strips which are represented by elements connected to Stations 31, 32, 33, and 34 on the sub-base. The sub-base is supported by elements connecting mass Stations 31, 32, 33, 34, with Stations 30, 35, 37, and 38.

The accelerator electrodes are cantilevered from ceramic insulators at mass Stations 45-46, 47-48, 57-58, 56-59. These were also modeled in detail to obtain loads in the accel, decel, and ceramic subassemblies. Stations 23 and 24 represent the cesium reservoir centers of gravity and were considered to be filled with 70.0 grams of cesium (each) for the dynamic analysis.

A damping coefficient of 3% was used for the sinusoidal vibration. This value was determined from experience with similar structures which have been verified by actual vibration tests. A lower value (1%) was used for the shock simulation, because a structure of this type has low damping when subjected to a shock pulse.

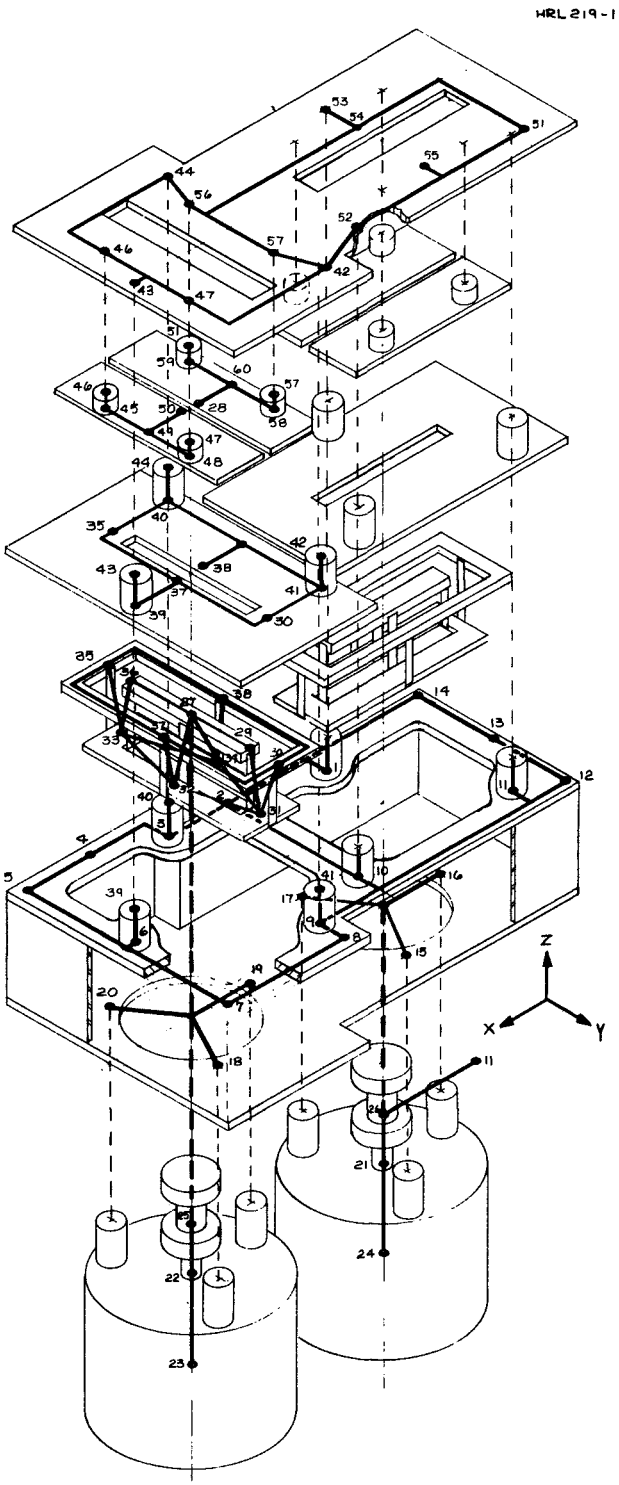

Fig. 27.
Mass Stations and Connecting Elements used for Computer Program.

- Computer Results — The mathematical model was subjected to nine g's sinusoidal vibration over the frequency range of 20 to 2000 Hz along each of the three mutually perpendicular axes, as shown in Fig. 27. The response of the lumped mass stations was calculated and 27 mode shapes were computed for the dual ion thruster assembly in the specified frequency range. The general mode descriptions, along with the natural frequencies are listed in Table II. In addition, eight selected mode shapes are plotted in Figs. 28 through 40, showing the deflections which occur at natural frequencies.

Comparisons of the computer load output show good correlation between corresponding mass stations in each half of the thruster assembly. This indicates the gross simulation of the model assumed in the right half is a good representation when compared with the detailed left half.

Table III shows the maximum acceleration response of the critical areas of the thruster assembly (i.e., cesium tank, ionizer subassembly, and accel electrodes). The maximum acceleration found was 214 g's at Stations 29 and 36, resulting in an amplification factor of 23.8. Because of the low masses involved, the deflections are small.

The maximum acceleration response to a 35 g, 8 msec, one-half sine wave shock input for critical areas is shown in Table IV. The maximum acceleration was also found at Stations 29 and 36 (ionizer) and resulted in an amplification factor of 1.25 or 44 g's. Less consideration should be given to this response, because when compared with the sinusoidal response, the shock load is obviously much less severe. If the structure can withstand the sinusoidal environment, the shock requirement evidently is satisfied.

TABLE II

Natural Frequencies and Modes

Mode	Frequency, Hz	Mode Shape Description
1	203	Y translation of ionizer
2	293	Rotation of ionizer assembly about center line
3	344	X translation of ionizer and sub-base
4	376	X translation of feed valve
5	383	Z translation of exit electrode
6	447	Y translation of feed valve
		Y translation of cesium tank
7	483	X translation of cesium tank
8	488	Y translation of cesium tank
		Y translation of feed valve
9	518	Y translation of exit electrode
10	526	X translation of cesium tank
		X,Y translation of exit electrode
11	532	Z translation of accel half
12	587	Z translation of accel half
13	611	X translation of exit electrode
14	635	Y translation of cesium tank
15	652	Z,Y translation of cesium tank
16	766	X translation of ionizer sub-base
		Z translation of focus electrode
17	799	Y translation of exit electrode
18	918	Z translation of accel
19	959	Z translation of cesium tank
20	1070	Y translation of ionizer base
21	1104	Z translation of accel half
22	1411	Z translation of exit electrode
23	1535	Z translation of ionizer
24	1551	Y translation of exit electrode
25	1557	Z translation of ionizer
26	1705	Z translation of accel
27	1757	Z translation of accel
28	2027	Y,Z translation of exit electrode

T191

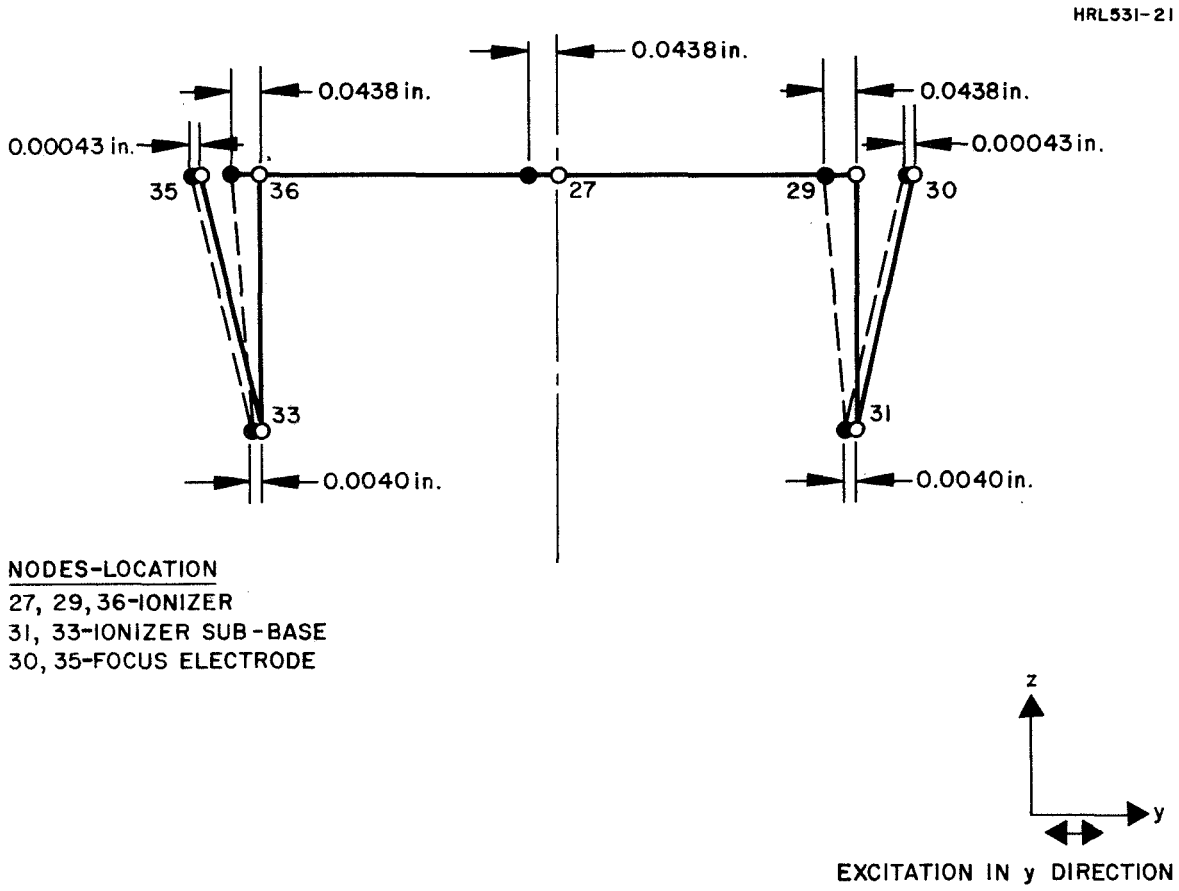

Fig. 28. First Mode Shape, f_1 = 203 Hz Ionizer Translation.

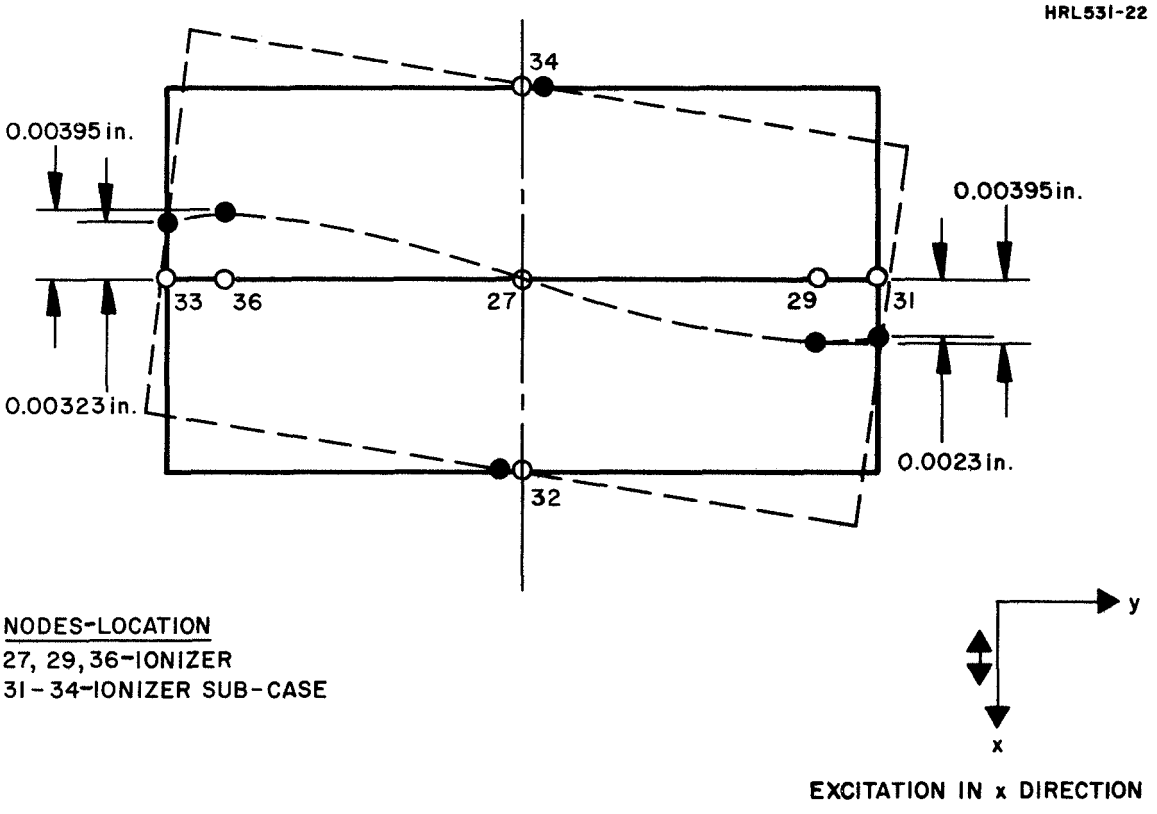

Fig. 29. Second Mode Shape, f_1 = 203 Hz Ionizer Thruster.

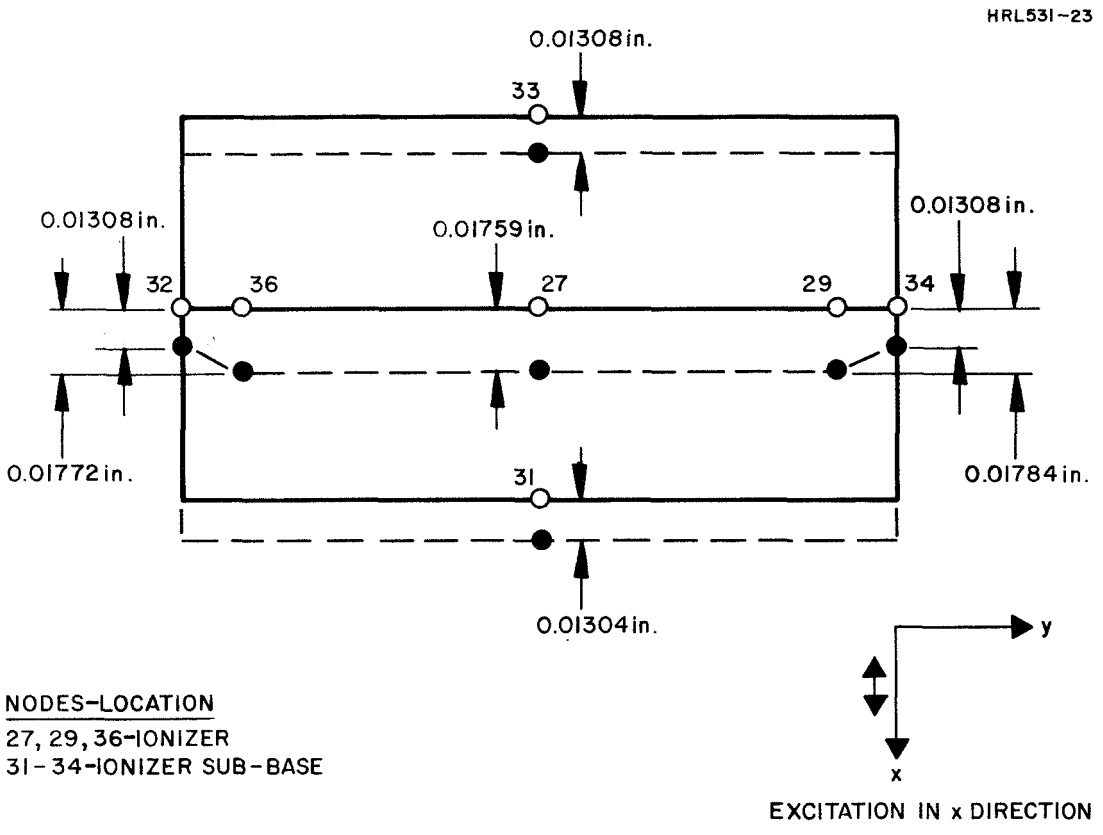

Fig. 30. Third Mode Shape, f_3 = 344 Hz Ionizer and Sub-base Translating WRT Focus Electrode.

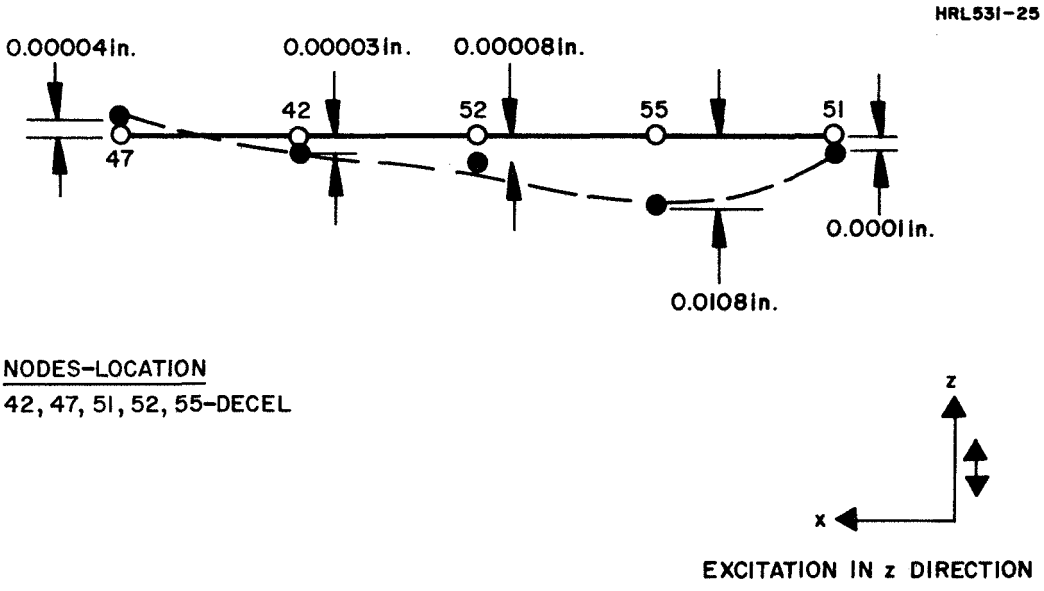

Fig. 31. Fifth Mode Shape f_5 = 383 Hz Deflection of Exit Electrode.

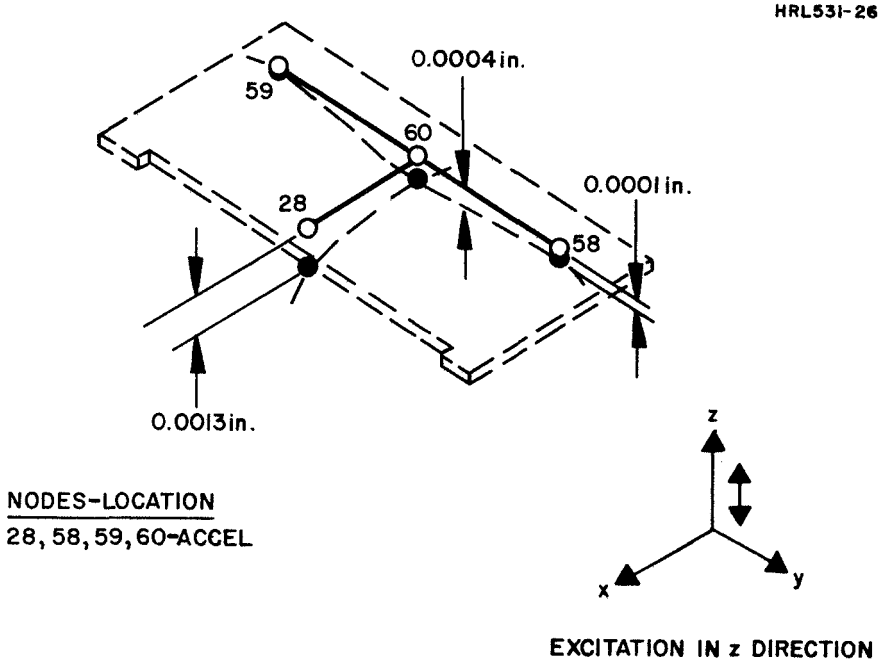

Fig. 32. Eleventh Mode Shape, f_{11} = 532 Hz Deflection of Accel Half.

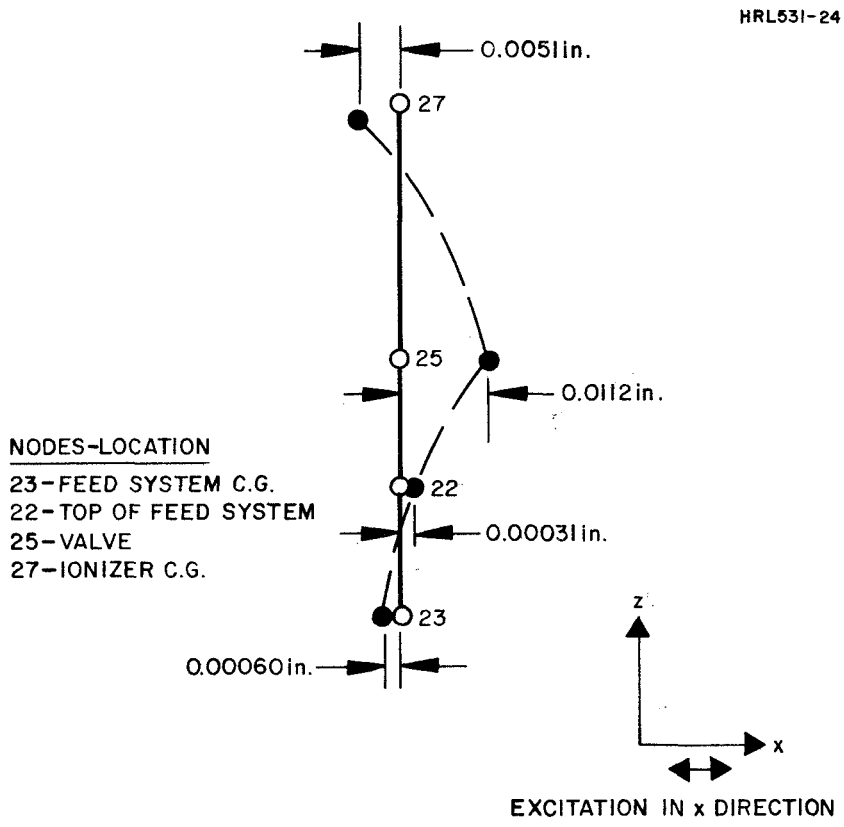

Fig. 33. Fourth Mode Shape, f_4 = 376 Hz X-Translation of Feed Valve.

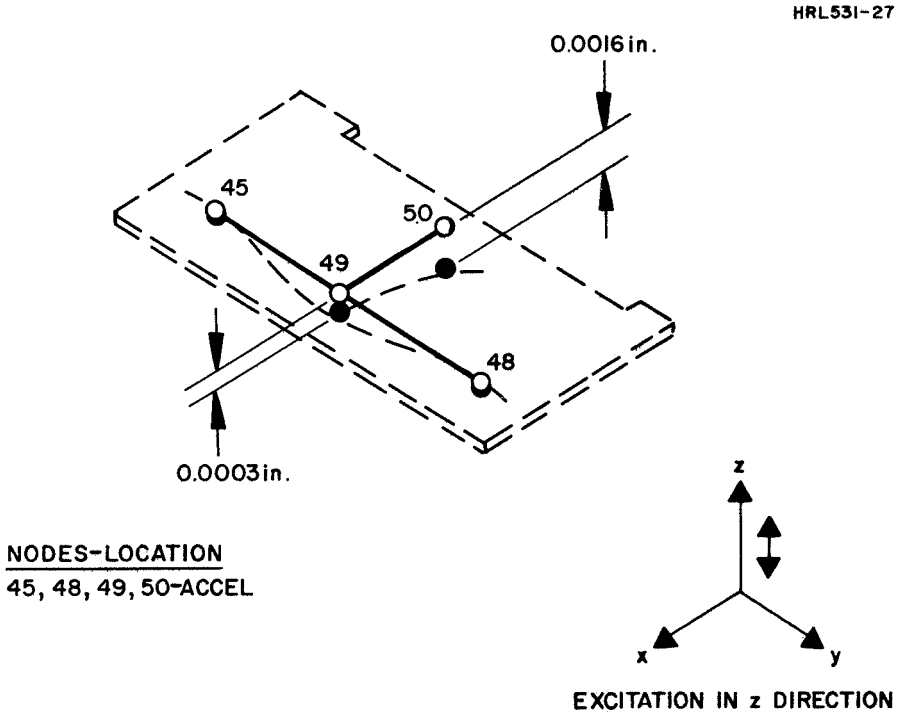

Fig. 34. Twelfth mode Shape, f_{12} = 587 Hz Deflection of Accel Half.

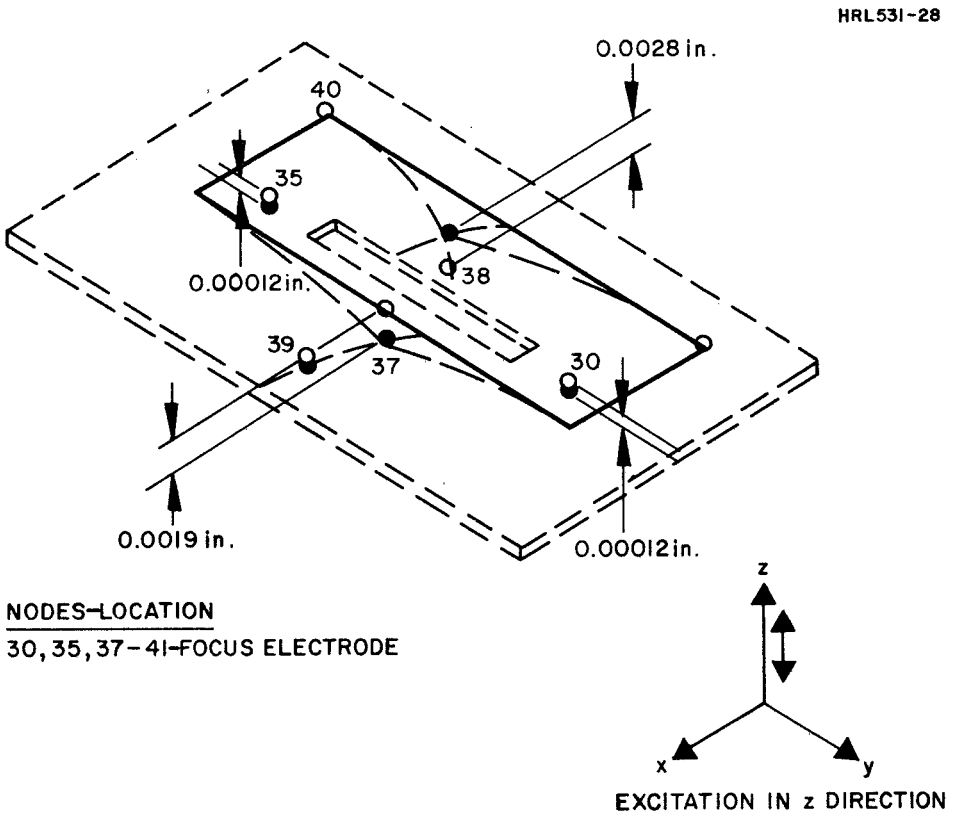

Fig. 35. Sixteenth Mode Shape, f_{16} = 766 Hz Deflection of Focus Electrode.

TABLE III

Selected Acceleration Response of Critical Areas on the Ion Thruster Assembly Maximum Accelerations (G's)

Mass Station	Description	Excitation Direction		
		X Axis	Y Axis	Z Axis
23	Cesium Tank	137	135	99
24	Cesium Tank	118	147	169
29, 36	Ionizer	214	185	138
28	Accelerator	114	91	186
50	Accelerator	116	75	225

T192

TABLE IV

Response of a Selected Number of Mass Points To the Base-Applied 35 G, One-Half Sine Wave Shock Maximum Accelerations (G's)

Mass Station	Description	Excitation Direction	
		X Axis	Z Axis
29, 36	Ionizer	44	36
28	Accelerator	37	39
50	Accelerator	37	39
55	Lumped Accelerator	37	41

T193

- Stress Analysis — The output listing of the computer program includes the axial load, shear load, twisting and bending moments at each end of the 96 elements connecting the mass stations. These values are computed for all three axes, resulting in a total of 3456 individual stress values for each frequency, and also are summarized for each element so the maximum loads for each element are determined easily. The maximum axial, shear, torsional, and bending stresses are computed by hand from load values listed in the summaries to determine critical stress areas. Table V is a listing of the computed stresses for most subassemblies.

As a result of this analytical study of the vibration characteristics of the thruster assembly and subsequent stress analysis, two minor design changes were made.

1. The thread size of the metal cap which is brazed to the ceramic accel insulator was increased from No. 1-72 to No. 2-56 in order to increase the insulator assembly's resistance to shear and bending loads.

2. The angular position of the diagonal support straps which join the ionizer base and sub-base were changed so they have double width at all attachment points. The weight of the sub-base also was reduced to decrease bending moments.

No additional design changes are anticipated as a result of the vibrational-stress analysis of the dual beam ion thruster. The specified sinusoidal vibration of 9.0 g's, although of relatively high magnitude, does not appear to threaten the structural soundness of the system. The system also responds well to shock loads with low (1.25) transmissibility to component parts. After the vibrational analysis was completed and the thruster tested, a design change was made in the insulators which support the accel electrodes. These insulators differ from the original ones and were not used in the vibrational analysis.

TABLE V

Maximum Stress Values

Element	Maximum Axial Stress, psi	Maximum Shear Stress, psi	Maximum Torsional Stress, psi	Maximum Bending Stress, psi
Cesium Tank	350	560	1	170
Wick Housing	390	1,080	1	5,280
Feed Tube	6,130	825	1	4,750
Feed System Supports	2,270	1,380	22,700	64,000
Accel Insulator	2,900 (2,100)[a]	13,800 (9,900)	188,000 (120,000)	136,000 (83,000)
Ionizer Support Straps (Inner)	27,070	11,700	16,600	80,000
Ionizer Support Straps (Outer)	14,660 (7,330)	24,200 (12,100)	170,000 (69,800)	205,000 (134,000)
Thruster Support Insulators	8,100	24,400	930	16,900
Housing Assembly	500	1,280	33,800	5,800

[a]Numbers in parentheses are stress values after design modification.

T194

SECTION IV

NEUTRALIZER DEVELOPMENT

The objective of this task was the development of a filament capable of emitting 20 mA of electron current per watt of input power for a 15,000 hour period. When developed, this filament was used as a neutralizer in the linear strip thruster. The work involved the selection of the neutralizer material, development of the technique for processing the filament, testing to determine the operating conditions which produce the best efficiency and operating life, and the operation of a filament for a life test.

Thoriated tungsten was selected as the filament material. Tests were made to determine the optimum conditions for carburization of the surface. Filaments were tested using a guarded cylindrical diode. The space charge limited current and the saturation current were measured for filament temperatures from 1800 to 2400°K. Filaments were developed that produced emission currents of about 40 mA/W of input power and operated more than 2000 hours with no sign of degradation.

A. FILAMENT MATERIAL SELECTION

The choice of materials for use in this application, was limited by the emission efficiency and geometrical requirements and have been placed on the filament. The high emission efficiency necessitates the use of a low work function emitter.

Dispenser cathodes and impregnated cathodes have the highest emission efficiencies and also have long operating lifetimes. They were not used in this application because of their button-shaped geometry. Although these cathodes are not suitable for use as filament type neutralizers, which are used in the present design, the dispenser cathodes should be considered if future designs permit a button-shaped neutralizer.

Oxide coated filament cathodes have high emission efficiency. They have been ruled out for this study because the oxide coating on the filament is both fragile and of limited life. It is possible the coating could be sloughed off during vibration tests.

The material selected was thoria impregnated tungsten. This material is formed by the addition of about 1/2 to 2% thoria to a tungsten slurry which is then reduced to tungsten metal. The thoria is distributed uniformly throughout the tungsten powder which is then formed into wire. The thoria is converted to thorium metal by a brief (15 to 30 sec) heating to temperatures as high as 2500°K. When the filament is operated at lower temperatures (1800 to 2000°K), the thoria diffuses to the surface to form a low work function surface. The lifetime of the filament is limited by the gradual loss of thorium by evaporation from the surface.

The lifetime of the thoriated tungsten filament can be extended by a factor of six by forming a carbide layer (W_2C) over the surface of the cathode. The carbide serves to reduce the loss of the thorium. Because tungsten carbide is much more brittle than tungsten, the extent of carburization of the filament must be limited in order not to weaken the filament. The extent of carburization of the filaments was established from previous studies which were reported in the literature.

In order to estimate the lifetime, it is necessary to specify the filament diameter, which is set by the power limitation of the neutralizer supply. Because the conduction losses are negligible for a long filament of small diameter, it is possible to assume that all power is lost as radiation. Thus, by means of the Stefan-Boltzmann equation, it is possible to calculate the diameter of a carburized thoriated tungsten filament of given length, temperature, and radiated power. For example, a 7 cm long, 5×10^{-3} cm (2 mil) diameter carburized filament, operating at 1900°K, radiates 2.5 W of power. Because of the over-all power limitations, the filament wire was limited to a 5×10^{-3} cm diameter. Smaller diameter wire was not used because the extent of carburization needed for the smaller wire could result in a significant loss of strength.

Estimation of the extent of carburization was based on the values reported by Ayers.[13] He presents a graph of the carbide loss rate (as an equivalent thickness of W_2C shell lost per hour) as a function of emission efficiency. There are three points given: 70 mA/W at 1950°K, 100 mA/W at 2000°K, and 130 mA/W at 2050°K. Extrapolating this to 20 mA/W gives an equivalent loss rate of 5×10^{-7} mils/hour. Thus, for 15,000 hours operating time, the equivalent loss is 0.19 μm. This carbide thickness corresponds to 1.4% of a 52.4 μm diameter wire.

For a 50 mA/W emission efficiency, the equivalent loss rate is 1.3×10^{-5} mils/hour which correspond to an equivalent loss of 5 μm over 15,000 hours. This represents a 35% carburization of a 52.4 μm wire. This value represents an upper limit for the carbide thickness of the filament processing used in this study. Values in the range of 15 to 25% were used for filaments developed in this program.

B. CARBURIZATION PROCESS

The optimum conditions for carburization of the thoriated tungsten filaments were established in a series of tests performed in the first part of this program. The general conditions were based on the works of Schneider[14] and Horsting[15]; Schneider found the optimum conditions to process the filaments were in an atmosphere of hydrogen, containing from 0.18 g to 0.45 g of benzene per 10 ℓ (STP) of hydrogen, and at a filament temperature below 2200°K.

Processing the filaments at temperatures above 2200°K resulted in the formation of WC and ThC_2. The WC is undesirable because it is solid (rather than laminated as is the W_2C), and thus restricts the diffusion of thorium metal to the surface of the filament. The ThC_2 compound is much more stable than the ThO_2, and therefore, is not easily reduced by flash heating (as is ThO_2). This results in a decrease in the amount of available thorium. A lower limit exists at about 1800°K, as a consequence of the limited diffusion of the carbon (or tungsten carbide) into the wire.

According to Schneider, the benzene concentration was important, because processing at lower concentrations failed to produce carburization, and processing at higher levels caused the formation of WC and free carbon on the surface. Both are unfavorable to the operation of the cathode.

A significant change was made in the design of the apparatus. Schneider "controlled" the benzene concentration by adjusting the height of a tube above a benzene surface and by regulating the flow of hydrogen gas over the benzene surface. It is impossible to define the benzene concentration by this method.

In the present work, a stream of hydrogen gas (of known flow rate) is bubbled through benzene to saturate the hydrogen. The partial pressure of benzene is controlled by the benzene temperature. Thus, the mole fraction of benzene in hydrogen is fixed. The benzene concentration is reduced to the desired level by diluting the saturated stream with a stream of pure hydrogen. This system is shown in schematic form in Fig. 36.

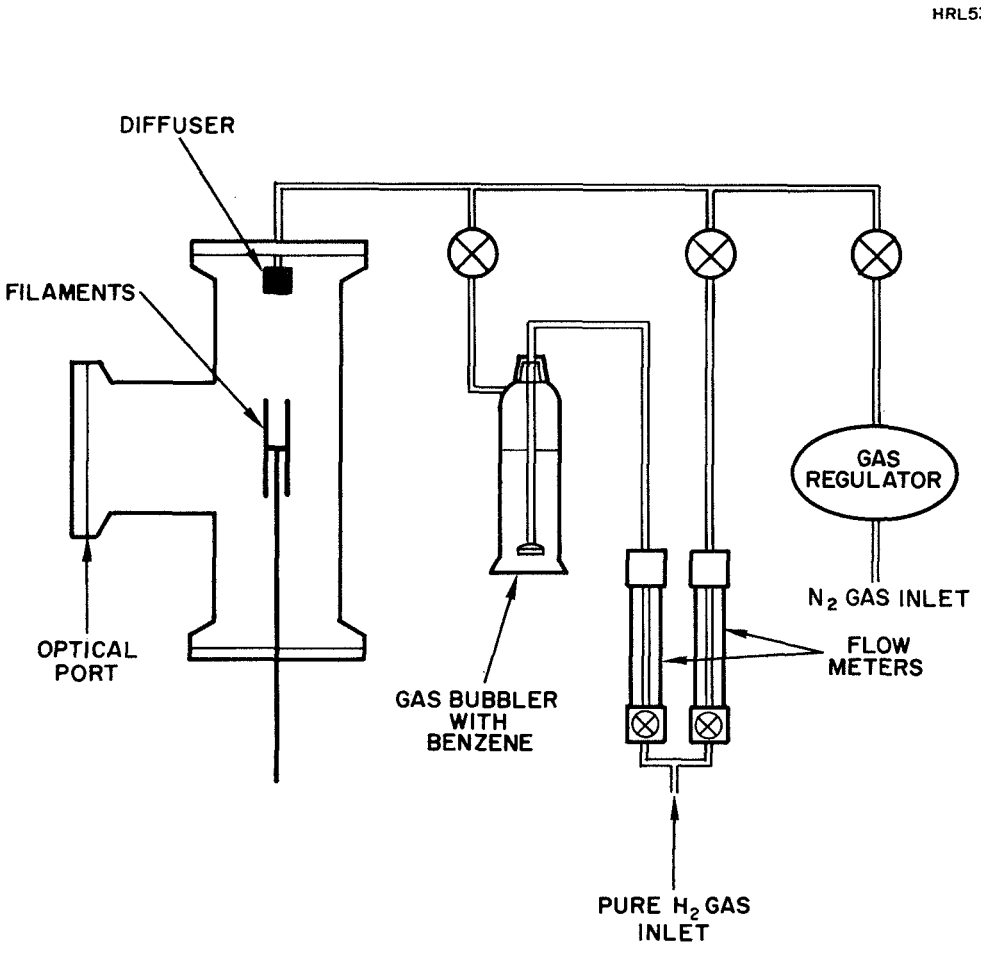

Fig. 36. Diagram of Filament Carburization System.

The reaction chamber is formed from a 6 in. diameter T-shaped Pyrex glass pipe. The optical window is a flat plate Pyrex glass. The diffuser is a cylinder type (12 mm diameter) coarse porosity fritted Pyrex gas dispersion tube. The "bubbler" is a gas absorption cylinder having a coarse porosity fritted disk. The flowmeters are 150 mm tube types with Pyrex and stainless steel floats. Figure 37 shows the electrical circuit for heating the filaments.

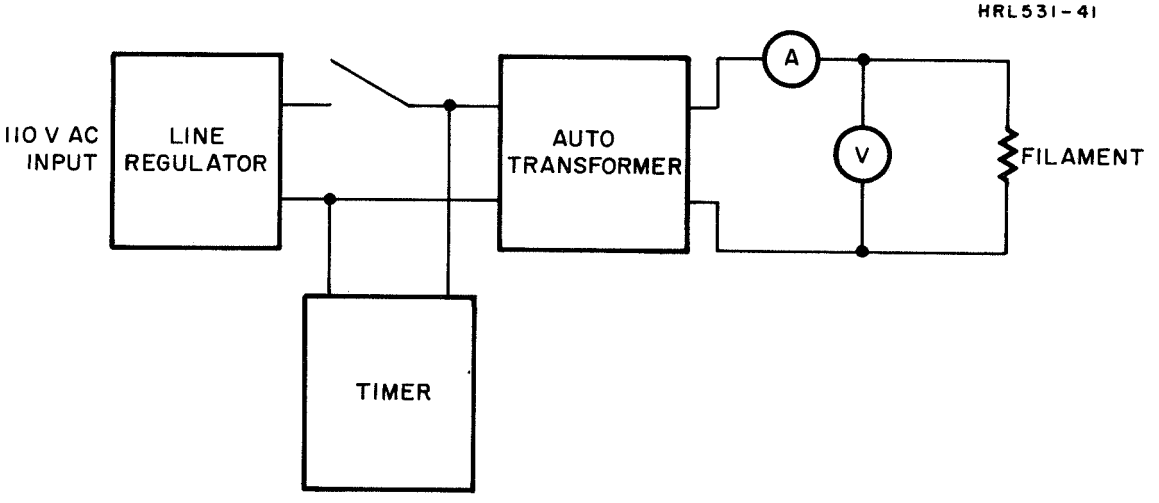

Fig. 37. Schematic of Electrical Circuit for Filament Processing System.

The carburization process consists of the following operations. Four filament assemblies (with lead wires attached) are mounted on a rotating post which is positioned inside the reaction chamber opposite the optical port. A flow of nitrogen gas is maintained at all times when the system is turned off to prevent the diffusion of air or water vapor into the reaction chamber. The chamber is then purged with hydrogen gas for about one hour. The cold resistance of the filaments is measured. The filaments are heated at a temperature of about 2030 ± 50°K to stabilize the filament. The heating time (on the order of 15 ± 5 sec) is set by the

point at which the filament current becomes constant. During this process, the filament temperature is measured with a disappearing filament pyrometer. The system is allowed to come to equilibrium at room temperature and the cold resistance of the filament is again measured.

Benzene vapor is now introduced into the system in a concentration of 0.5 mole percent (which is equal to 0.18 g benzene/10 ℓ (STP) H_2). Preliminary experiments showed this to be an optimum concentration. The benzene concentration is set by the temperature of the benzene liquid in the bubbler (which establishes the vapor pressure), and by adjustment of the ratio of the flow rate of benzene-saturated hydrogen to pure hydrogen. A minimum flow of about 2 ℓ (STP)/min is used to prevent erosion of the filament. When lower flow rates were used, erosion was observed near the ends of the filaments.

The carburization is accomplished by heating the filament to a temperature of 2030 ± 50°K in the benzene-hydrogen atmosphere until about 35% of the wire is converted to W_2C. The process requires about 20 to 25 sec. The end point is set by an increase in the resistance to 1.22 of the original value. This value was obtained from Cailey's[16] work and was confirmed by observations in this program. The temperature was measured with an optical pyrometer.

When the processing was completed, the benzene vapor source was shut off and the system was flushed with pure hydrogen. After measuring the cold resistance, the system was filled with nitrogen until the next set of filaments were processed.

The filaments were removed, taken out of the assemblies, sealed into thick walled uranium glass capillary tubing, then mounted and prepared for photomicrographic examination. A representative example is shown in Figs. 38(a), (b), and (c). These examples are sections of filament 102 LD taken

M 7885

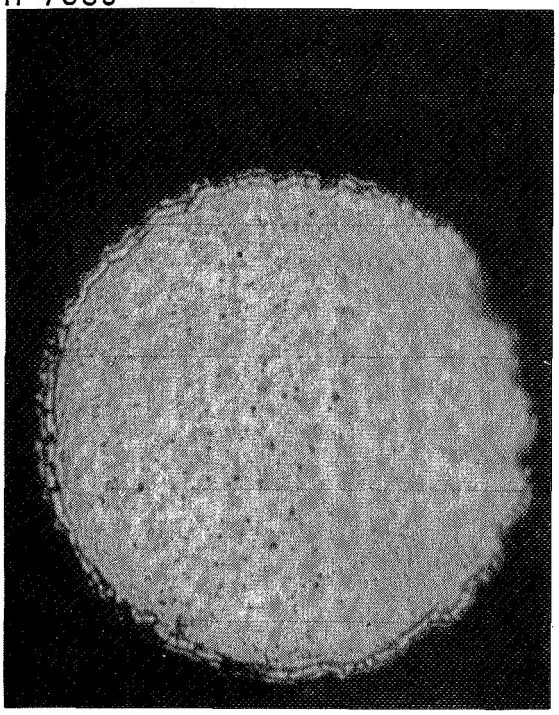

(a)

M 7884

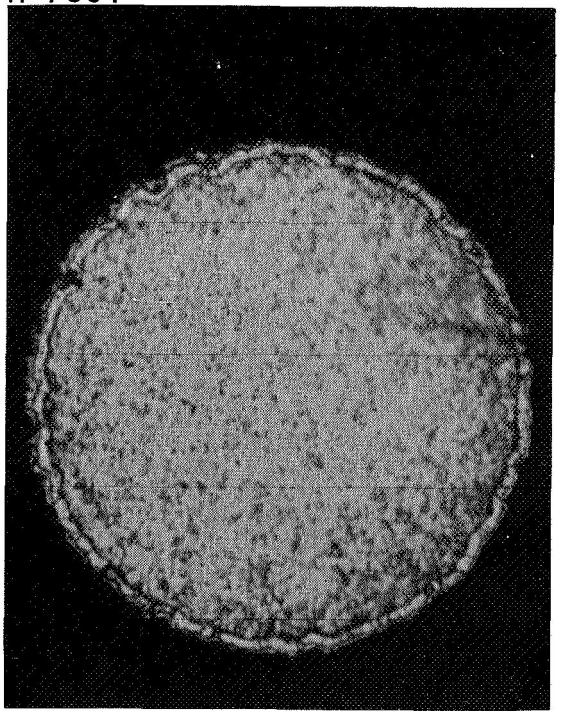

(b)

M 7883

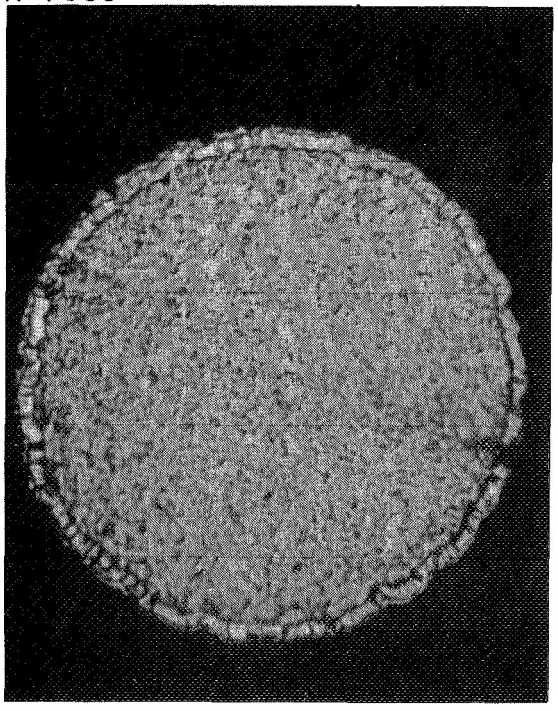

(c)

Fig. 38.
Photomicrograph of Carbuized Cross Section of Filament (1250x).

approximately 2 cm below center, at center, and at about 2 cm above center. The carbide shell is about 18% of the total wire.

C. FILAMENT ACTIVATION AND EMISSION TESTS

A procedure for activation of the carburized thoriated tungsten filaments was developed, based on the method described by Schneider.[14] This work was performed as part of the thermionic emission studies. The test data in these studies included cold resistance of the filaments, heating power, filament temperature, diode voltage and emission current, pressure in the test chamber, and cathode to anode distance. In this section, diode design and vacuum facility will be discussed first, then measurement of the filament temperature, resistance, and I-V characteristics, followed by a summary of the results.

Two types of diode assemblies were designed. One was a guarded cylindrical diode (shown in Fig. 39), which was used to determine the thermionic emission properties of the carburized thoriated tungsten. A planar diode (shown in Fig. 40) was used to simulate the operation of the neutralizer filament on the ion thruster. Both units used the filament mounting structure which had been approved for use in the thruster.

The cylindrical diode assembly consists of a 4.65 cm long center collector and two, 1.07 cm long guard electrodes. The inside diameter of the anodes is 1.01 cm. The planar diode has a 4.65 cm long anode. The anode-to-cathode distance is 0.477 cm. The anode simulates a 0.315 cm thick by 4.65 cm long ion beam. The cathode is located 0.158 cm from the ground plane electrode, which simulates the decelerator electrode used in the ion thruster.

HRL 531-35

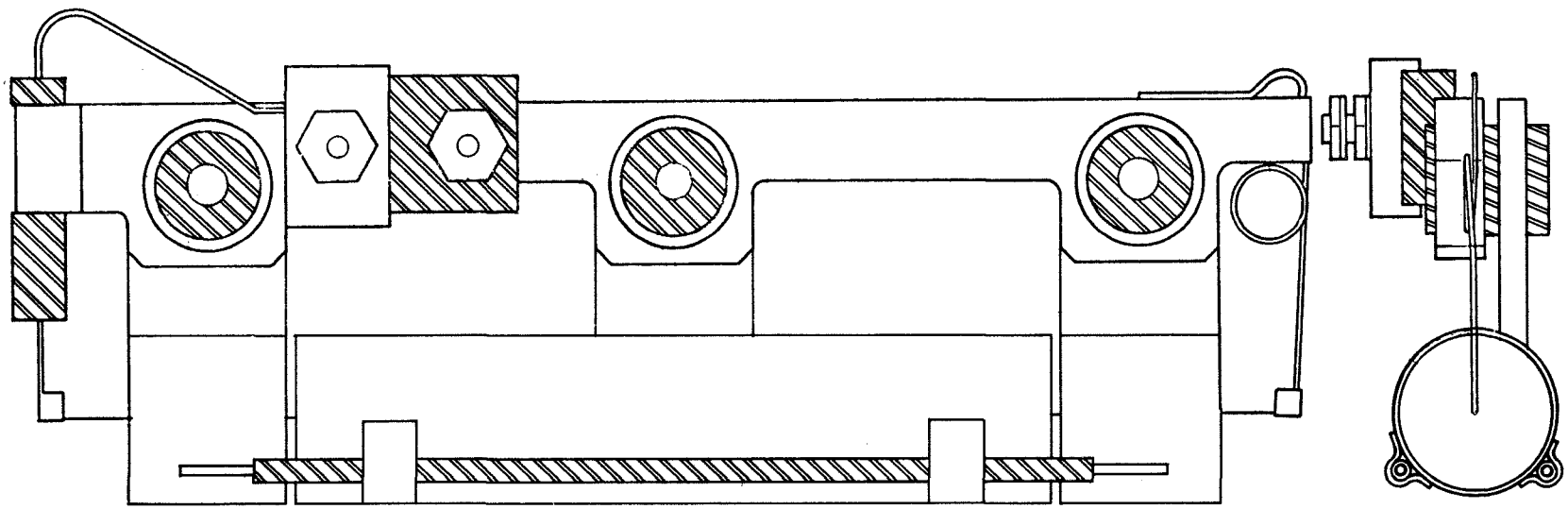

Fig. 39. Guarded Cylindrical Diode (Scale about 2.4x).

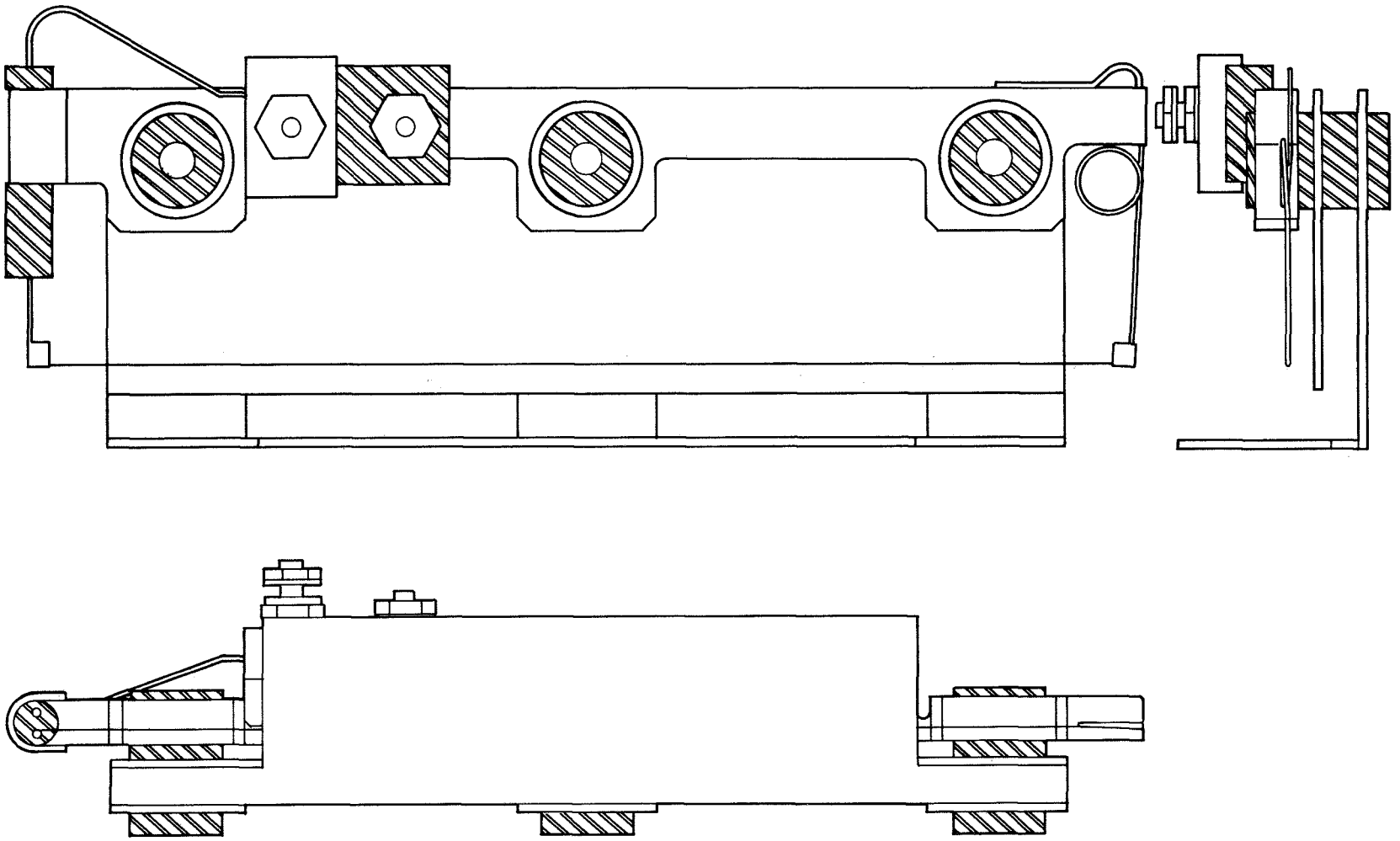

Fig. 40. Planar Diode (Scale ~ 2.4x).

An estimate of the end effects due to the filament supports, was made to demonstrate that the filament temperature over the central portion of the filament was uniform. This was based on Langmuir's work.[17] For a total length of 7.36 cm, the central 5.76 cm is uniform in temperature to 1% (i.e., the temperature at the end of this distance is 99% of the center). The central 6.34 cm has an edge-to-center temperature ratio of 95%.

A small vacuum station was used to test the neutralizer emission. This all-metal system was designed for UHV operation in order to prevent the contamination or poisioning of the emitter surfaces by oil or water vapor. The system, which is shown in Fig. 41 in outline form, consists of the following components. The test chamber is a 6 in. diameter T-section with six test ports. The fore pumps used are a gas aspirator pump and a zeolite sorption pump. The high vacuum pumps consist of a 250 ℓ sec^{-1} triode sputter ion pump and a 1600 ℓ sec^{-1} titanium sublimation pump. The six ports are used as follows: two are optical ports for optical pyrometric measurement of the neutralizer's temperature; one port contains a 20 pin header, which is used for power and signal leads for the four diodes that are tested each run; another two ports are used for vacuum diagnosis (one for a nude ion gauge tube and the other for a quadrupole mass spectrometer tube); and the last port is used for the fire line.

The temperature of the filaments was obtained by means of a disappearing filament brightness pyrometer. Corrections for the emissivity of the surface, absorption in the glass port, and reflection at the surface of the window, were made to obtain the absolute temperature. The values for the tungsten emissivity used in this study were those of Roeser and Wensel.[18] In a more recent work, Larabee[19] presents

values that are substantially the same in the temperature range of interest. The emissivity values used with the carburized filaments, were those reported by Barnes.[20] The window corrections were measured in the laboratory by comparing the apparent temperature of a lamp with and without the window in the light path. Corrections for reflective losses, which occur when measurements are made at an angle to the normal to the window, were obtained from Benford's paper.[21]

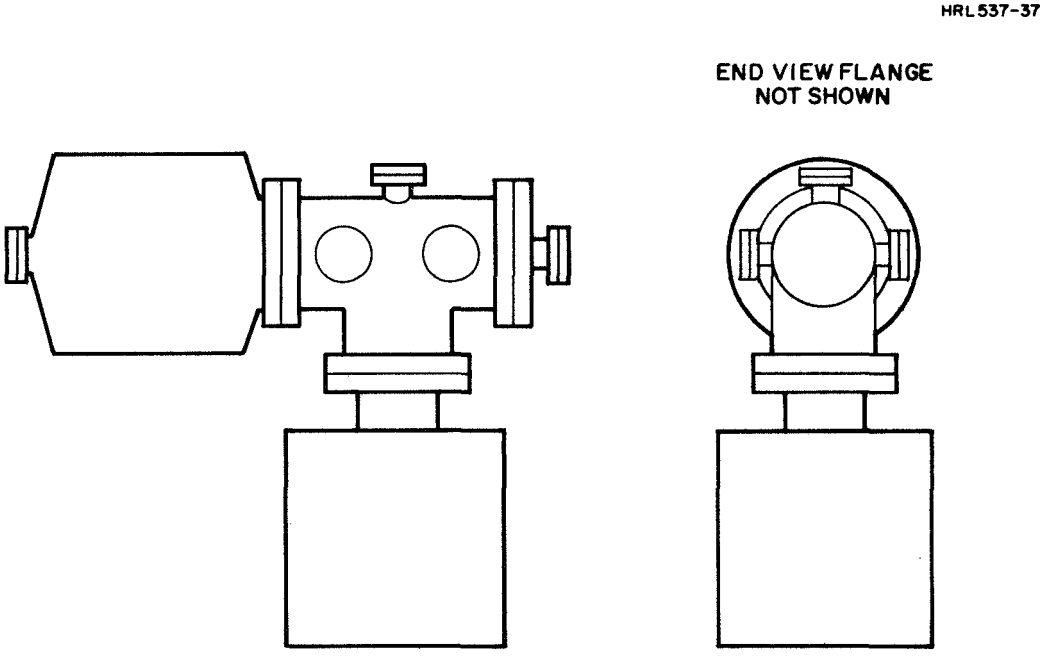

Fig. 41. Vacuum Test Station.

The cold resistance of the filaments was measured using a wheatstone bridge circuit with a galvanometer null detector. It was necessary to modify the circuit to limit the current flow through the filament to 3 mA, because larger

currents would cause appreciable heating of the filament when the measurements were made on a filament that was under vacuum. The reproducibility of the measurements, which is mainly limited by variations in the lead wire junctions, is better than 1 part in 10^4.

The emission current/diode bias relationship was determined by means of the circuit shown in Fig. 42. The filament power is obtained from I_F and E_F. The cathode to anode bias is E_B. The sum of the collector current I_C and the guard current T_G equals the total emission current I_T.

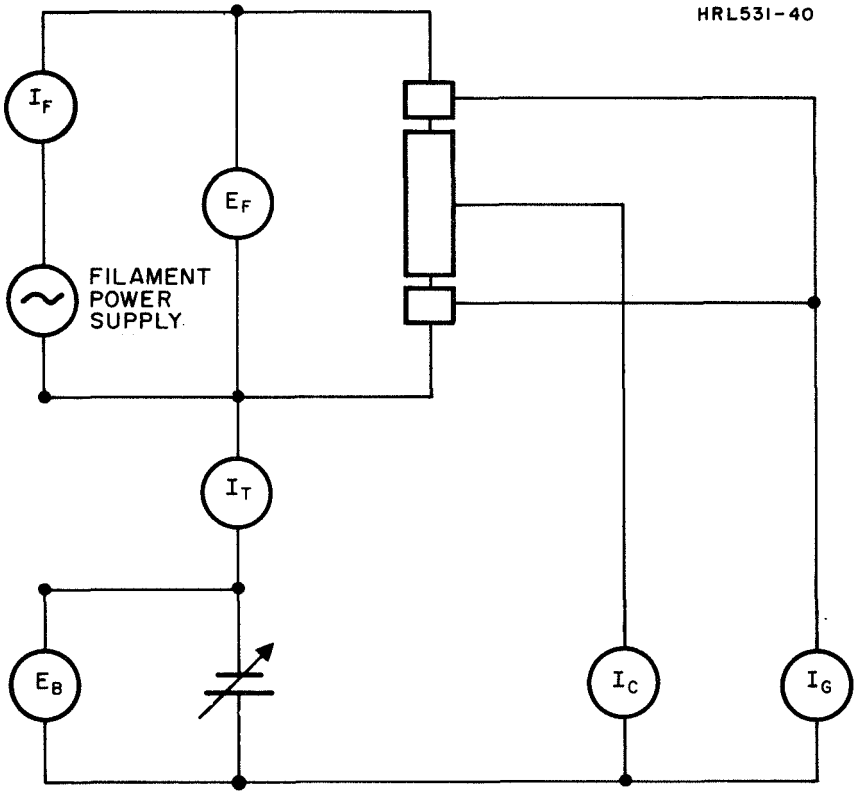

Fig. 42. Diode Circuit used in Neutralizer Tests.

The development of the activation procedure consisted of the following steps. The filament diode assemblies were mounted in the vacuum chamber. (A typical assembly is shown in Fig. 43.) The system was evacuated to a pressure of about 5×10^{-9} Torr. The filaments were processed one at a time. The power was gradually increased so that the filament was heated in about 50°K increments. Evidence of thermionic emission was first observed at a temperature of about 1650 to 1700°K. When the filament temperature reached the 1750 to 1800°K range, the emission gradually increased as a function of time, indicating the activation had begun at this temperature level. Complete activation was achieved by brief flashing (15 to 30 sec) at temperatures between 2200 and 2400°K. Flash heating to 2600°K was attempted and found to produce no change from the 2200 to 2400°K flashing. The lower temperature activation is recommended because of the possibility of damage to the cathode as a result of the loss of thorium metal due to evaporation. At about 2500°K, the loss of thorium becomes significant. Consequently, operation at this point could cause a premature depletion of the thorium metal, thus limiting the cathode life.

All filaments exhibited a unique behavior in the first heat cycle. As the filaments were heated above 1750°K, the apparent temperature increased while the input power remained constant. Subsequent temperature cycles were all on this new power-versus-temperature curve. This irreversible change is shown in Fig. 44. Barnes[20] noted a similar change in emissivity, which he ascribed to the presence of surface roughness resulting from carburization of the filament.

M 7503

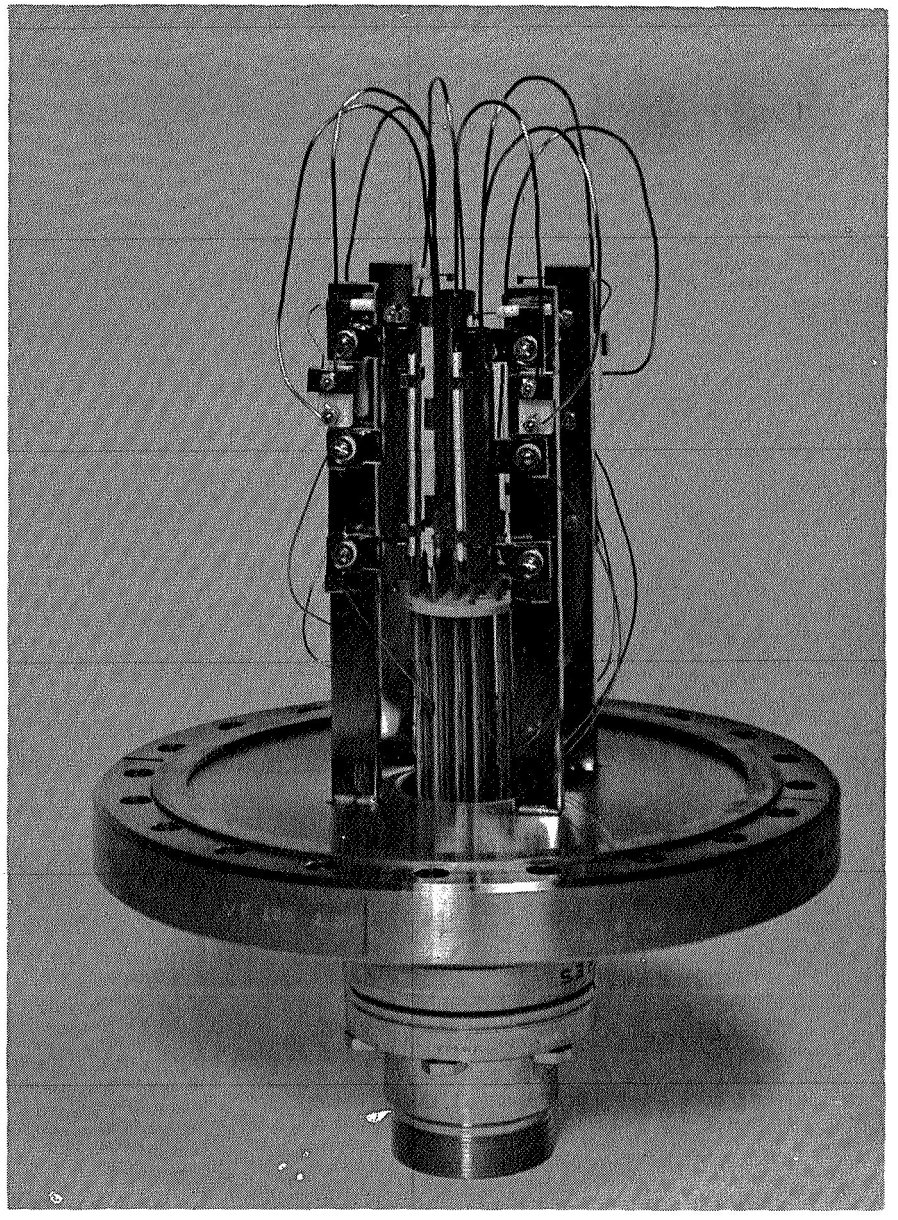

Fig. 43. Photograph of Neutralizers Used in Test.

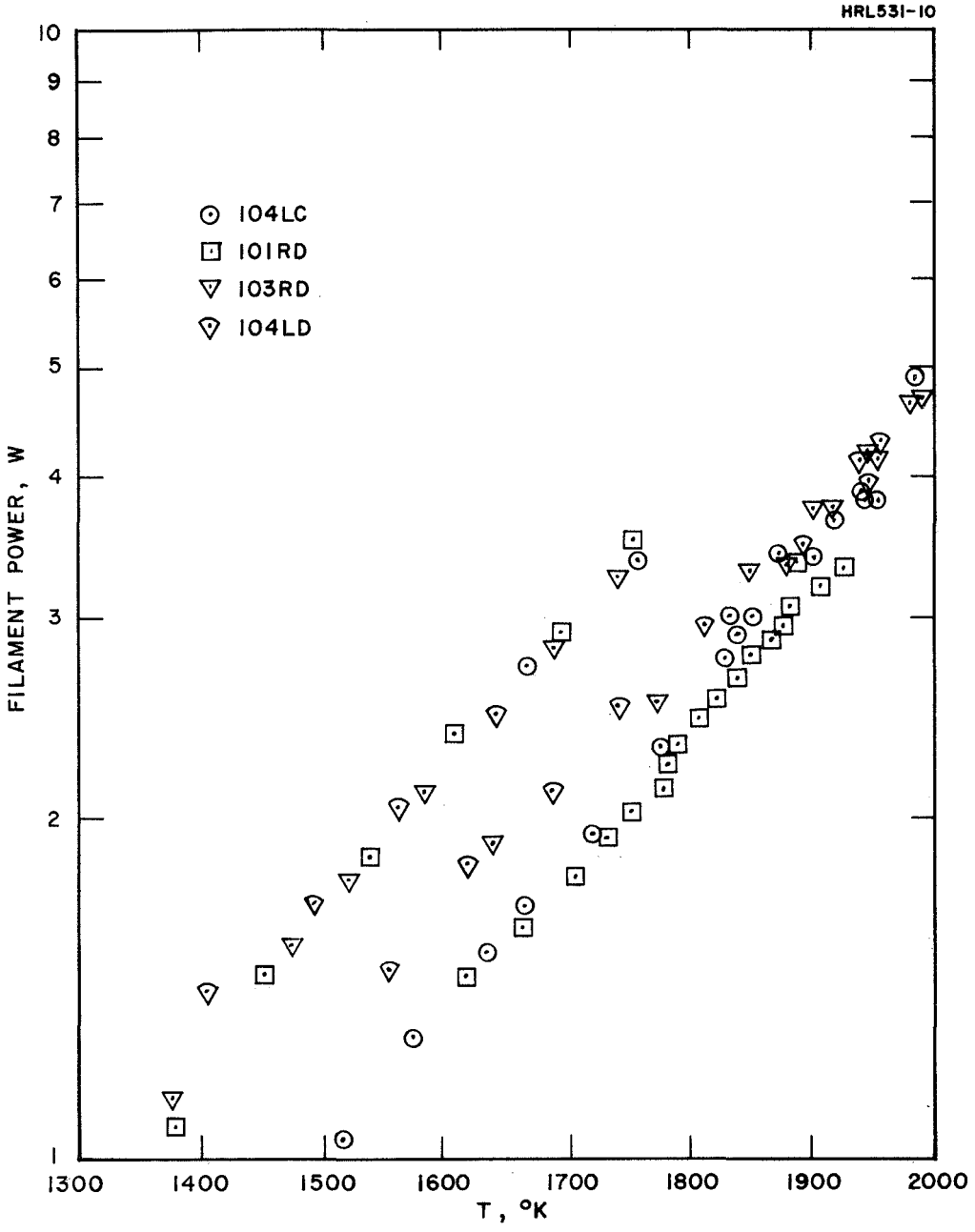

Fig. 44. Filament Power Versus Temperature.

Another possible cause for this change in emissivity is the presence of a thin carbon deposit on the surface. At the end of the carburization process, when the filament heater power is turned off, the temperature decreases to below ∿1800°K, where the diffusion of carbon is very slow but the pyrolysis of the benzene continues to a lower temperature. When the filament is heated to activate it, the carbon film is diffused into the filament, where it reacts to form the carbide. This causes a change in the surface emissivity.

Figure 45 shows the typical I-V characteristics of a filament. The cathode emission and the diode voltage could not be safely increased above these values because 25 W of power being used caused the anode to be heated to about 1000°K. A typical graph of the temperature dependence of the thermionic emission is shown in Fig. 46. The activated filaments exhibited work functions of 3.2 ± 0.1 eV. The filaments produced emission currents of 20 mA/W of input power at temperatures of about 1800 to 1850°K.

Operation of filament 103 LC at 2510°K for three hours resulted in a reduced emission. Prior to the high temperature operation the filament had a 3.15 eV work function at approxi-1900°K. After the 2510°K operation, the work function increased to 3.30 eV. After several days of operation, the emission became unstable and decreased, even though attempts were made to reactivate the surface.

Tests were performed using the planar diode assemblies. The most significant point was the inferior coupling between the cathode and anode. The perveance of this assembly is about 6% of the cylindrical diode. This is seen by comparing the perveance plot for the planar diode (Fig. 47), with that of the cylindrical diode (Fig. 45). In all other respects, the filament operation was similar to the cylindrical diode case.

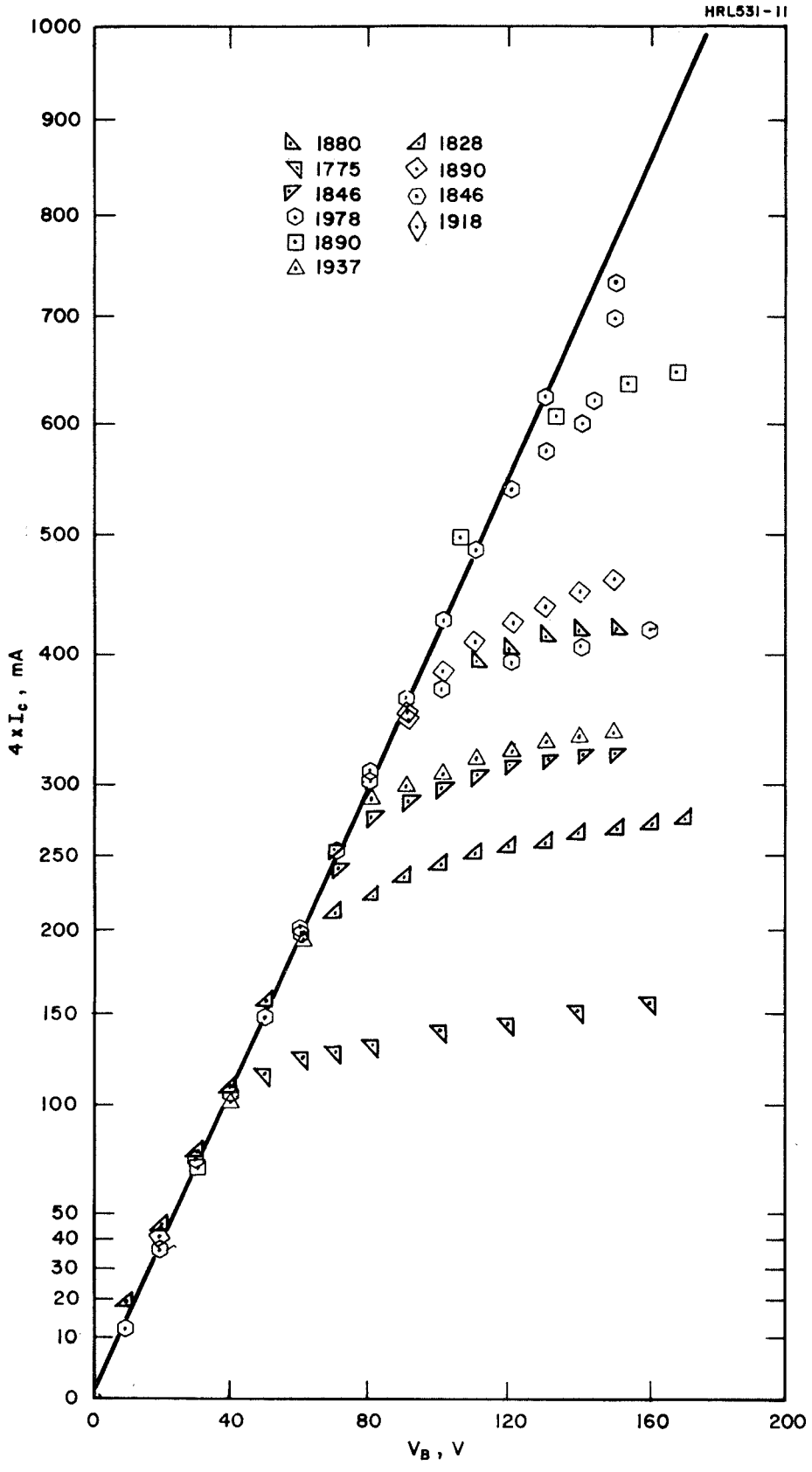

Fig. 45. I-V Characteristics for a Filament.

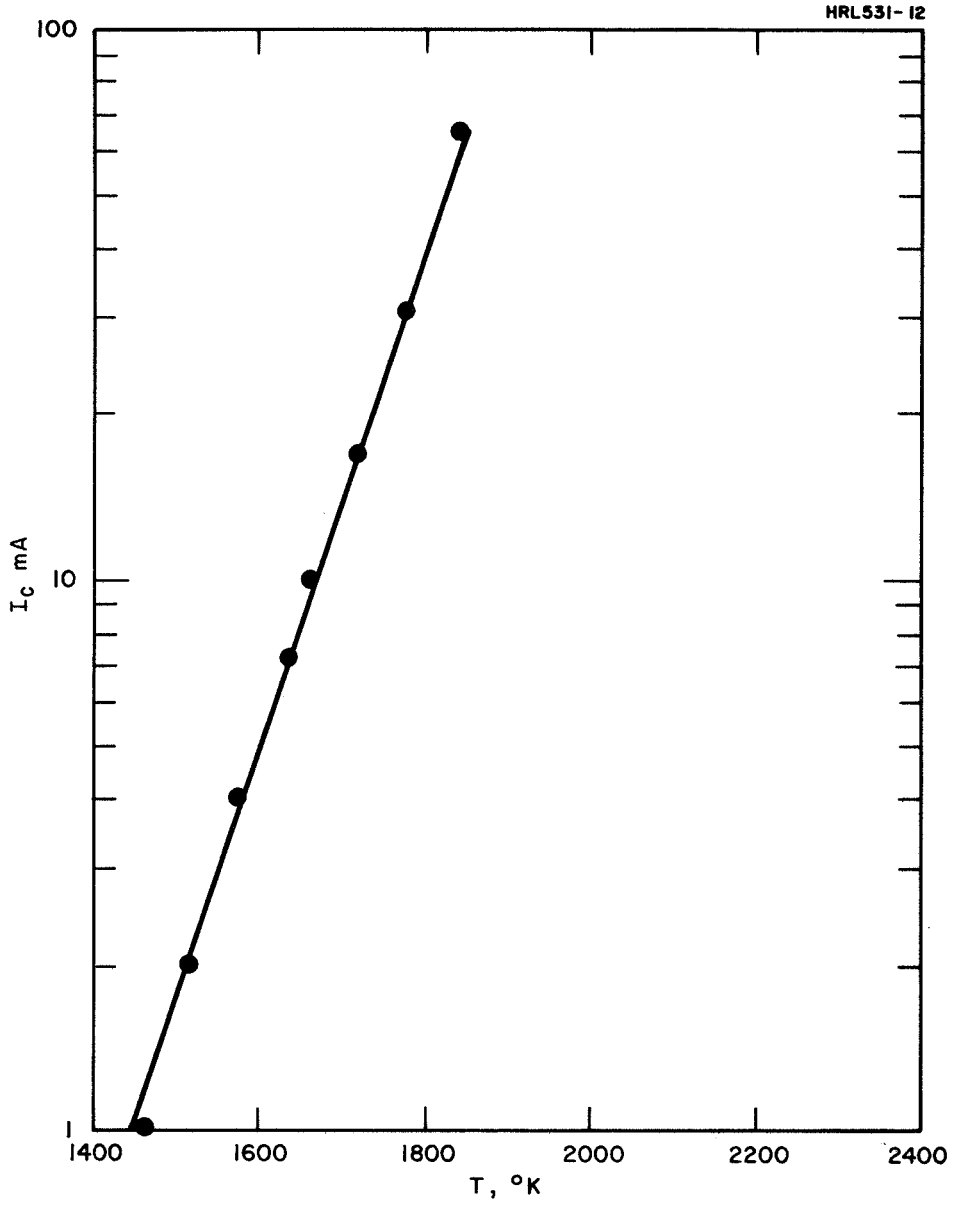

Fig. 46. Emission Current Versus Temperature.

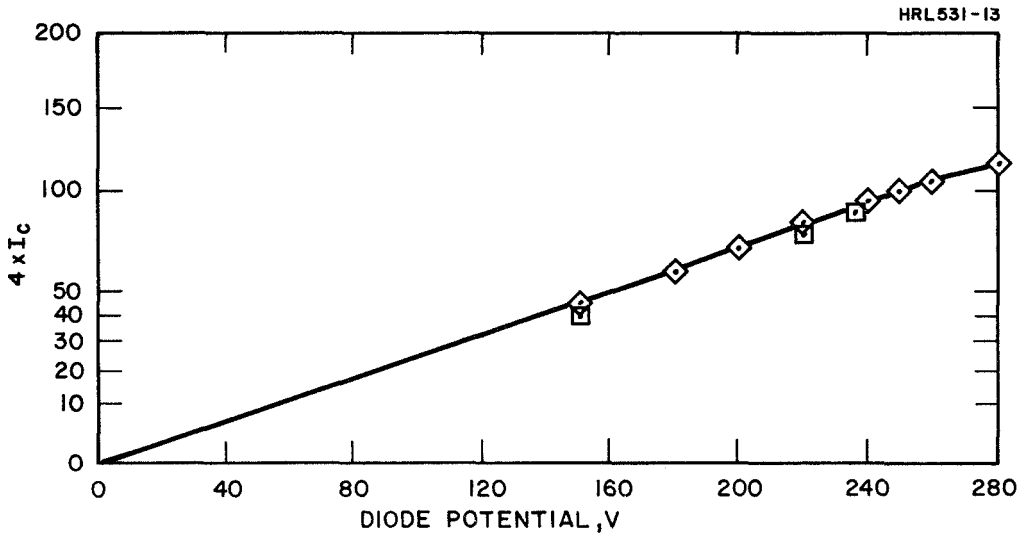

Fig. 47. Perveance Curve for Planar Diode.

D. LIFE TEST

A life test was planned to test the stability of the carburized thoriated tungsten filaments. A 500 hour test was called for in the contract; however, this test ran for nearly 2400 hours and was terminated at the end of the contract period. The results are summarized in Table VI. The cathode emission efficiency gradually increased over this period. This change may be associated with the gradual improvement in the vacuum conditions during the course of the test. The change may be due to a slight variation in temperature associated with a surface change. Also the amount of thorium on the surface may have changed gradually.

The most significant result was the observation that both filaments were capable of producing more than 40 mA/W for periods greater than 2000 hours.

Before the life test was completed, the dual beam thruster system was delivered to NASA Lewis Research Center. The filaments delivered with this thruster were processed in the same way as those prepared for the neutralizer life test.

TABLE VI

Life Test of Neutralizers

Filament	Hours	W	Total mA	T°K	mA/W	P
103 RD	Start	3.36	94	1874	28	1.0×10^{-8}
	528-1/2	3.33	123	—	37	3.5×10^{-9}
	1272-1/2	3.32	142	1903	43	1.9×10^{-9}
	1938-1/2	3.38	159	1929	47	1.7×10^{-9}
	2390-1/2	3.375	158	1934	47	1.7×10^{-9}
104 LD	Start	2.98	102	1863	34	1.6×10^{-8}
	504	2.95	108	—	37	3.5×10^{-9}
	1248	2.94	120	1881	41	1.9×10^{-9}
	1914	2.94	125	—	42.5	1.7×10^{-9}
	2366	2.93	125	—	42.6	1.7×10^{-9}

T195

SECTION V

THRUSTER TEST RESULTS AT HUGHES RESEARCH LABORATORIES

The testing performed for this program was accomplished in a 4 ft diameter by 10 ft long vacuum chamber. This chamber has been used only to test cesium ion thrusters and is pumped with a large oil diffusion pump and a liquid nitrogen cryo-liner. The chamber is capable of producing pressures on the 10^{-7} Torr scale.

The first phase of the test plan was to obtain neutral fraction data, perveance measurements, and critical temperatures. The thruster was mounted with two neutral detectors which were similar to the one described in Ref. 22. Figure 48 is a photograph of the neutral detectors and the thruster. The front of the thruster can be seen in the center of the ground shield and support plate. One neutral detector was aligned so that it viewed the central position of strip 1 on the ionizer axis. The second detector was aligned so it viewed a central portion of Strip 2 slightly off axis. The purpose of the off-axis measurement was to evaluate the effect of the voltage gradients formed by the deflection voltages. The beam of Strip 1 when deflected, does not intersect the beam of the orthogonal strip, designated Strip 2.

After the thruster and detectors were placed in the vacuum chamber and the pressure in the chamber was 10^{-7}Torr, the feed systems were vented by turning on the vent valve power supplies and manually keeping the current level at 2 A. The pressure rise, caused by the gas escaping from the system, was readily observed on the pressure monitoring system of the vacuum chamber. These pressures are shown as a function of time in Fig. 49. It can be seen that the pressure changed from the low 10^{-7} Torr range,

M 7881

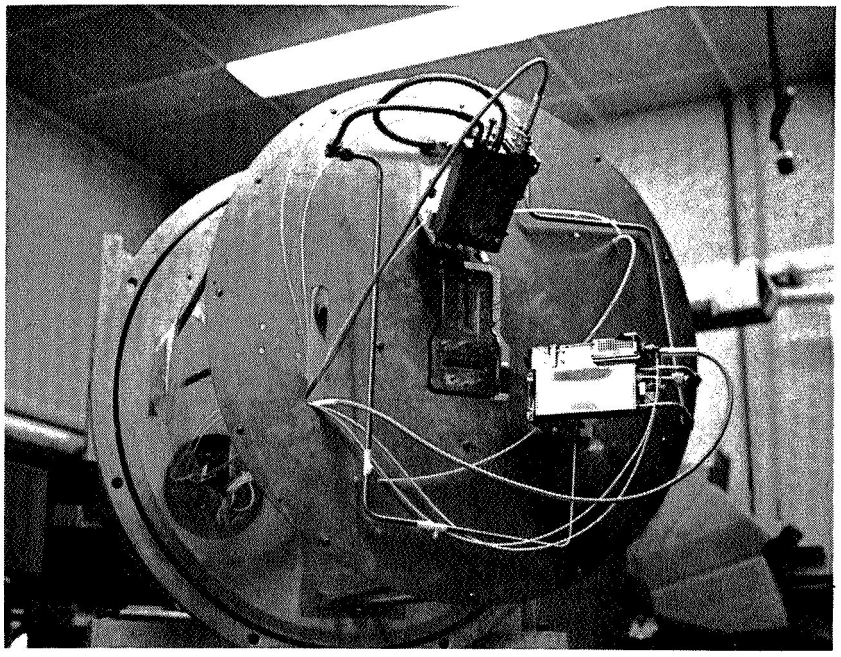

Fig. 48. Neutral Atom Detectors and Dual Beam Thruster System.

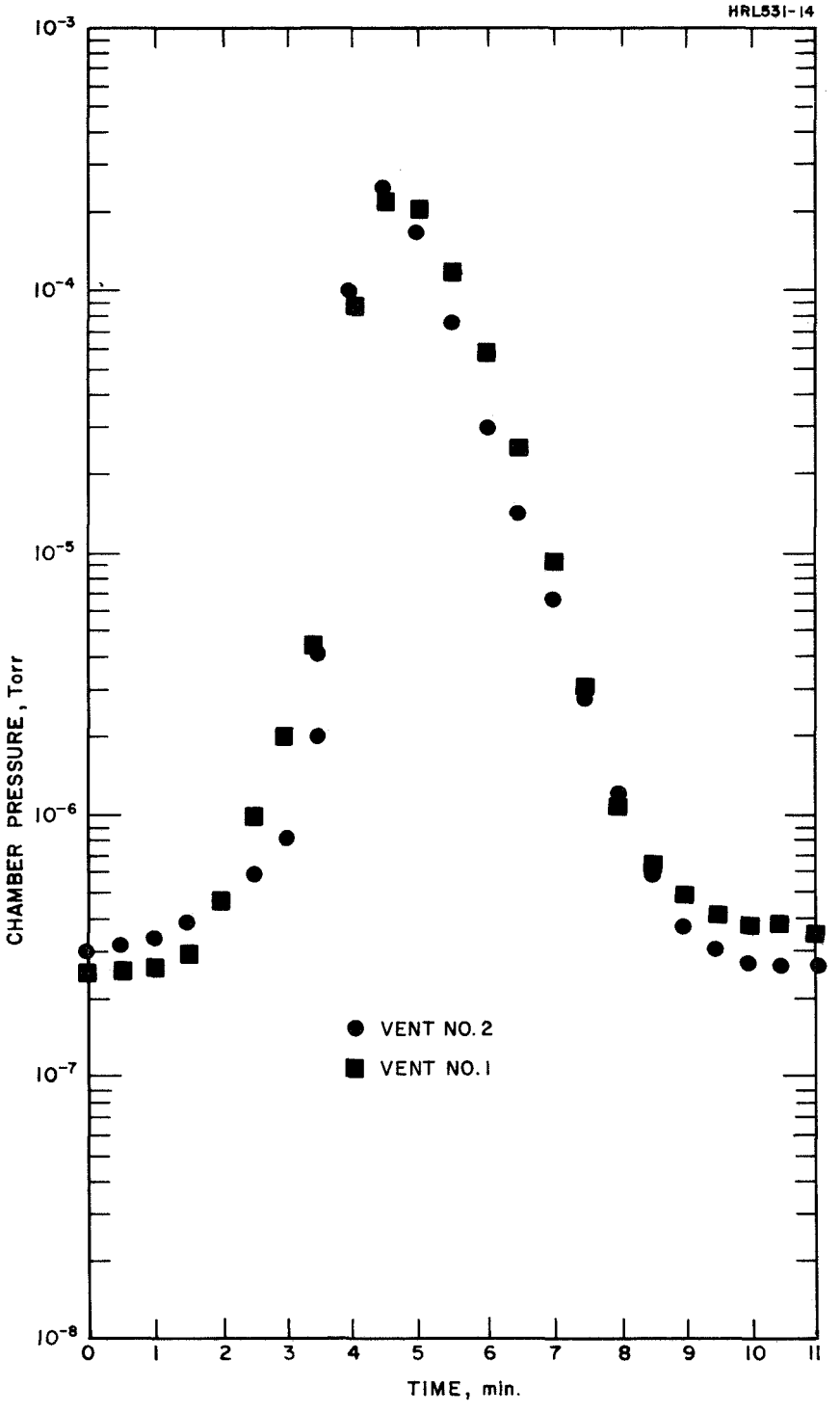

Fig. 49. Pressure Versus Time for Vent Valves Opening.

to the low 10^{-4} Torr range, and back to the low 10^{-7} Torr range during the 10 min venting cycle. Throughout the test phase, ionizer power versus ionizer temperature curves were recorded. Typical results shown in Fig. 50, were obtained with an optical pyrometer located at the end of the chamber. These results have been corrected for emissivity of the porous tungsten and loss in the window and show the strip temperatures are nearly the same for equal power levels. Strip 1 was used first to obtain an ion beam. A beam was obtained approximately ten minutes after the vaporizer was turned on. The control loop regulated the beam without any difficulties. Four thrust levels were obtained, as shown in Table VII. The data were taken over a 3-1/2 hour period. The ionizer temperature was operated much higher than necessary because the condition of the ionizer was unknown. For this reason 125 W was used for the full thrust ion beam.

After the full thrust level had been reached and appeared to be stable, an attempt was made to take a perveance curve. Unfortunately, the excess cesium vapor created by these measurements, caused excessive leakage currents and the test was terminated. During these tests, arcing was observed in the vicinity of the leads going from the thruster electrical terminals to the accelerating electrodes. These Kapton covered leads were replaced with bare wire leads and the arcing disappeared in subsequent tests.

Strip 2 was operated at the four thrust levels. The results, comparable to Strip 1 results, are shown in Table VIII.

Neutral fraction data were obtained for various current densities for Strip 1 and Strip 2 and are shown in Fig. 51. Strip 2 has a lower neutral flux and it is not as "clean"

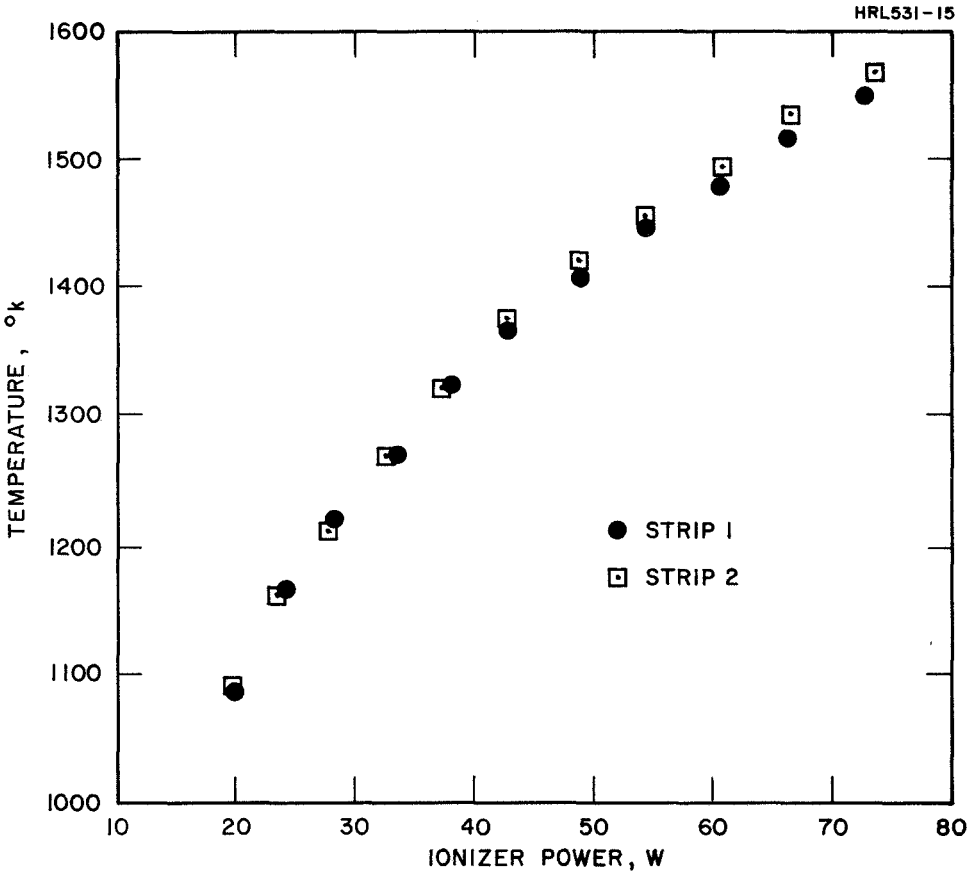

Fig. 50. Ionizer Temperature Versus Ionizer Power.

TABLE VII

Strip 1 Initial Test

Beam Voltage	1.67 kV	1.67 kV	1.67 kV	1.67 kV
Beam Current	5 mA	10 mA	14.7 mA	19.7 mA
Accel Voltage	-5 kV	-5 kV	-5 kV	-5.5 kV
Accel Current	0.04 mA	0.02 mA	0.22 mA	0.38 mA
Ionizer Temperature	1443°K	1443°K	1558°K	1598°K
Ionizer Power	54 W	54 W	73.8 W	80.7 W
Vaporizer Power	4.97 W	6.27 W	7.9 W	6.52 W
Vent Power	2.45 W	2.45 W	2.45 W	2.45 W
Beam Power	8.39 W	16.7 W	24.5 W	32.9 W
Accel Power	0.2 W	0.1 W	1.1 W	1.9 W
Total Power	70 W	80 W	110 W	125 W

T196

TABLE VIII

Strip 2 Initial Test

Beam Voltage	1.67 kV	1.67 kV	1.67 kV	1.67 kV
Beam Current	5 mA	10 mA	15 mA	20 mA
Accel Voltage	-5.5 kV	-5.5 kV	-5.5 kV	-5.5 kV
Accel Current	0.12 mA	0.15 mA	0.65 mA	1.15 mA
Ionizer Temperature	1595°K	1595°K	1595°K	1595°K
Ionizer Power	73.70 W	73.70 W	73.70 W	73.70 W
Vaporizer Power	8.39 W	9.05 W	9.50 W	9.35 W
Vent Power	2.78 W	2.78 W	2.78 W	2.78 W
Beam Power	8.34 W	16.70 W	25.00 W	33.40 W
Accel Power	0.66 W	0.83 W	3.58 W	6.32 W
Total Power	94 W	103 W	115 W	126 W

T197

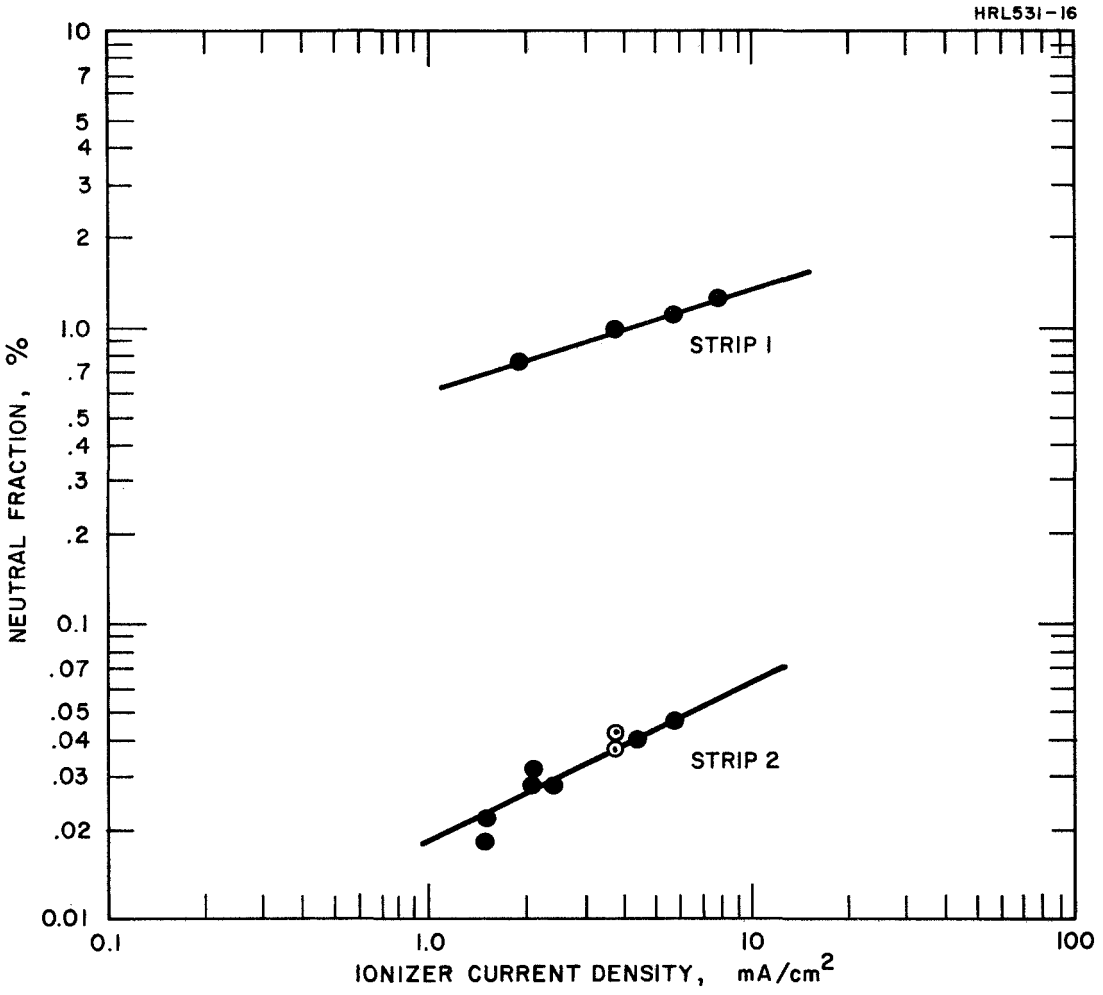

Fig. 51. Neutral Fraction Versus Ionizer Current Density for Strip 1 and Strip 2.

as Strip 2. These curves were not taken at the same time, thus the history of operating times for each strip are different. These results indicate that the critical temperature of each strip also should be different. Figure 52 illustrates this difference. The critical temperature for Strip 2 was 1325°K, and 1440°K for Strip 1, again showing that Strip 1 was not as clean as Strip 2. There is no data point shown for Strip 1 below 1459°K, because at 1425°K the neutral flux increased so quickly that the measurement had no meaning, other than the neutral flux was quite high.

Neutral fraction data also were taken for a deflected 25 mA beam on Strip 2. The deflection voltage across the accel electrodes was ±700 V. It was believed this would give a beam deflection of ±20°. The neutral fraction was 1.15% and 1.31% for the respective deflections. Although there is a slight difference, it is quite small. The effect would have been more pronounced if the neutral detector viewed the edge of the ionizer, but the mount for the detector did not allow this freedom of movement.

One of the problems encountered in these earlier tests was the dependence of the accel currents upon neutral flux. For this reason, the neutral detectors were used to determine the critical temperatures and the knee of the perveance curves. The detectors provided a more sensitive measurement than the conventional method of measuring the beam current. The knee of the perveance curves were found for the two strips and are shown in Fig. 53. This data shows that for a 5 mA beam, the total accelerating voltage should be above 3.5 kV to minimize the neutral flux. A conventional perveance curve taken on Strip 1 is shown in Fig. 54; it shows that the break is not sharp between the flow limited and space charge limited case. The two 20 mA points shown

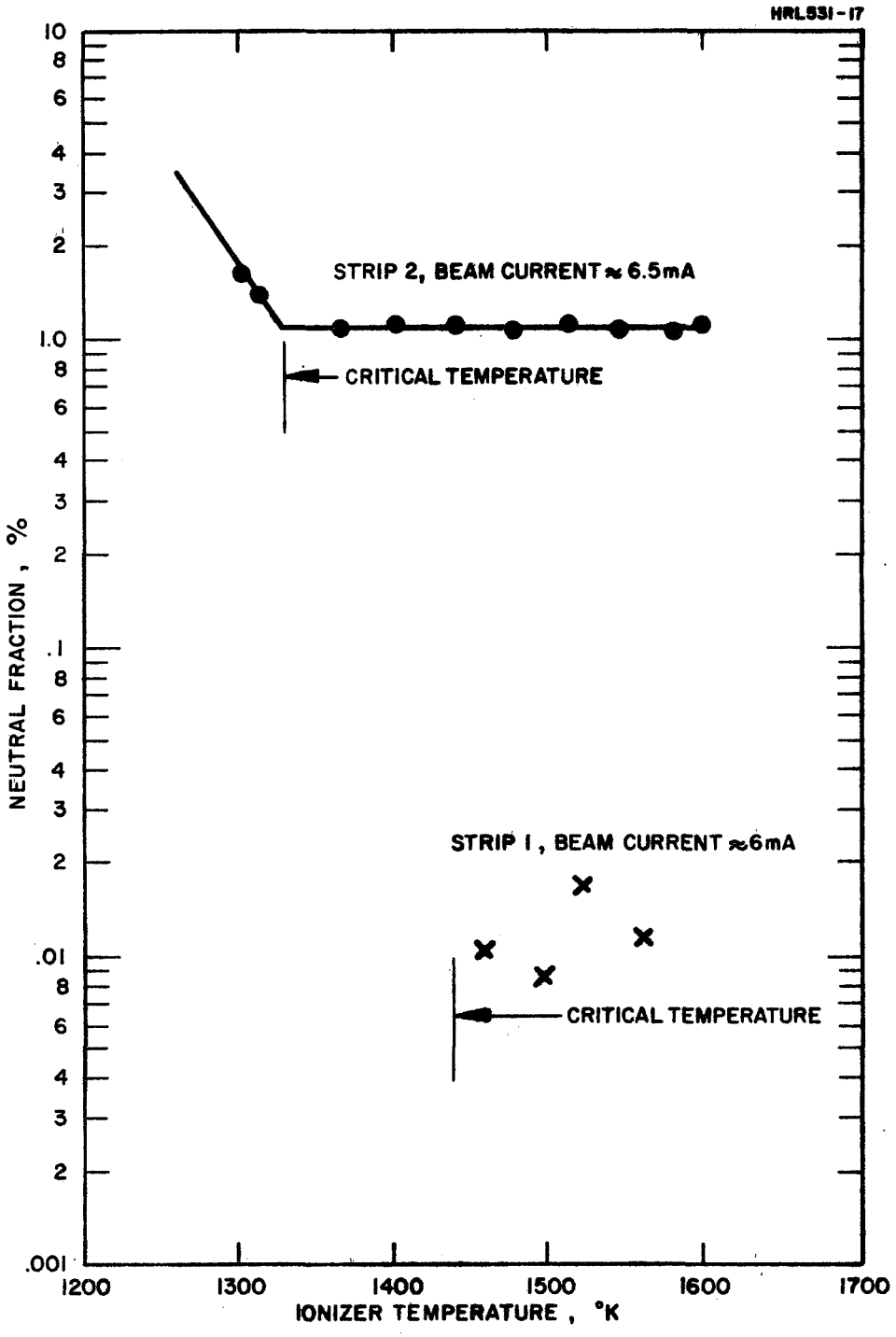

Fig. 52. Neutral Fraction Versus Ionizer Temperature for Strip 1 and Strip 2.

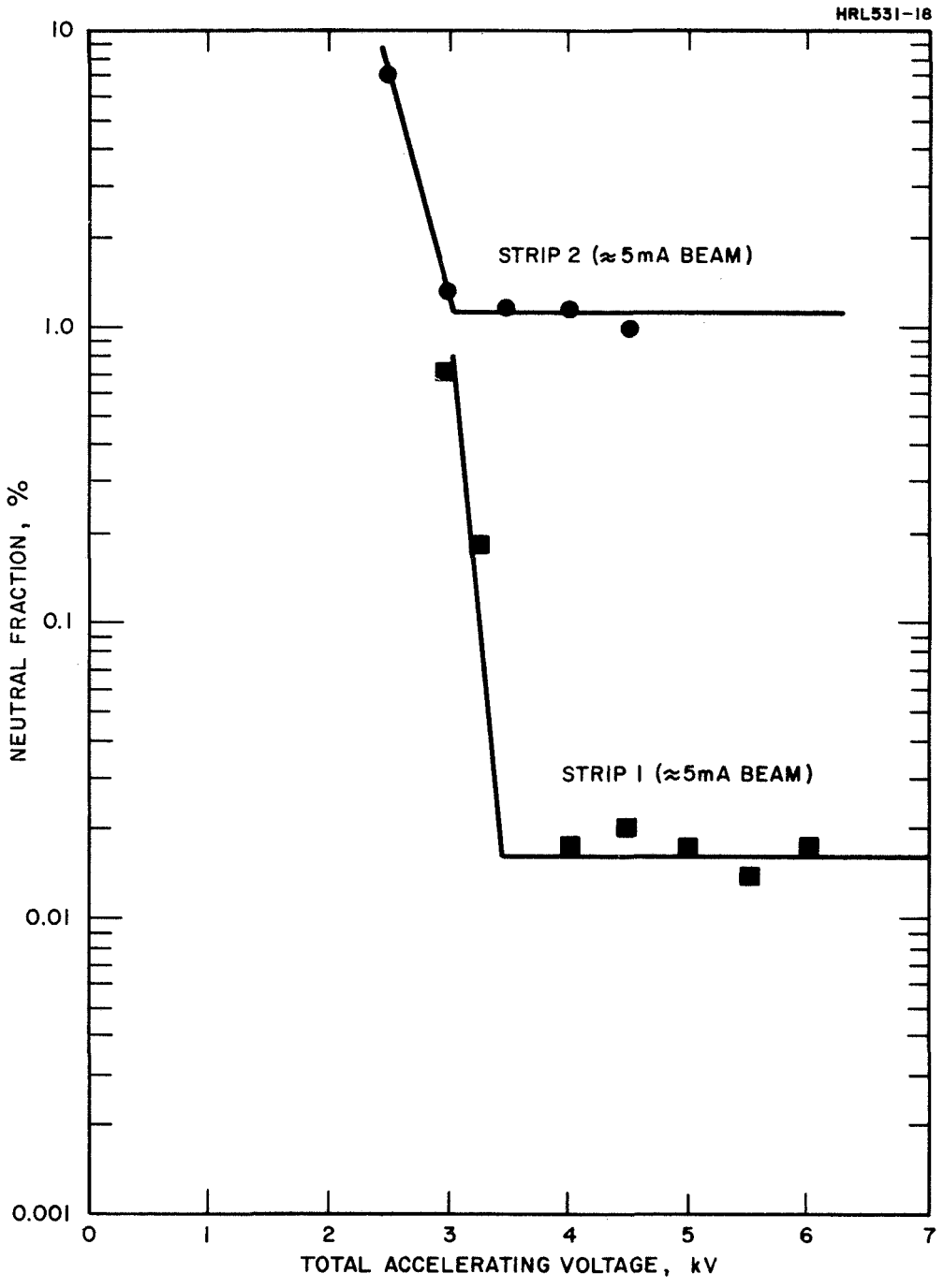

Fig. 53. Determination of Knee of Perveance Curve for Strip 1 and Strip 2.

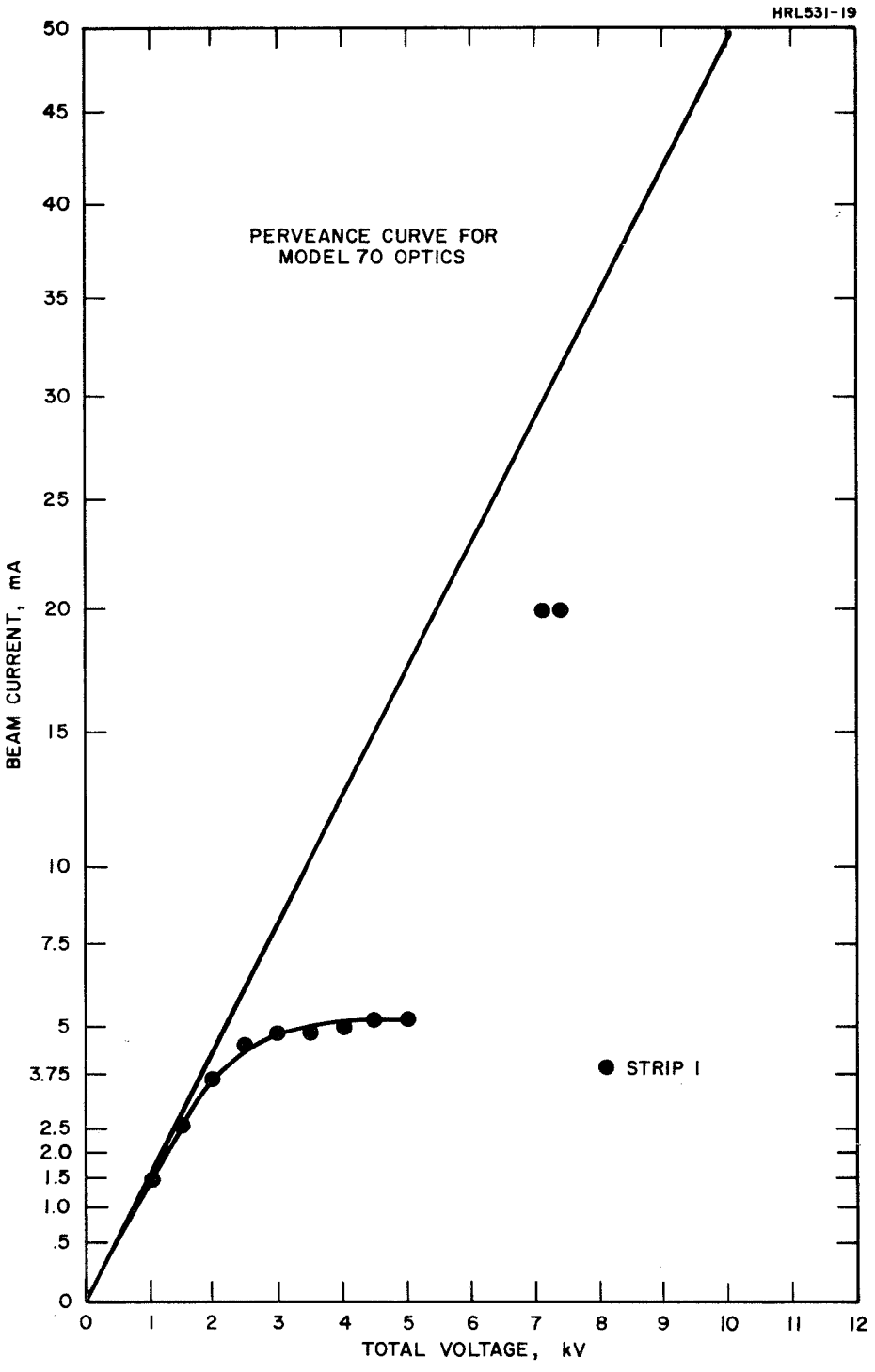

Fig. 54. Perveance of Strip 1.

in Fig. 54 were taken at 20 mA just before the accel voltage was dropped, and the accel current became too large to continue the curve.

At the end of these measurements it was decided to change the design of the insulators that supported the accel electrode. The insulator was changed from a cylindrical shape to a mushroom shape. The mushroom design was used to provide a larger insulator surface between the accel and exit electrode. After this change was completed, the deflection measurements were made.

Two scanners were used for the deflection experiments. The scanners were swung along an arc of a circle, whose center was on the axis of the ionizer, as shown in Fig. 55. The scanners were Faraday type collectors with a slit 0.020 in. wide and 12 in. long. Figure 56 shows the scanners with the thruster mounted on an endplate. The scanner for Strip 1 is moved aside and the scanner for Strip 2 is directly opposite Strip 2. Most of the data were taken with the scanners 12 in. from the ionizers. One group of scans was taken at a distance 18 in. from the ionizer; the results were identical to the 12 in. scan.

A typical scan is shown in Fig. 57. The data shown is from an x-y recorder. The collector intensity is shown along the y-axis, and the position of the detector is shown along the x-axis. The collector swings 140° for each trace and is driven by a 1 rpm electric rotor. The first trace taken is for the undeflected beam (i.e., -5 kV on each deflection electrode), and is designated by $2\delta V = 0$ in Fig. 57. The second trace is displayed one-half inches along the y-axis for clarity and is for a measured $2\delta V = 400$ V across the deflection electrodes, i.e., -5.2 kV on one deflecting electrode and -4.8 kV on the other electrode. The $2\delta V$ is

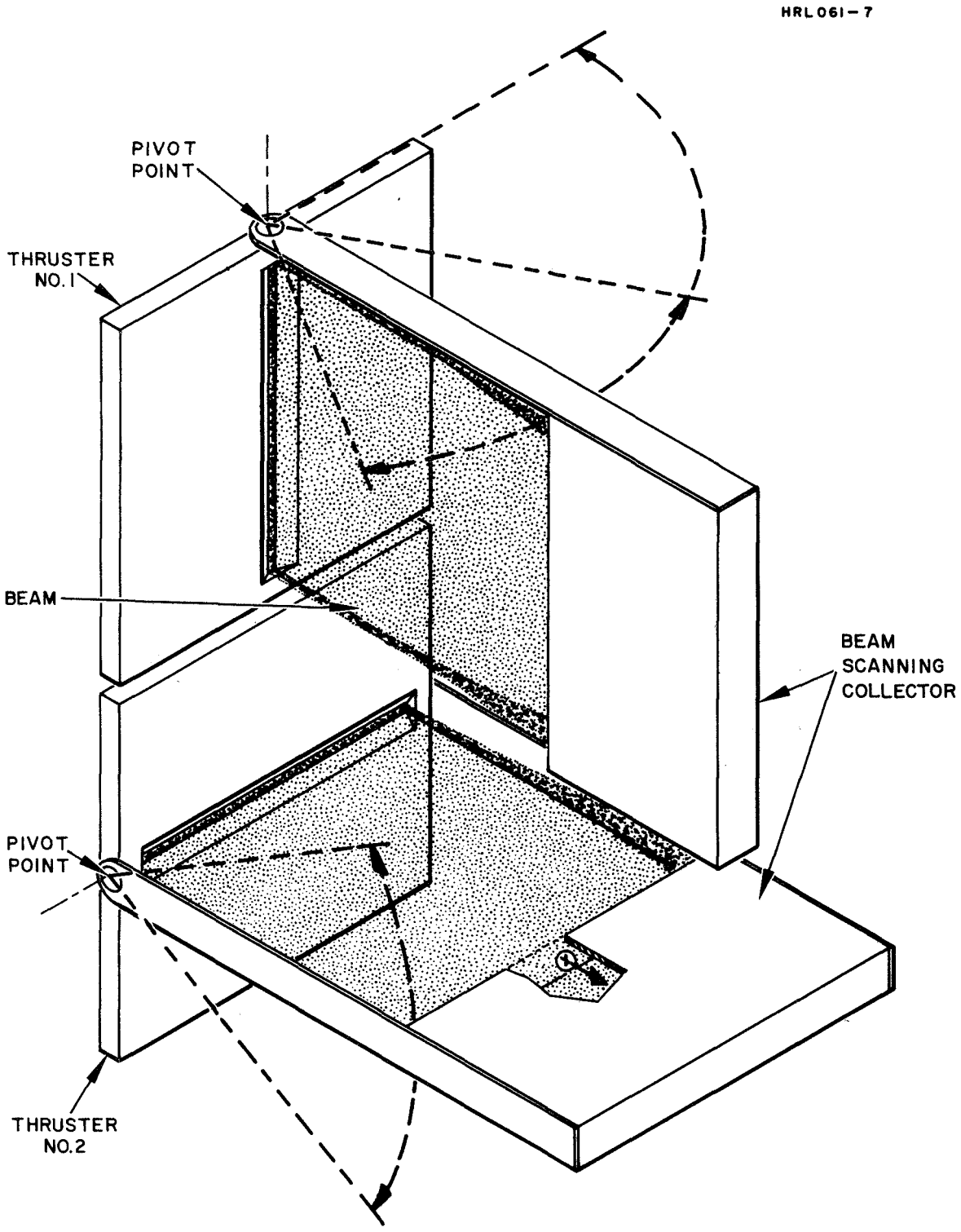

Fig. 55. Artist Concept of Beam Scanners.

M 7880

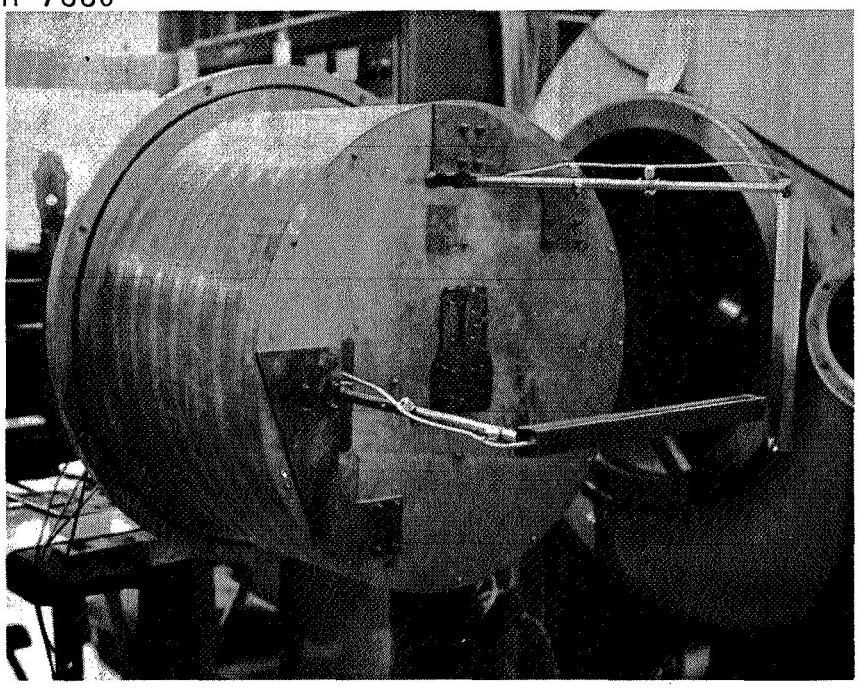

Fig. 56. Beam Scanners and Front View of Dual Beam Thruster.

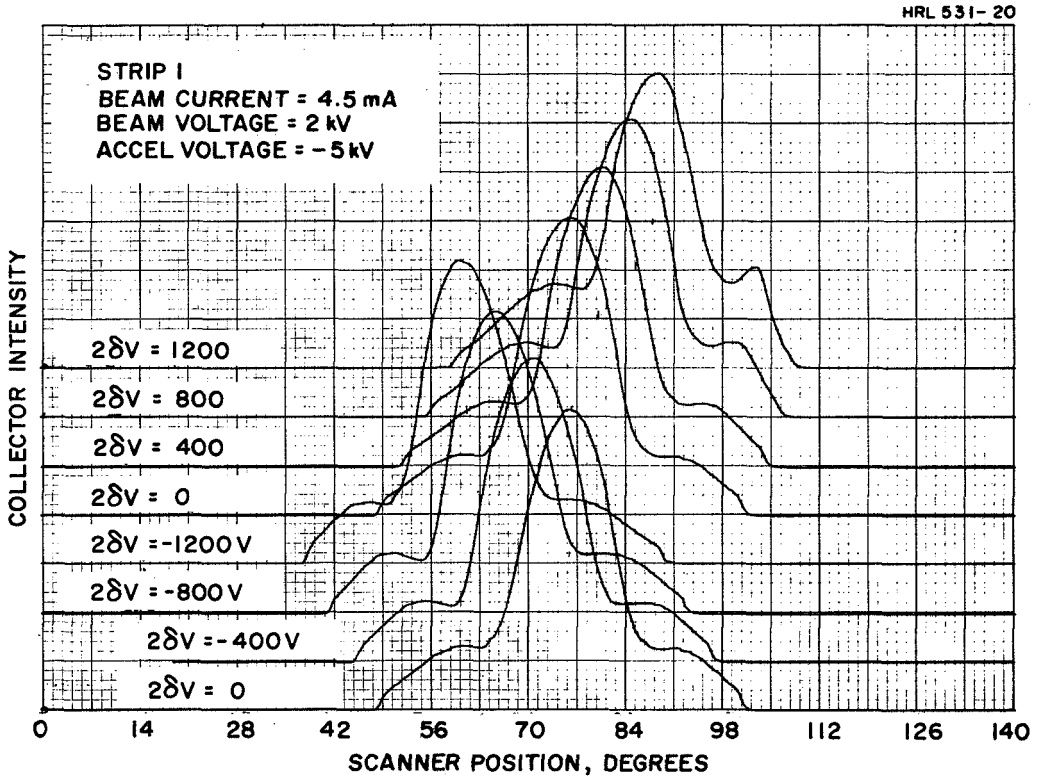

Fig. 57. Typical Beam Scans for Strip 1.

increased in 400 V steps to 1200 V, and then reversed so the beam is deflected in the opposite direction. The minus sign on the $2\delta V$ means the beam is deflected toward electrode X_1 and toward X_2 for a positive $2\delta V$ (see Fig. 58). The angular deflection of the beam calculated is an average and is measured with respect to the undeflected beam. The angular deflection for Strip 1 is shown in Fig. 59. Most of the data were taken with a 12 in. scanning distance. One set of data was taken with an 18 in. scan for a 4.5 mA beam. These data are shown as empty circles. Three of the four points were identical to those obtained with a 12 in. scan.

As the beam increases, it can be seen that deflection increases. The maximum deflection obtained was 24° for an 18 mA beam. The voltages required for this deflection are in agreement with those predicted by the analytical studies. These voltages can produce leakage currents across accel insulators by using the present design. This leakage can be avoided with longer insulation path lengths, and will be discussed later.

Figure 60 shows the deflection data for Strip 2. It is practically the same as Strip 1 with no more than a 1° difference in the two strips. Figures 59 and 60 are the calibration curves for the deflection system.

These experimental results have already been discussed and compared with the analytical results in Section III-D.

The final test to be performed before delivery, as defined in the contract, was a 24 hour operation of the thruster system. The thruster was taken apart and cleaned. The copper gaskets between the feed system and ionizers were replaced when the thruster was assembled. The thruster was then ready for the 24 hour test. The test was successfully completed with the pressure in the chamber never higher than 4×10^{-6} Torr, nor lower than 7×10^{-8} Torr.

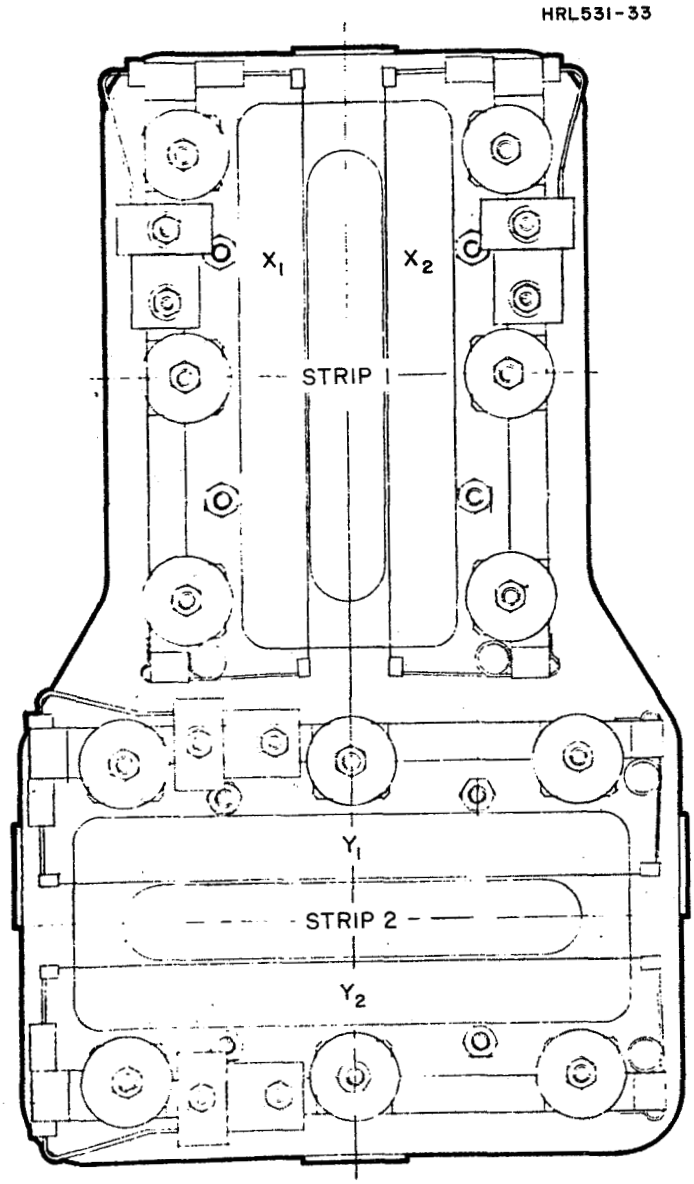

Fig. 58. Front View of Dual Beam Thruster Showing X_1, X_2, Y_1, and Y_2 Designations.

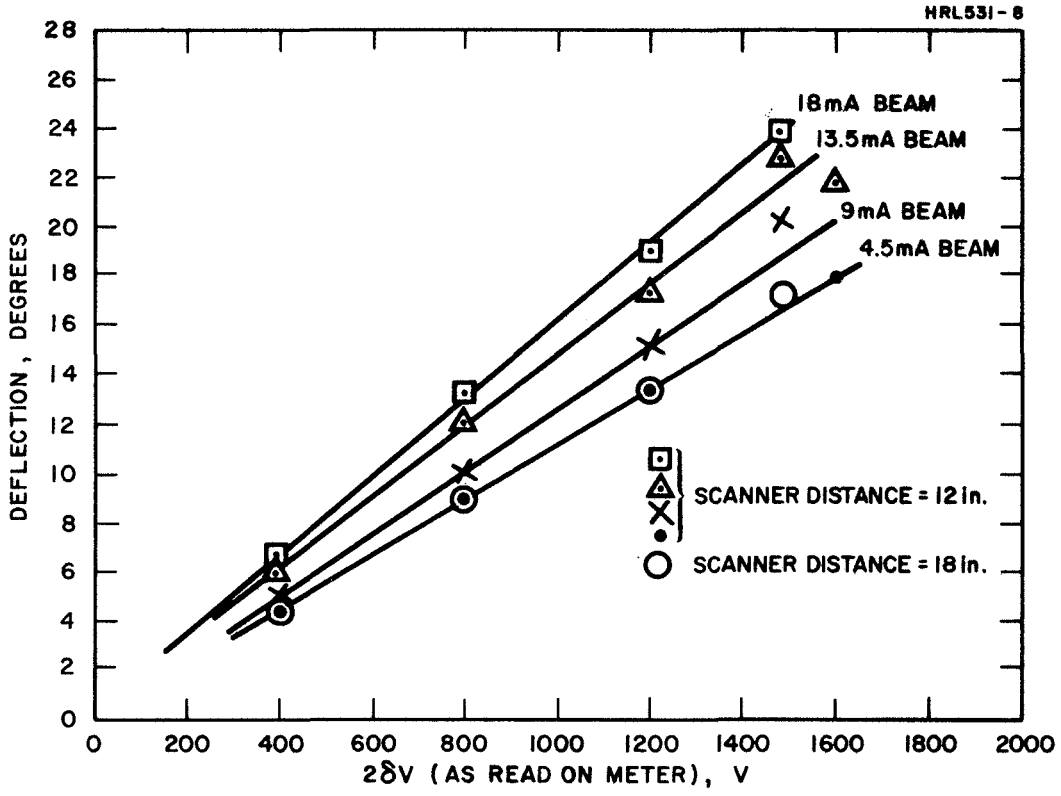

Fig. 59. Deflection Data for Strip 1.

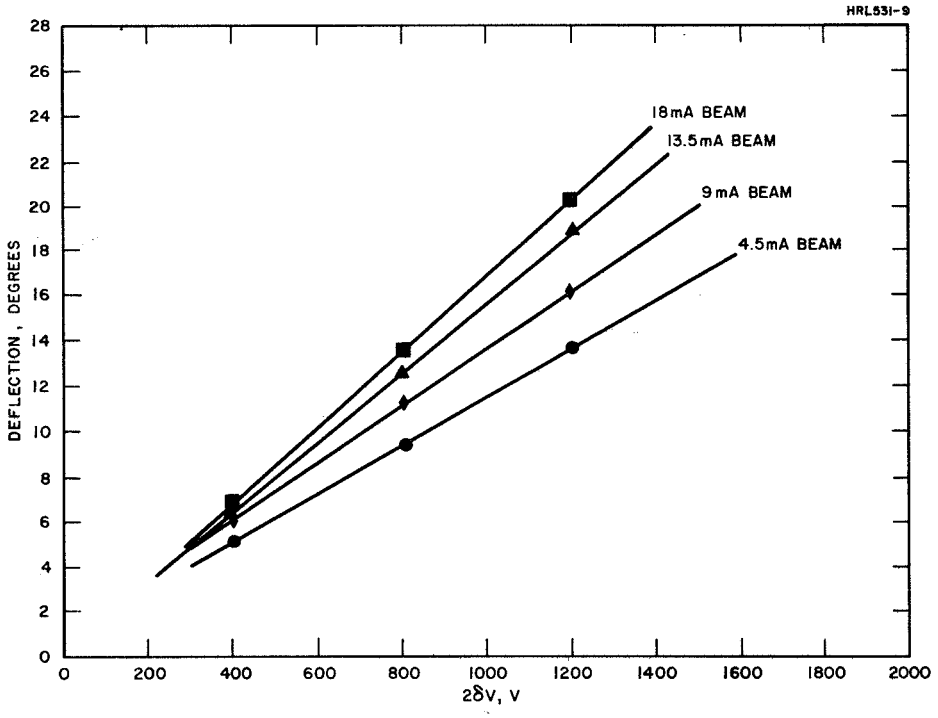

Fig. 60. Deflection Data for Strip 2.

The quantities measured during the 24 hour test can best be shown with the aid of the electrical schematic in Fig. 61. The operational times during the test for each thrust level and strip are shown in Table IX. Operational times shown for Strip 1 include the time it was operated alone and with Strip 2. Strip 2 was operated only when Strip 1 was operating. The 24 hour test was defined as a total of 24 hours of operation of both strips at equal thrust levels. From the results in Table IX, it can be seen that Strip 1 was run for a total time of 33 hours, 58 min, and both strips were run at equal thrust levels for 24 hours and 18 min. Transition times were not included in the table. This would add approximately 30 min to each strip. Some typical data points taken from the test prior to any beam deflection, while both strips were operating, are shown in Table X. The largest amount of power used in each strip goes to the ionizer at the 100% thrust level, because the ionizers are not clean. Past experience shows that 100 to 200 hours of operation are required for the ionizers to clean up in the oil diffusion-pumped vacuum systems used for testing the thruster. The cleanup time in space or in an ultra high vacuum chamber is believed to be less. When an ionizer is clean, it will operate satisfactorily at 1550°K. Table X shows that a temperature of 1523°K was required. By referring to Fig. 50 again, it can be seen that for a clean ionizer, the ionizer power would drop to about 40 to 45 W for each strip. This is a decrease of 20 to 25 W for each strip from the power used at the 100% thrust level shown in Table X.

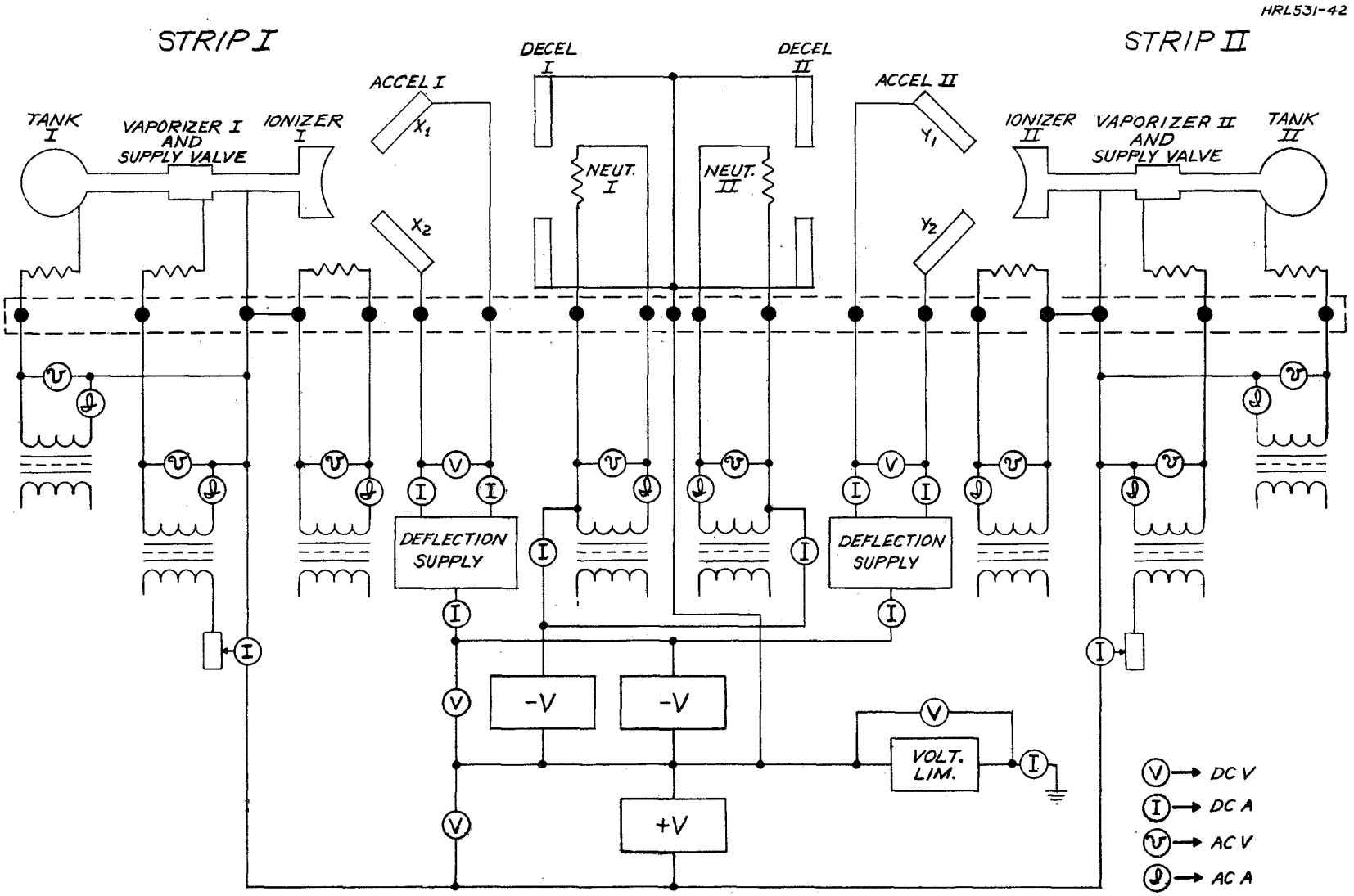

Fig. 61. Electric Schematic Dual Beam Thruster System.

TABLE IX

Thrust Levels Versus Time

	Strip 1				Strip 2			
Thrust Level, %	25	50	75	100	25	50	75	100
Operating Time, Hours:Min	8:48	14:19	3:02	7:50	5:05	12:33	2:57	3:43

T200

During the test, the beam was deflected at different thrust levels and the deflection voltage and accel currents recorded. Figure 58 shows a front view of the thruster and the designation of neutralizers and accel electrodes. The neutralizers and accel electrode location for Strip 1, are designated X_1 and X_2, while the Y_1 and Y_2 designations refer to those of Strip 2. The results of the beam deflection are shown in Tables XI, XII, and XIII. The $2\delta V$ in the first column is the voltage across the pair of deflecting electrodes. The minus sign means electrodes X_2 and Y_2 are more negative, while X_1 and Y_1 are more positive than the case for the undeflected case where $2\delta V = 0$. All cases show that increased currents in the accel electrodes are the result of resistive leakage to ground, and not interception.

In order to obtain the average value of the angle of deflection, the calibration curves for the various thrust levels are used (Fig. 59 and Fig. 60). It can be shown that the calibration curves were obtained for a beam voltage of +2 kV and accel voltage of -5 kV. Since the deflection angle is related to ($2\delta V$/accel voltage), there would be a slight correction factor for the deflection values. When the accel voltage is -5.5 kV, the deflection is slightly less than that presented in Figs. 59 and 60, while it would be greater for accel voltages of -4 kV and -3.5 kV. Precise correction

TABLE X

Thruster Performance

Strip 1				
Thrust Level	25%	50%	75%	100%
Beam Voltage	2 kV	2 kV 2	2 kV	2 kV
Beam Current	4.5 mA	9 mA	13.5 mA	18 mA
Accel Voltage	-5.5 kV	-5.5 kV	-5.5 kV	-5.5 kV
Accel Current	0.33 mA	0.45 mA	0.92 mA	1.1 mA
Ionizer Temperature	1455°K	1454°K	1496°K	1523°K
Ionizer Power	54.7 W	54.7 W	60.7 W	66 W
Vaporizer Power	5.03 W	6.4 W	7.1 W	10.32 W
Beam Power	9.0 W	18.0 W	27 W	36 W
Accel Power	1.8 W	2.47 W	5.06 W	6.05 W
Neutralizer Power	2.63 W	2.63 W	2.63 W	2.63 W
Total Power	73.2 W	84.2 W	102.5 W	121 W
Strip 2				
Thrust Level	25%	50%	75%	100%
Beam Voltage	2 kV	2 kV	2 kV	2 kV
Beam Current	4.5 mA	9 mA	13.5 mA	18 mA
Accel Voltage	-5.5 kV	-5.5 kV	-5.5 kV	-5.5 kV
Accel Current	0.21 mA	0.26 mA	0.45 mA	1.24 mA
Ionizer Temperature	1458°K	1462°K	1462°K	1532°K
Ionizer Power	54.7 W	54.7 W	55.3 W	67.4 W
Vaporizer Power	5.25 W	6.32 W	6.76 W	9.62 W
Beam Power	9.0 W	18.0 W	27 W	36 W
Accel Power	1.15 W	1.43 W	2.48 W	6.87 W
Neutralizer Power	2.63 W	2.63 W	2.63 W	2.63 W
Total Power	72.7 W	83.1 W	94.17 W	122.5 W

T201

TABLE XI

Beam Deflection Results at 100% Thrust Level
Beam Voltage = 2 kV; Beam Current = 18 mA; Accel Voltage = -5.5 kV

Deflection Voltage $2\delta V$, V	Strip 1			Strip 2		
	Accel Current X_2, mA	Accel Current X_1, mA	Beam Toward Electrode	Accel Current Y_2, mA	Accel Current Y_1, mA	Beam Toward Electrode
-0	1.1	1.0		0.49	0.76	
-300	1.2	0.9	X_1	0.58	0.62	Y_1
-600	1.4	0.8	X_1	0.68	0.52	Y_1
-900	1.6	0.7	X_1	0.78	0.42	Y_1
-1080	1.75	0.7	X_1			
-1200				0.90	0.36	Y_1
0	1.0	1.1		0.48	0.79	
+300	0.9	1.2	X_2	0.43	1.0	Y_2
+600	0.8	1.4	X_2	0.37	1.1	Y_2
+900	0.75	1.6	X_2	0.34	1.4	Y_2
+1200	0.65	1.7	X_2	0.31	1.6	Y_2
0	1.0	1.0		0.49	0.73	

T202

TABLE XII

Beam Deflection Results at 75% Thrust Level
Beam Voltage = 2 kV; Beam Current = 13.5 mA; Accel Voltage = -4 kV

Deflection Voltage $2\delta V$, V	Strip 1			Strip 2		
	Accel Current X_2, mA	Accel Current X_1, mA	Beam Toward Electrode	Accel Current Y_2, mA	Accel Current Y_1, mA	Beam Toward Electrode
0	1.8	0.62		0.39	0.52	
-300	2.1	0.50	X_1	0.44	0.40	Y_1
-600	2.4	0.42	X_1	0.50	0.30	Y_1
-900	2.8	0.36	X_1	0.58	0.23	Y_1
-1200				0.66	0.17	Y_1
0	1.45	0.60		0.37	0.53	
+300	1.30	0.79	X_2	0.32	0.66	Y_2
+600	1.20	0.97	X_2	0.30	0.82	Y_2
+900	1.0	1.2	X_2	0.28	1.0	Y_2
+1200	0.8	1.4	X_2	0.26	1.1	Y_2
0	1.7	0.62		0.35	0.46	

T203

TABLE XIII

Beam Deflection Results at 50% Thrust Level
Beam Voltage = 2 kV; Beam Current = 90 mA; Accel Voltage = -3.5 kV

Deflection Voltage 2δV, V	Strip 1			Strip 2		
	Accel Current X_2, mA	Accel Current X_1, mA	Beam Toward Electrode	Accel Current Y_2, mA	Accel Current Y_1, mA	Beam Toward Electrode
0	0.90	0.34		0.06	0.12	
-300	1.1	0.28	X_1	0.08	0.08	Y_1
-600	1.2	0.26	X_1	0.10	0.05	Y_1
-900	1.4	0.23	X_1	0.14	0.04	Y_1
-1200	1.6	0.20	X_1	0.18	0.03	Y_1
0	0.74	0.32		0.06	0.12	
+300	0.64	0.40	X_2	0.05	0.18	Y_2
+600	0.53	0.49	X_2	0.05	0.23	Y_2
+900	0.44	0.60	X_2	0.05	0.31	Y_2
+1200	0.33	0.70	X_2	0.06	0.40	Y_2
0	0.82	0.32		0.06	0.09	

T204

values could be obtained by generating new sets of calibration curves for the various accel-to-decel ratios; however, the calibration curves obtained were limited to A/D = 3.5.

After the deflection data were obtained, the test was continued to complete the 24 hour operation of both thrusters. The thrust level was varied among the 75%, 50%, and 25% thrust level. The last segment of the run was a 5-1/2 hour operation with both thrusters at the 50% thrust level.

As shown in Fig. 61, there is a voltage limiting circuit and ammeter between the power supply common and ground, which was used to check the effectiveness of the beam neutralization. The voltage buildup was limited to 150 V if the electrons from the neutralizers were not coupling with the beam.

The neutralization technique was first tried during the 24 hour test. The first test attempted to heat the neutralizers to the proper temperature with a 4.5 mA beam. There was no evidence of neutralization. A second attempt, using a negative bias, was equally unsuccessful. The neutralizers were left on during the part of the test although they were not neutralizing. After the 24 hour test, the positions of the neutralizers were measured. It was discovered that the neutralizer filaments were located too far from the beam to neutralize. Another set of neutralizer filaments were fabricated, so they could be properly located. Because carburized thoriated filaments were unnecessary to study the beam neutralization, these filaments were operated as pure tungsten filaments. The only difference was that more power was needed to obtain the necessary electron emission.

A representative set of results for the thruster system at full thrust is shown in Table XIV. Results at 50% thrust are shown in Table XV. When the coupling is good the floating ground potential, and the current-to-ground would

TABLE XIV

Neutralization Results at 100% Thrust

Strip 1			Strip 2			Strip 1 and Strip 2		
Beam Voltage - 2 kV Beam Current = 18 mA Accel Voltage = -5 kV			Beam Voltage = 2 kV Beam Current = 18 mA Accel Voltage = -5 kV					
Neutralizer Used	Neutralizer Power, W	Neutralizer Emission, mA	Neutralizer Used	Neutralizer Power, W	Neutralizer Emission, mA	Neutralizer Bias, V	Floating Ground, V	Current-to-Ground mA
X_1	8.95	23	Y_1	9.20	>25	-80	-15	0
X_1	8.95	17	Y_1	9.20	>25	-60	-39	0
X_1	8.95	6	Y_1	9.20	>25	-50	-54	0

T205

TABLE XV

Neutralization Results at 50% Thrust

Strip 1			Strip 2			Strip 1 and Strip 2		
Beam Voltage = 2 kV Beam Current = 9 mA Accel Voltage = -5 kV			Beam Voltage = 2 kV Beam Current = 9 mA Accel Voltage = -5 kV					
Neutralizer Used	Neutralizer Power, W	Neutralizer Emission, mA	Neutralizer Used	Neutralizer Power, W	Neutralizer Emission, mA	Neutralizer Bias, V	Floating Ground, V	Current-to-Ground mA
X_1	6	>25	Y_1	6.5	23	-100	-137	0.8
X_1	6	>25	Y_1	6.5	>25	-120	- 88	0.5
X_1	6	>25	Y_1	6.5	>25	-140	- 40	0.3

T206

drop. For the 100% thrust level a neutralizer bias of about -50 V was needed to keep the floating ground at -50 V. The 50% thrust level required a -140 V bias to keep the floating potential at -40 V. The emission of the neutralizers was higher than the total current because some of the electrons moved to the decel. At lower beam current more than -150 V were required in the bias circuit. A second repositioning of the neutralizer, prior to delivery, was made to improve the neutralization at lower current densities. This change was accomplished and the thruster was delivered to NASA LeRC.

SECTION VI

THRUSTERS TEST RESULTS AT NASA LEWIS RESEARCH CENTER

The acceptance test of the thruster system was performed at NASA Lewis Research Center. The chamber used for the test was an oil diffusion pumped system with a liquid nitrogen cryoliner. This sytem was capable of operating in the 10^{-8} Torr range.

The thruster, which had to be mounted at LeRC, was attached to a rectangular frame, but isolated from it. In turn, the frame was mounted to the fixture, which was also electrically isolated from the chamber. A grounded disc (3 ft in diameter) with a center opening was mounted in line with the thruster face and a cylindrical ground screen was placed around the thruster.

Before the thruster and mounting fixture were placed in the chamber, a resistance check was made on, and between, various components. The high resistance measurements were made with a megohm meter at 1000 V, but the resistance between the neutralizer and ground was at a 200 V setting. Low resistance readings were made with a low range ohmmeter. The results of the measurement are shown in Table XVI. Ground in the table is the exit electrode and thruster support structure.

After the resistance check, the thruster and support plate were placed in the chamber and electrical leads were connected to the thruster. A final check for shorts revealed that one accel was shorted to the exit electrode. A quick check showed that one of the shields around the insulator supporting the accel had been moved during the installation. This was repaired easily. The chamber was evacuated, and several hours later the power supplies were turned on briefly for a final electrical check. The system was pumped overnight and the testing started the next day.

TABLE XVI

Impedance Check of Thruster at NASA Lewis Research Center (In Air)

Description	Strip 1, Ω	Strip 2, Ω
Ionizer and Accel 1 (X_1 and Y_1)	7×10^{10}	5×10^{10}
Ionizer and Accel 2 (X_2 and Y_2)	10^{11}	5×10^{10}
Ionizer and Ground	6×10^{10}	5×10^{9}
Accel 1 and Accel 2	7×10^{10}	3×10^{10}
Accel 1 and Ground	8×10^{10}	2.4×10^{10}
Accel 2 and Ground	2×10^{10}	3.4×10^{10}
Neutralizer 1 Common and Ground	9×10^{9}	6×10^{10}
Neutralizer 2 Common and Ground	9×10^{9}	6×10^{10}
Vent and Ionizer	0.96	1.15
Vaporizer and Ionizer	0.99	0.92
Ionizer Heater and Ionizer	0.86	0.88
Vent and Ground	5×10^{10}	6×10^{10}
Vaporizer and Ground	5×10^{10}	6×10^{10}
Ionizer and Ground	5×10^{10}	6×10^{10}
Outer Frame and Ionizer	6×10^{10}	7×10^{10}
Ionizer to Ionizer		
Outer Frame to Ground	6×10^{10}	6×10^{10}
Accel 1 to Accel 1	7×10^{10}	7×10^{10}
Neutralizer 1	3.13	3.07
Neutralizer 2	3.07	3.04

T207

The thruster acceptance test called for an 8 hour test. Figure 62 shows the operational levels for the test. The thrust levels were chosen by the NASA Project Manager. Both strips were kept at full thrust for more than four hours at the start of the test and one hour at the end of the test. The results shown in Fig. 62, follow the test plan (except for a delay between the seventh and eighth hour) for the following reason. Near the end of the seventh hour of operation, a thermocouple on vaporizer 2 was lost. As a precaution, Strip 2 was turned off. A few minutes later Strip 1 was turned off and a plan for the remainder of the test was made. Because there were power settings recorded at the full thrust level, no thermocouple readings were required.

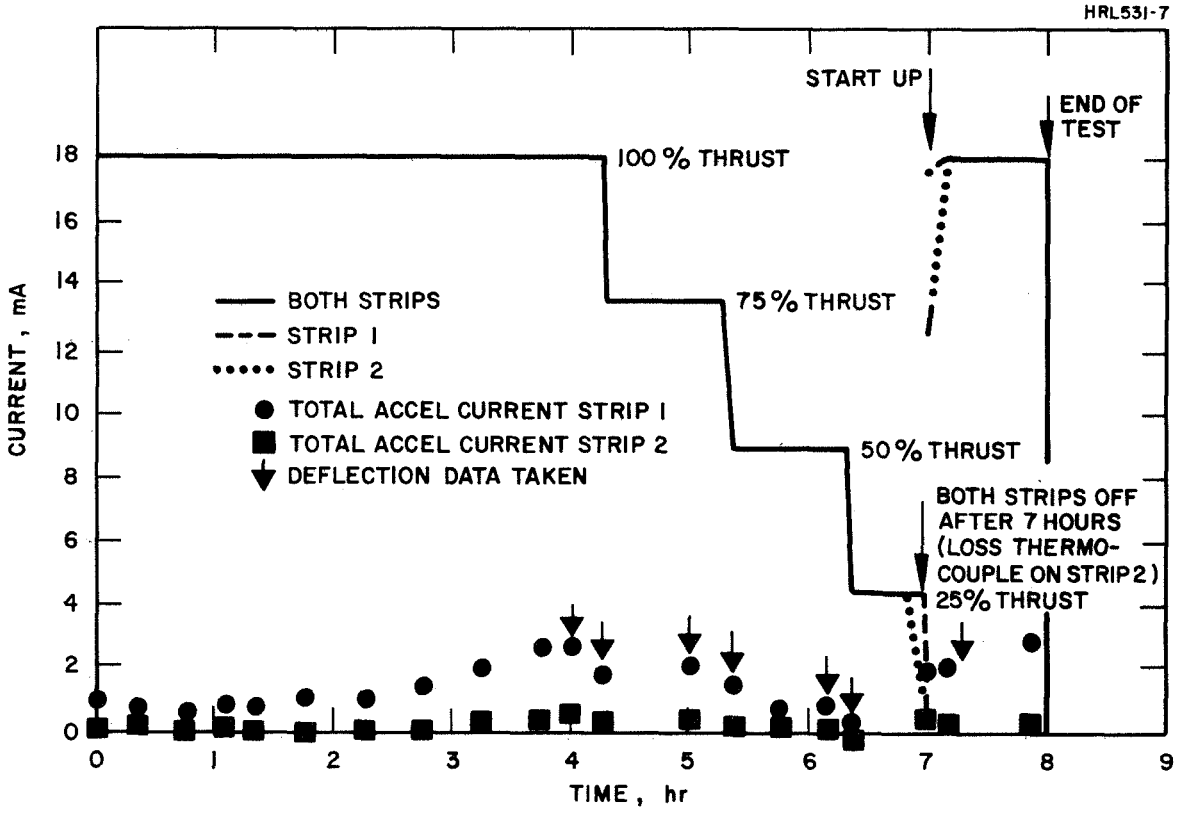

Fig. 62. Eight Hour Acceptance Test at LeRC.

All power to the thruster was turned off and resistance measurements were made (Table XVII). The final hour of the test was completed.

Accel current of Strip 2 was lower than that of Strip 1. The accel current on Strip 2 never exceeded 0.6 mA, while the highest value for Strip 1 was 3 mA. Since the short between the accel and exit electrode before the test start was on Strip 1, it is plausible that the shield over the accel insulator moved close enough to the exit electrode to emit electrons by field emission.

The operational parameters recorded during the eight hour test are shown in Tables XVIII and XIX. Both strips were operating while the data were taken. From the data taken, the current to ground quantity warrants explanation. This is the current flowing between the floating point on the power supplies to ground. When this value is zero, the ion beam is achieving neutralization. A significant result proved that it was easier to neutralize the beam at lower current densities than those experienced at the testing at Malibu. This was because the lower accel voltage did not "push" the electrons away from the beam and the new position of the neutralizers. This result indicates that the space in the exit electrode should be smaller, so the negative fields can be screened from the neutralizers. This change would make the neutralization much easier and would require less neutralizer bias.

During the eight hour test, deflection data also were taken. (See Tables XVIII and XIX.) The data recorded for the various thrust levels and two strips are shown in Tables XX, XXI, XXII, and XXIII. The angular deflection can be obtained from Figs. 59 and 60. The $2\delta V = \pm 1200$ V corresponds to approximately $\pm 20°$ for an 18 mA beam.

TABLE XVII

Impedance Check of Thruster at NASA Lewis Research Center
(In Vacuum)

Description	Strip 1, Ω	Strip 2, Ω
Ionizer and Accel 1 (X_1 and Y_1)	∞	∞
Ionizer and Accel 2 (X_2 and Y_2)	∞	∞
Ionizer and Ground	4×10^7	5×10^7
Accel 1 and Accel 2	∞	1.5×10^{13}
Accel 1 and Ground	2.5×10^{13}	1.5×10^9
Accel 2 and Ground	4.5×10^8	1×10^9
Neutralizer 1 Common and Ground	5×10^9	3×10^9
Neutralizer 2 Common and Ground	5×10^9	5×10^9
Vent and Ionizer	1.03	1.08
Vaporizer and Ionizer	1.03	1.05
Ionizer Heater and Ionizer	0.77	0.78
Vent and Ground	1.8×10^7	2×10^9
Vaporizer and Ground	1.5×10^7	2×10^9
Ionizer and Ground	1.5×10^7	2×10^9
Outer Frame and Ionizer	2.5×10^9	∞
Ionizer to Ionizer	7×10^9	7×10^9
Outer Frame to Ground	7×10^{11}	7×10^{11}
Accel 1 to Accel 1	7×10^{12}	7×10^{12}
Neutralizer 1	3.10	2.90
Neutralizer 2	2.90	2.90

T208

TABLE XVIII

Strip 1 Test at Nasa Lewis Research Center

Date	Time	Ionizer Heater		Vaporizer Heater		Beam		Accel		Neutralizer Heater		Neutralizer		Current-to-Ground mA	Pressure, Torr
		V	A	V	A	kV.	mA	-kV	mA	V	A	Bias, V	Emission, mA		
3/3/71	0944	17.0	3.90	6.5	1.95	2.0	18	5.5	1.0					36	7.6×10^{-7}
	1005	17.0	3.90	6.0	1.70	2.0	18.4	5.5	0.6	9.5	0.40	120	16	0	3×10^{-7}
	1030	17.0	3.91	5.75	1.65	2.0	18	5.5	0.6	9.6	0.395	120	15	0	1.8×10^{-7}
	1049	17.0	3.91	5.6	1.63	2.0	18	5.5	0.9	9.6	0.395	120	13.3	2.3	2.3×10^{-7}
	1105	17.0	3.91	5.6	1.60	2.0	18	5.5	0.9	9.6	0.395	120	12.5	3.0	1.7×10^{-7}
	1130	17.0	3.91	5.6	1.60	2.0	18	5.5	1.1	9.6	0.395	120	11	10.0	1.2×10^{-7}
	1200	17.0	3.91	5.4	1.6	2.0	18	5.5	1.1	9.6	0.395	120	12	9.6	1.1×10^{-7}
	1230	17.0	3.91	5.4	1.65	2.0	18	5.5	1.5	9.6	0.395	120	18	6.5	1.1×10^{-7}
	1300	17.0	3.92	5.4	1.62	2.0	18	5.5	2.05	9.6	0.395	120	20.5	5.5	9.3×10^{-8}
	1330	17.0	3.92	5.5	1.63	2.0	18	5.5	2.7	9.5	0.380	120	17.8	7.2	9.5×10^{-8}
	1345	17.0	3.92	5.5	1.65	2.0	18	5.5	2.9	9.5	0.38	120	15.5	9.2	9.2×10^{-8}
						Deflection data taken for 18 mA beams									
	1400	17.0	3.92	5.0	1.55	2.0	13.5	4.5	1.7	9.5	0.40	120	21	0	
						Deflection data taken for 13.5 mA beams									
	1445	17.0	3.92	5.7	1.65	2.0	13.5	4.5	2.2	9.5	0.4	110	22	0	5.9×10^{-8}
						Deflection data taken for 13.5 mA beams									
	1505	17.0	3.95	5	1.5	2.0	9.2	3	1.6	9.5	0.39	70	14	0	
						Deflection data taken for 9.2 mA beams									
	1530	17.0	3.95	4.8	1.43	2	9.5	3	0.85	9.5	0.395	75	15.8	0	6.1×10^{-8}
	1554	17.0	3.95	5.0	1.57	2	9.5	3	0.90	9.5	0.395	75	15.8	0	4.9×10^{-8}
						Deflection data taken for 9.3 mA beams									
	1606	17.0	3.97	4	1.4	2	4.5	2	0.38	9.5	0.395	70	11.5	0	
						Deflection data taken for 4.5 mA beams									
	1635					Lost thermocouple on Strip 2									
	1645	17.0	4.0	3.8	1.45	2	4.5	2	0.42	9.5	0.395	75	10.5	0.6	5.2×10^{-8}
	1646					Both strips turned off									
3/4/71	0930	17	3.95	7	1.95	2.5	17.6	5.2	2.1	0		0			8.6×10^{-8}
	0940	17	3.95	6.5	1.9	2.0	18	5.2	2.0	10.3	0.76	120	25	3	2×10^{-7}
						Deflection data taken for 18.0 mA beams									
	1025	17.3	3.93	5.5	1.75	2.0	17.9	5.0	3.2	10.1	0.77	120	24	0.5	8.8×10^{-8}
						Critical temperature check									
	~1035					All power off									

T209

TABLE XIX

Strip 2 Test at Nasa Lewis Research Center

Date	Time	Ionizer Heater		Vaporizer Heater		Beam		Accel		Neutralizer Heater		Neutralizer		Current-to-Ground mA	Pressure, Torr
		V	A	V	A	kV		-kV	mA	V	A	Bias, V	Emission, mA		
3/3/71	0944			6.5	2.02	2	18.2	5.5	0.2					36	7.6×10^{-7}
	1005	17.0	3.90	6	1.9	2	18.1	5.5	0.6	9.5	0.41	120		0	3×10^{-7}
	1030	17	3.90	6	1.8	2	18	5.5	0.1	9.5	0.41	120		0	1.8×10^{-7}
	1049	17	3.90	5.6	1.77	2	18	5.5	0.2	9.5	0.41	120		2.3	2.3×10^{-7}
	1105	16.8	3.92	5.6	1.75	2	18	5.5	0.1	9.5	0.41	120		3.0	1.7×10^{-7}
	1130	16.8	3.92	5.5	1.7	2	18	5.5	0.15	9.5	0.41	120		10.0	1.2×10^{-7}
	1200	16.8	3.92	5.5	1.72	2	18	5.5	0.12	9.2	0.4	120		9.6	1.1×10^{-7}
	1230	16.8	3.92	5.5	1.70	2	18	5.5	0.15	9.2	0.4	120		6.5	1.1×10^{-7}
	1300	16.8	3.92	5.5	1.73	2	18	5.5	0.2	9.2	0.4	120		9.3	9.3×10^{-8}
	1330	16.7	3.93	5.5	1.74	2	18	5.5	0.5	9.5	0.42	120		9.5	9.5×10^{-8}
	1345	16.7	3.93	5.5	1.73	2	18	5.5	0.5	9.5	0.41	120		9.2	9.2×10^{-8}
		Deflection data taken for 18 mA beams													
	1400														
		Deflection data taken for 13.5 mA beams													
	1445														5.9×10^{-8}
		Deflection data taken for 13.5 mA beams													
	1505														
		Deflection data taken for 9.2 mA beams													
	1530	16.7	3.95	5.5	1.73	2	9.4	3	0.1	9.4	0.4	75	12.7	0	6.1×10^{-8}
	1554	16.7	3.95	5.5	1.73	2	9.4	3	0.1	9.4	0.4	75	13.2	0	4.9×10^{-8}
		Deflection data taken for 9.3 mA beams													
	1606	16.7	3.95	4.5	1.58	2	4.5	3	0	9.5	0.4	70	13	0	
		Deflection data taken for 4.5 mA beams													
	1635					Lost thermocouple on Strip 2									
	1645	16.7	3.95	6	1.82	2	2	2	0	9.5	0.4	75	6.5	0.6	5.2×10^{-8}
	1646					Both strips turned off									
3/4/71	0930	17.4	3.90	6	2	2.5	12.5	5.2	0.4						8.6×10^{-8}
	0940	17.5	3.90	7	2	2	18	5.2	0.3	8.7	0.74	120	25	3	2×10^{-7}
		Deflection data taken on 18 mA beams													
	1025	17.5	3.95	5.6	1.75	2.0	17	5.0	0.4	8.75	0.75	120	24	0.5	8.8×10^{-8}
		Critical temperature check													
	1035	All power off													

T210

TABLE XX

Beam Deflection Results at 100% Thrust Level
Beam Voltage = 2 kV; Beam Current = 18 mA; Accel Voltage = -5.5 kV

Deflection Voltage $2\delta V$, V	Strip 1			Strip 2		
	Accel Current X_2, mA	Accel Current X_1, mA	Beam Toward Electrode	Accel Current Y_2, mA	Accel Current Y_1, mA	Beam Toward Electrode
0	1.0	2.1		0.07	0.44	
-300	1.1	1.9	X_2	0.07	0.40	Y_2
-600	1.2	1.7	X_2	0.09	0.36	Y_2
-900	1.4	1.5	X_2	0.11	0.32	Y_2
-1180	1.5	1.3	X_2			
-1200				0.13	0.29	Y_2
0	1.0	2.1		0.06	0.45	
300	0.9	2.6	X_1	0.05	0.49	Y_1
600	0.8	3.0	X_1	0.04	0.54	Y_1
900	0.7	3.2	X_1	0.04	0.61	Y_1
1200	0.7	3.3	X_1	0.04	0.68	Y_1
0	1.0	2.2		0.07	0.44	Y_1

T211

TABLE XXI

Beam Deflection Results at 75% Thrust Level
Beam Voltage = 2 kV; Beam Current = 13.5 mA, Accel Voltage = -4.5 kV

Deflection Voltage 2δV, V	Strip 1			Strip 2		
	Accel Current X_2, mA	Accel Current X_1, mA	Beam Toward Electrode	Accel Current Y_2, mA	Accel Current Y_1, mA	Beam Toward Electrode
0	0.6	1.3		0.02	0.28	
-300	0.7	1.1	X_2	0.02	0.24	Y_2
-600	0.7	1.0	X_2	0.03	0.22	Y_2
-900	0.8	0.8	X_2	0.04	0.19	Y_2
-1200	1.05	0.65	X_2	0.05	0.17	Y_2
0	0.5	1.3		0.02	0.28	
300	0.5	1.6	X_1	0.02	0.32	Y_1
600	0.4	2.3	X_1	0.01	0.36	Y_1
900	0.5	2.4	X_1	0.01	0.44	Y_1
1200	0.5	2.2	X_1	0.01	0.48	Y_1
0	0.6	1.3		0.02	0.27	

T212

TABLE XXII

Beam Deflection Results at 50% Thrust Level
Beam Voltage = 2 kV; Beam Current = 9 mA; Accel Voltage = -3 kV

Deflection Voltage 2δV, V	Strip 1			Strip 2		
	Accel Current X_2, mA	Accel Current X_1, mA	Beam Toward Electrode	Accel Current Y_2	Accel Current Y_1, mA	Beam Toward Electrode
0	0.35	0.45		0	0.08	
-300	0.34	0.36	X_2	0	0.075	Y_2
-600	0.35	0.30	X_2	0	0.06	Y_2
-900	0.45	0.25	X_2	0	0.05	Y_2
-1200	0.45	0.20	X_2	0	0.04	Y_2
0	0.30	0.50		0	0.09	
300	0.26	0.64	X_1	0	0.1	Y_1
600	0.20	0.80	X_1	0	0.13	Y_1
900	0	1.20	X_1	0	0.15	Y_1
1200	0	1.30	X_1	0	0.18	Y_1
0	0.34	0.46		0	0.09	

T213

TABLE XXIII

Beam Deflection Results at 25% Thrust Level
Beam Voltage = 2 kV; Beam Current = 4.5 mA; Accel Voltage = -2

Deflection Voltage 2δV, V	Strip 1			Strip 2		
	Accel Current X_2, mA	Accel Current X_1	Beam Toward Electrode	Accel Current Y_2	Accel Current Y_1, mA	Beam Toward Electrode
0	0.33	0.05		0	0.02	
-300	0.16	0.04	X_2	0	0.02	Y_2
-600	0.17	0.03	X_2	0	0.015	Y_2
-900	0.18	0.02	X_2	0	0.015	Y_2
-1200	0.18	0.02	X_2	0	0.01	Y_2
0	0.15	0.05		0	0.02	
300	0.12	0.08	X_1	0	0.03	Y_1
600	0.18	0.12	X_1	0	0.03	Y_1
900	0.17	0.18	X_1	0	0.04	Y_1
1200	0.18	0.22	X_1	0	0.05	Y_1
0	0.14	0.06		0	0.02	

T214

The deflection experiment was repeated on the 18 mA beam during the last hour of testing. All four neutralizers were used with a -120 V bias. The coupling was better than with only two neutralizers. The neutralization also was complete (i.e., current-to-ground = 0), for the slightest deflection. This was anticipated because the ion beam was moved closer to the beam.

SECTION VII

CONCLUSIONS AND RECOMMENDATIONS

Based on the results of the tests performed under this contract, there are several changes which could improve the thruster operation. These are (1) shaping the back side of the ionizer, (2) location of insulators which support the accel electrodes, (3) location of neutralizers, and (4) electrical terminals.

The electrode system used in this thruster is the Model 70 optics. There have been some changes in the accel electrodes to improve the beam deflection, but these have not affected the perveance. During the testing, it was found that the transition from a flow limited condition to the space charge limited condition is not sharp; there is a rounding effect. The probable cause for this, is that the cesium flow through the ionizer is not matched to the ions required at that surface of the ionizer. More ions are needed along the edge of the ionizer than at the center. Figure 63(a) shows the cross section of the ionizer used in this program. It favors more flow at the center rather than the edge. Figures 63(b) and (c) show two possible configurations which would provide a better match of flow to the ions required. This change should flatten the flow limited portion of the curve and permit lower accel voltages to be used; consequently, larger beam deflections could be obtained with the same 2δV voltages now used.

In the first tests made on the thruster system, it became apparent that the thruster operation was very sensitive to neutral flux. The accel currents were particularly affected when critical temperature or perveance data were taken. The first insulators which were cylindrical,

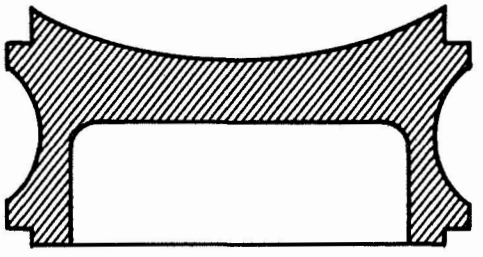

(a)

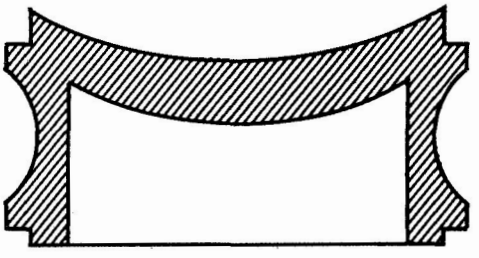

(b)

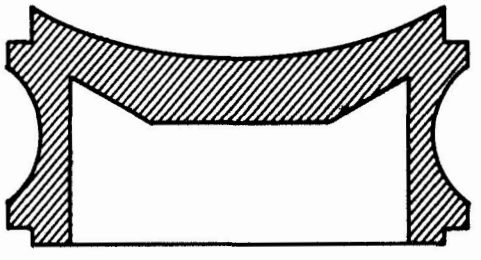

(c)

Fig. 63.
Cross Section of
Present Ionizer and
Alternate Designs.

shielded, and supported the accel from the decel. A second set was designed and built. These were located in the same place, but were mushroom shaped to provide a longer surface path to minimize surface leakage. Although this was an improvement, because the insulators are still near the ionizer, and subject to high temperature and cesium flux, there is a better solution to the problem. In some ways the problem is similar to those experienced with a cesium μ-thruster which was built at HRL and delivered to NASA Goddard Space Flight Center. In that program, drain currents and leakage currents were a constant source of problems. The problem disappeared only when the insulators for the accel electrode were moved toward the rear of the thruster. By moving the insulators away from the ionizer, lower temperatures and cesium flux minimized the accel drain problems. This was accomplished by mounting the accels off a ground structure located in the vicinity of the feed system. Figure 64 illustrates the possibility of the same treatment for the dual beam thruster. The ground structure can be seen horizontally in the figure near the flanges which join the ionizer and feed system. The accel electrodes are supported by long fluted insulators away from the ionizer. The focus electrode and feed system are supported by shorter insulators since they stand off a lower voltage. This change would substantially improve the thruster performance and lower accel currents.

The neutralizers have been shown to neutralize beam with a negative bias on the neutralizer. This bias is the order of -70 to -150 V for the present location of the neutralizers. Further studies concerning the location of the neutralizers should permit the lowering of the bias voltage and decrease electron flow to the decel electrode. Narrowing the gap on the exit electrode would also improve beam neutralization.

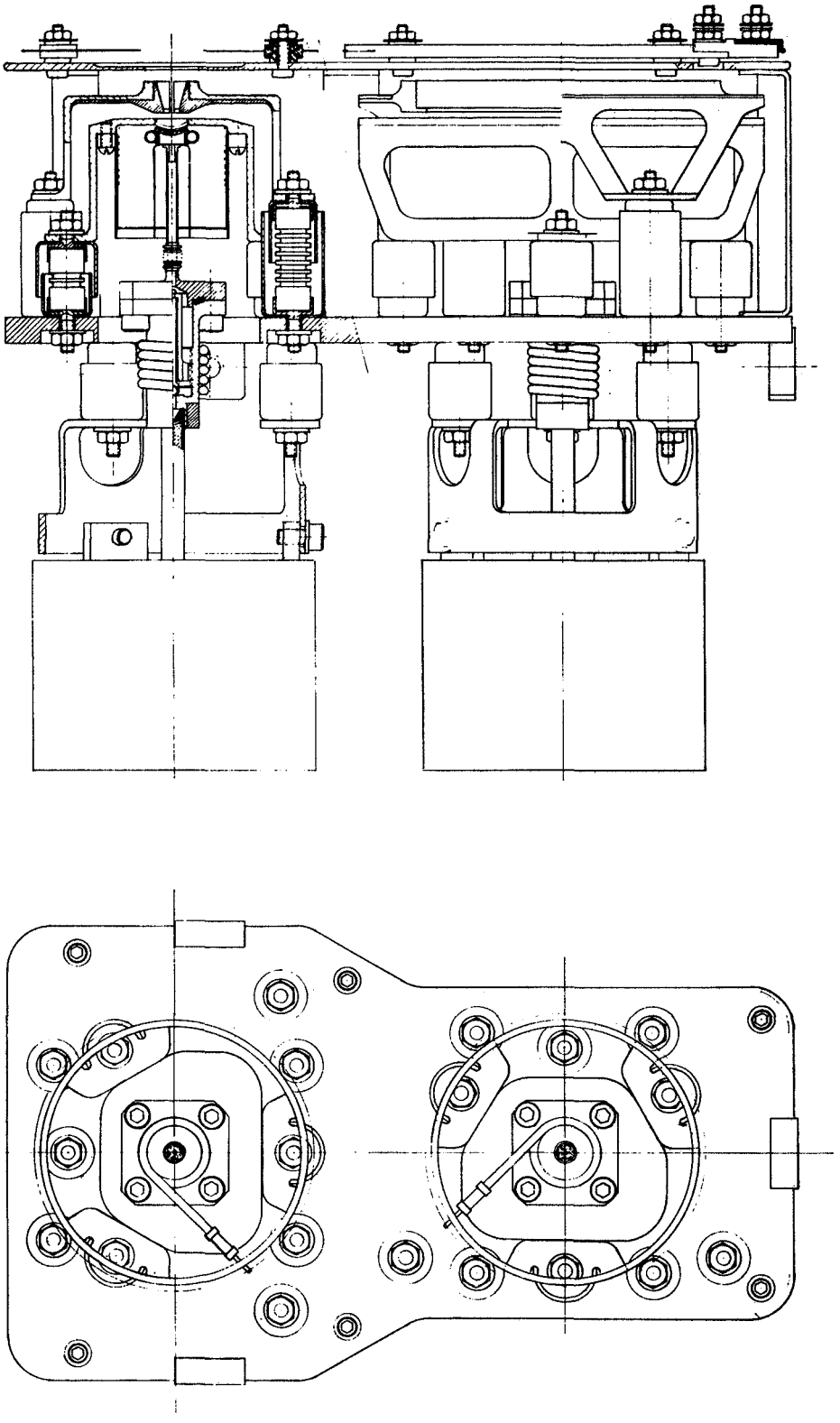

Fig. 64. New Dual Beam Thruster Design.

The electrical terminals were added after the original design was presented for review. As a result, they were located at various points on the ground structure wherever space permitted. A more orderly terminal strip should be placed on the thruster. When breakdown problems were discovered on the accel electrode terminals, these terminals were increased in size and moved. These terminals also will have to be located on the terminal strip. Breakdown experience should be considered seriously.

These changes would improve the thruster performance. It is clear that the thruster system would use less than 200 W when the ionizer surface becomes clean. The deflectable beam concept has been shown to be feasible for deflection angles of ±20° and could be used for station keeping.

REFERENCES

1. J.R. Anderson, et al., "Development of Linear-Strip Ion Thrusters for Attitude Control," NASA CR-54673, Summary Report, Contract No. NAS 3-4117, Hughes Research Laboratories (13 January 1966).

2. C.R. Dulgeroff, C.R. Collett, and J.M. Simpkins, "Cesium Microthruster System," AIAA Paper No. 69-292, Presented at AIAA Seventh Electric Propulsion Conference, Williamsburg, Virginia (March 1969).

3. J.R. Anderson, et al., "Development of Linear Strip Ion Thrusters," Monthly Progress Report No. 10, Contract NAS 3-7927, Hughes Research Laboratories (May 1966).

4. G. Sohl, R.C. Speiser, and J.A. Wolters, "Life Testing of Electron Bombardment Cesium Ion Engines," AIAA Paper No. 66-233, Fifth Electrical Propulsion Conference, San Diego, Calif. (1966).

5. A.T. Forrester and F.A. Bureatta, "Surface tension storing and feed systems for ion engines," J. Spacecraft Rockets 3, 1080-1085 (1966).

6. J.R. Anderson, et al., "Development of Linear Strip Ion Thrusters," HRL-7927-SA, NASA-CR54684, Contract No. NAS 3-7927 (January 1966).

7. K. Spangenberg, Vacuum Tubes, p. 394 (McGraw-Hill, New York, 1948).

8. A.E. Scheidegger, The Physics of Flow Through Porous Media, p. 183 (MacMillan Co., New York, 1960).

9. N.B. Kramer and E.G. Todd, J. Appl. Phys. 34, 3140 (1963).

10. G.R. Brewer, J. Appl. Phys. 28, 7 (1959).

11. H.E. Gallagher, IRE Trans. ED-6, 390 (1959).

12. Hughes Research Laboratories Staff, "Ion Engine Thrust Vector Study," Final Report, Contract JPL 952129, Hughes Research Laboratories (1969).

13. R.B. Ayers, Proc. IRE 40, 591 (1952).

14. P. Schneider, J. Chem. Phys. 28, 675 (1958).

15. C.W. Horsting, J. Appl. Phys. 18, 95 (1947).

16. H.J. Dailey, Electronics p. 107 (January 1948).

17. I. Langmuir, S. MacLane, and K.B. Blodgett, Phys. Rev. 35, 478 (1930).

18. Tabulated in the 31st Edition of the Handbook of Chemistry and Physics.

19. R.D. Larabee, J. Opt. Soc. Am. 49, 619 (1959).

20. B.T. Barnes, J. Phys. Chem. 33, 688 (1929).

21. F. Benford, J. Opt. Soc. Am. 29, 162 (1939).

22. Staff Members, "Ion Engine Development," NASA CR-54676, Contract No. NAS 3-6271, Hughes Research Laboratories (August 1966).